Alma Mater Studiorum - Università degli Studi di Bologna

Dottorato di Ricerca in Chimica - XXIX Ciclo

Settore Concorsuale: 03/B1
Settore Scientifico Disciplinare: CHIM/03

Operating Molecular Machines: Thermodynamic and Kinetic Aspects

Giulio Ragazzon

Relatore:
Prof. Alberto Credi

Correlatrice:
Dott.ssa Serena Silvi

Coordinatore:
Prof. Aldo Roda

Dipartimento di Chimica "G. Ciamician"

Bologna 2017

Sunto divulgativo

Credo che divulgare la propria scienza sia un dovere dello scienziato, ad ogni livello.
Le tesi di dottorato solitamente non sono comprensibili ad un pubblico generalista; rappresentano la frontiera in un determinato campo e per questo si rivolgono ad altri scienziati e devono parlare il linguaggio della comunità di riferimento. Questa tesi in larga parte non fa eccezione. Tuttavia vorrei spiegare brevemente qual è stato l'ambito del mio lavoro e quali sono stati i risultati più rilevanti, in parole semplici e comprensibili da un pubblico ampio.

Il corpo umano può essere interpretato come una macchina: un robot, ma non fatto di plastica e metallo, bensì di molecole e composti naturali. Ci sono immense aree della struttura umana che non conosciamo, ma fino a dove (non lontano) arriva la comprensione della comunità scientifica, la descrizione proposta regge. I robot hanno bisogno di energia per funzionare e allo stesso modo si comportano gli esseri umani: mangiamo, respiriamo, e se non lo facciamo, muoriamo. L'energia che guadagnamo mangiando e respirando viene usata per compiere delle funzioni a livello molecolare, ad esempio, quando contraiamo un braccio (i muscoli), ciò accade perchè un numero gigantesco di molecole si sta contraendo in maniera sincronizzata. Perciò possiamo pensare agli uomini come a un assembramento di molecole, che interagiscono fra loro e svolgono funzioni utili fintanto che viene fornita energia. In altre parole tre caratteristiche importanti sono[1]: (1) l'abilità di assemblare molecole diverse, (2) l'abilità di svolgere delle funzioni a livello molecolare, (3) l'utilizzo di un continuo input energetico.
I chimici hanno dedicato sforzi ingenti per sviluppare i temi (1) e (2), e il loro lavoro è stato riconosciuto con l'attribuzione di due Premi Nobel. Nel 1987 è stato attribuito a Cram, Lehn e Pedersen, per "il loro sviluppo e utilizzo di molecole che sviluppano, per la loro struttura specifica,

[1]Vorrei sottolineare che la Vita si distingue da molte altre caratteristiche, spesso estremamente complesse e lontane dall'essere comprese. Questo lavoro è completamente scollegato con lo svilupo della vita artificiale

interazioni ad alta selettività", cioò le interazioni che fanno assemblare molecole diverse in maniera controllata. Al giorno d'oggi ci si riferisce a questo campo come alla chimica supramolecolare, che è spesso descritta come "la chimica oltre la molecola". Appena qualche mese fa il Premio Nobel è stato assegnato a Sauvage, Stoddart e Feringa, per "il design e la sintesi delle macchine molecolari", che sono molecole capaci di svolgere funzioni a livello molecolare.[1] Il terzo argomento, cioè lo studio di sistemi chimici che hanno bisogno di un continuo apporto energetico per funzionare o esistere, è ancora sottosviluppato in confronto agli altri due, ma è per certi versi di moda nella chimica di oggi.
L'argomento più importante di cui tratta questa tesi è lo studio di un sistema semplice che unisce le tre caratteristiche descritte in precedenza: assemblaggio di molecole diverse, funzionalità e operazione automatica sotto l'azione di un costante apporto energetico. Al meglio delle mie conoscenze il sistema allo studio rappresenta — ad oggi — l'unico sistema chimico artificiale capace di unire queste tre caratteristiche. La funzione svolta è analoga a quella di una pompa, infatti una molecola allungata, descrivibile come un asse molecolare, attraversa con una direzione preferenziale una molecola ciclica, un anello molecolare. L'energia usata per far avvenire il pompaggio è formita dalla luce e l'"informazione chimica" che fa assemblare le due molecole (l'anello e l'asse) è codificata nella loro struttura molecolare, grazie all'appropriata ingegnerizzazione "di molecole che sviluppano, per la loro struttura specifica, interazioni ad alta selettività".

Allo stato attuale non ci sono applicazioni pratiche significative per il lavoro presentato in questa tesi. Onestamente neppure le macchine molecolari da Premio Nobel ne hanno. Questo lavoro si colloca nell'ambito della scienza di base: il mio compito è stato studiare un comprendere qualcosa di nuovo, non migliorare qualcosa che già esisteva.
L'illuminazione a candele era lo strumento comune per illuminare le case e le strade un tempo, anche mentre Volta stava facendo brillare un filo di rame per la prima volta. Anni dopo, grazie al contributo di molti, incluso Edison, l'illuminazione elettrica entrò in commercio e divenne d'uso comune. Lavorare alle macchine molecolari artificiali oggi può essere visto come far brillare un filo di rame all'inizio del diciennovesimo secolo: non vogliamo fare candele migliori, vogliamo fare qualcosa di mai visto.

[1] Invito gli interessati a visitare il sito ufficiale del Premio Nobel all'indirizzo `https://www.nobelprize.org/nobel_prizes/chemistry/laureates/` e dare un'occhiata alla sezione `Popular information` o `Press release` dell'anno desiderato.

Contents

Sunto divulgativo **iii**

Popular information **1**

Summary & readership **3**

List of abbreviations **7**

I Introduction **9**

1 From supramolecular chemistry to molecular machines **11**

1.1 Supramolecular chemistry and nanoscience 11

1.2 Molecular devices and machines 13

1.3 References 17

2 Experimental part **21**

2.1 References 24

II Viologen-calix[6]arene based devices **25**

3 Introduction **27**

3.1 Calix[6]arene as nonsymmetric molecular wheels 27

3.2 References 28

4 Calix[6]arene functionalized with naphthyl units **31**

4.1 Introduction 31

4.2 Calix[6]arene bearing naphthalene units at its lower rim 32

4.3 Calix[6]arene bearing naphthalene units at its upper rim . . . 37
4.4 Electrochemical pseudorotaxanes switching . . . 42
4.5 Conclusions . . . 43
4.6 References . . . 44

5 Calix[6]arene based rotaxanes with one recognition site 47
5.1 Introduction and design . . . 47
5.2 Spectroscopic and electrochemical investigation . . . 49
5.3 Conclusions . . . 54
5.4 References . . . 54

6 Calix[6]arene based rotaxanes with two recognition sites 57
6.1 Introduction and design . . . 57
6.2 Spectroscopic and electrochemical investigation . . . 58
6.3 Conclusions . . . 64
6.4 References . . . 65

III Acid-base switchable rotaxanes 67

7 Introduction 69
7.1 pH-switchable rotaxanes: from fundamentals to applications . . . 69
7.2 References . . . 70

8 Characterization of a bistable pH-switchable rotaxane 73
8.1 Introduction . . . 73
8.2 Design . . . 75
8.3 Determination of the ring distribution from luminescence measurements . . . 76
8.4 Determination of the ring distribution from acid/base titrations . . . 80
8.5 Conclusions . . . 84
8.6 References . . . 85

9 Redox switching of pKa through mechanical allostery 89
9.1 Introduction . . . 89
9.2 Electrochemical investigation . . . 90
9.3 Energetic considerations . . . 92

9.4 Conclusions . . . 95
9.5 References . . . 95

10 A molecular transporter **97**
10.1 Introducition . . . 97
10.2 Design and individual components . . . 97
10.3 Transporter operation . . . 101
10.4 Conclusions . . . 104
10.5 References . . . 105

IV A photochemically driven dissipative system **109**

11 Introduction **111**
11.1 Introduction . . . 111
11.2 Dissipative systems . . . 112
11.3 Photochemically driven dissipative systems . . . 113
11.4 References . . . 117

12 An autonomous artificial molecular pump **121**
12.1 Introduction . . . 121
12.2 System characterization . . . 122
12.3 Autonomous operation . . . 129
12.4 Conclusions . . . 134
12.5 References . . . 134

13 Insights in the operation of a dissipative pump **139**
13.1 Lessons from other fields . . . 139
13.2 Building an apparent potential energy surface . . . 141
13.3 Conclusions . . . 144
13.4 References . . . 145

V Radicals in supramolecular polymers **147**

14 A radical-cation based supramolecular polymer **149**
14.1 Aim & introduction . . . 149

14.2 Synthesis and stability of triphenylamine radical cations 149
14.3 Polymerization attempts 156
14.4 Conclusions 160
14.5 References 161

Conclusions **163**

List of publications **165**

Acknowledgments **169**

Popular information

I do believe that communicating science to the general public is mandatory, at any level in science. PhD thesis are usually not understandable by the general public; they represent the frontier in a specific field, therefore they are meant for other scholars and they must speak the language of the scientific community of reference. This thesis is largely not an exception. However in these first lines I would like to shortly explain what has been the subject of this work and what is the most relevant finding, in simple and broadly understandable words.

The human body can be seen as a machine: a robot, but not made of plastic and metal, rather by naturally occurring molecules and compounds. There are immense areas of the human architecture that are unknown, but as far (short) as the scientific community understands, the given picture holds. Robots need energy to perform any useful action, and so humans do: we eat and breath, and if we don't, we die. The energy that we gain by eating and breathing is used to perform tasks at the molecular level, e.g. when our arm (our muscles) contracts, it happens because a huge amount of molecules are acting synchronously. Therefore one can think about humans as collections of molecules that are interacting together and perform useful functions as long as energy is supplied. In other words three important features[1] are (1) the ability to bring different molecules together, (2) the ability to perform molecular-level tasks, (3) the exploitation of a continuous supply of energy. Chemists devoted huge efforts in developing themes (1) and (2), and their work has been recognized with the award of two Nobel Prizes. In 1987 it was awarded to Cram, Lehn and Pedersen, for "their development and use of molecules with structure-specific interactions of high selectivity", namely the interactions that bring molecules together in a controlled fashion. Nowadays one would refer to this field as supramolecular chemistry, that is often described as "the chemistry beyond the

[1] I wold like to stress the fact that Life is characterized by several other features, often extremely complex and far from being understood. This work is completely unrelated with the development of artificial life

molecule". Just a few months ago the Nobel Prize in Chemistry has been awarded to Sauvage, Stoddart and Feringa, for "the design and synthesis of molecular machines", that are molecules capable of performing molecular-level tasks.[1] The third topic, i.e. the study of chemical systems that need a continuous supply of energy to operate or exist, is still underdeveloped in comparison with the other two, but it is somehow trendy in chemistry nowadays.
The most important subject described in this thesis is the investigation of a minimal system that collects all the three outlined features: assembly of different molecules, functionality and automatic operation under a constant energy supply. To the best of my knowledge the studied system represents — to date — the only artificial chemical system combining these characteristics. The function resembles that of a pump, indeed an elongated axle-like molecule travels with one preferential direction across a cyclic ring-like molecule. The energy used to power the pumping is provided by light and the "chemical information" that brings the two molecules (the ring and the axle) together is encoded in their molecular structure, thanks to the careful engineering "of molecules with structure-specific interactions of high selectivity".

At the present stage there is no significant practical application for the work presented in this thesis. Honestly, not even the Nobel Prize-awarded molecular machines have. This work lies in the domain of basic science: my task has been to study and understand something new, not to optimize something already existing.
Candles lighting was the common way for illuminating houses and roads in the past, even while Volta was a making copper wire glow for the first time. Years later, thanks to the contribution of many, including Edison, electric lightning became commonly used and commercially available. Making artificial molecular machines today may be seen as making copper wires glow in the early nineteenth century: we do not intend to make better candles, we want to make something unprecedent.

[1] I encourage the interested reader to visit the official web site of the Nobel Prize at `https://www.nobelprize.org/nobel_prizes/chemistry/laureates/` and take a look at the `Popular information` or `Press release` section of the desired year.

Summary & readership

This manuscript is mainly devoted to artificial molecular machines. The award of the Nobel Prize to Sauvage, Stoddart and Feringa just few months ago recognized the oustanding ingenuity and creativity of the people working in this field. However, in comparison with their biological counterpart, artificial nanoscale devices and machines seem trivial, if not useless. Clearly this field requires further efforts to be beneficial — ultimately — for the society.

This thesis collects some of the work that I performed during my PhD, aimed at progressing the field, towards useful, structurally simple and autonomous machines. It is composed of five Parts, each comprising one or more Chapters.

Part I provides an introduction to the thesis work. In particular **Chapter 1** outlines the challenges that the field is currently facing, and **Chapter 2** provides the most relevant experimental details on the techniques that were used: mostly optical spectroscopy and electrochemistry.

Part II collects the work related to calix[6]arenes, that has been possible thanks to the fruitful collaboration with the group or Prof. Arduini and Prof. Secchi at the University of Parma. **Chapter III** introduces calix[6]arenes in the context of molecular devices and machines. In **Chapter 4** the possibility to functionalize the upper or lower rim of calix[6]arene with naphthyl units has been explored. It was found that the host retains its complexation ability and the coordination reaction modulates the photophysical properties of the host. In the following **Chapters 5** and **6** rotaxane and catenane architechtures with one or two recognition sites for the calixarene wheel have been studied: introduction of a secondary station was found to be necessary to displace the calixarene from its location, upon reduction of its electron-poor primary station. In this case our investigation has been complementary to the electron paramagnetic resonance (EPR) studies performed on the same systems by the group of Prof. Lucarini.

In **Part III** the main players are bistable rotaxanes based on the dialkylammonium:crown-ether recognition site as primary station. Such structures are introduced in **Chapter 7**. In the following **Chapter 8** it is shown that the affinity of the secondary station for the macrocycle controls the

basicity of the alkylammonium recognition site (primary station). This finding is exploited in the following **Chapter 9**, where it shown that, in a parent rotaxane architecture, an electrochemical stimulus at the secondary station can reversibly modulate the basicity of the alkylammonium in an allosteric-like manner. In this study EPR performed in the group of Prof. Lucarini has been beneficial to our aim. The final **Chapter 10** uses the same rotaxane architecture at study in the previous chapter to perform the pick-up, transport and release of a molecular cargo.
Part IV is based on a minimal molecular machine that operates away from equilibrium under continuous light stimulation, i.e. dissipatively. In particular, **Chapter 11** introduces molecular-level dissipative systems, with a particular focus on those powered by light. **Chapter 12** describes the dissipative operation of a minimal light-driven molecular pump and the following **Chapter 13** is intended to propose a novel strategy for conceptualizing light-driven dissipative systems. The rationalization is based on the energy span theory, that was developed for catalytic cycles, and is here applied to the studied molecular pump.
Finally, **Part V**, coinciding with **Chapter 14**, collects the work performed at the University of Tokyo under the supervision of Prof. Aida, who kindly hosted me in his group for half a year. The main players of this chapter are the radical cations of tripheylamine derivatives and their supramolecular aggregates.

Depending on the background of the reader, I would suggest to focus on different sections of the thesis.
As a general perspective, the most innovative findings are described in Part IV (chapters 11 to 13) and chapter 9: chapter 13 may even be considered, to some extent, controversial. Indeed chapters 11 and 13 might be of interest also for physicist working in the domain of dissipative systems. On the other hand, supramolecular chemist may be preferentially interested in the experimental counterpart of those chapters (i.e. chapter 12) and in chapter 9, that highlights the importance of "frustrated" noncovalent interactions within interlocked structures.
Photochemistry is of utmost importance in this work. Light is used as a tool to investigate and to operate molecular machines. In terms of investigation, chapter 4 collects a range of basic experiments with both absorption and emission techniques, including time-resolved and low temperature (77K) measurements. When considering the ability of light to operate nanomachines, chapter 10 provides an example of sequential operation, whereas chapter 12 describes the use of light under continuous irradiation. Some very unique properties of light as a driving force are discussed from

the theoretical perspective in chapters 11 and 13. Besides the highlighted chapters, almost every other section of the manuscript includes some photochemical feature.
Electrochemistry complements photochemistry. Also in this case the thesis contains sections where electrochemistry is a tool to investigate and operate nanoscale devices. Chapters 9 and 10 use extensively electrochemical techniques to investigate the studied devices, whereas in chapters 4, 6, 9 and 14, redox reactions serve as driving force for the system operation.
In a broader perspective — according to my personal taste — the key experiments shown in chapter 9 and 12 are elegant, and chapter 9 has an intrinsic didactic character.

A considerable amount of work that was done during my PhD has been excluded from this thesis. I do believe that I learned a lot from parts of my work that are not described here, including those projects that were abandoned. Therefore, I would like to mention the projects to which part of the PhD has been dedicated, but were not included.
As one might expect several of these projects are very close to the topics of the thesis. For what concerns calixarene chemistry, in collaboration with Prof. Arduini and Prof. Secchi at the University of Parma, the ability of this host to accelerate the alkylation of piridyl moieties to afford quaternary salts has been demonstrated [manuscript ready for submission], as well as the possibility to extend to calix[6]arene the strategy used in Chapter 12 to obtain the unidirectional transit of a molecular axle through a macrocycle. In collaboration with Prof. Lucarini at the University of Bologna and Prof. Di Valentin at the University of Padova, pulsed electron-electron double resonance (PELDOR) spectroscopy has been used to disclose the conformational preference of the crown-ether ring in the rotaxane architecture used in chapters 9 and 10 [see *Chem. Eur. J.*, **2016**, 22] of this thesis.
Host-guest complexes and azobenzene have been good companion: complexation of dibenzo-24-crown-8 with secondary alkylammonium salts has been exploited in different occasions, for examples in attempts to further build on [*Chem. Commun.*, **2015**, 51, 2810] and basic studies regarding the photophysical properties of such complexes (see the acknowledgments section in [*J. Am. Chem. Soc.*, **2014**, 136, 14245]). The ability of cyclobis(paraquat-*p*-phenylene) to complex thiophene and a number of its derivatives has been studied by means of optical spectroscopies and electrochemistry. Electrochemical experiments were also performed on some of the naphthalimide derivatives presented in chapter 8.
Discussion of the more theoretical aspects of the molecular pump described in Part IV have been a constant in these years, in particular with Emanuele Penocchio, first while he was a Collegio

Superiore student and even more now that the kinetic optimization of the molecular pump is being performed – in the context of a collaboration with Prof. Barone at Scuola Normale Superiore di Pisa.
In the time spent at the University of Tokyo in the labs of Prof. Aida, part of the work was dedicated to study the properties of optical second harmonic generation of a supramolecular ferroelectric material.
Besides the themes covered in the thesis, other topics that are commonly studied in the lab of Prof. Credi were explored. In collaboration with Dr. Armaroli, the ability of nitrogenous base recognition motif to guide the aggregation of CdSe quantum dots has been investigated. In collaboration with Prof. Armetano at University of Calabria and Dr. Pardo at University of Valencia, the optical absorption properties of metal-cluster containing metal-organic framework were studied. Moreover, developments of porosity photoswitching in the solid state [*Nat. Chem*, **2015**, 7, 634] were followed. Finally, part of my work has been carried out in collaboration with Infineum UK Ltd., and is covered by a non-disclosure agreement.

List of abbreviations

1-NPU	1-naphthyl-N'-phenylurea
2-MN	2-methoxynaphthalene
AFM	Atomic force microscopy
ATP	Adenosine triphospate
amH$^+$	Ammonium moiety
bpy	Bipyridinium moiety
CD	Circular dicroism
CH	Cyclohexane
CT	Charge transfer
CV	Cyclic voltammetry
DB24C8	Dibenzo-24-crown-8
DB24C8R	DB24C8 derivative, see figure 9.1
DCM	Dichloromethane
DOV^{2+}	1,1'-dioctyl-4,4'-bipyridinium
DPV	Differential pulse voltammetry
EPR	Electron paramagnetic resonance
IR	Infrared
MC	Metal-centered
MCH	Methylcyclohexane
MLCT	Metal-to-ligand charge transfer
MCC	Metastable co-conformation
NI	Naphthalimide moiety
NMR	Nuclear magnetic resonance
P$_1$-*t*Bu	N-*t*-butyl -N',N',N'',N'',N''',N'''-hexamethylphosphorimidic triamide
PES	Potential energy surface
PSS	Photostationary state
SCC	Stable co-conformation
TBA	Tributylamine
TBPA$^{+\bullet}$	Tris(4-bromophenyl)ammoniumyl radical cation
TPA	Triamide triphenylamine
TrH	Triflic acid
tria$^+$	Triazolium moiety
TsO$^-$	Tosylate
UV	Ultraviolet

Part I

Introduction

1

From supramolecular chemistry to molecular machines

1.1 Supramolecular chemistry and nanoscience

Using the words of Nobel Prize laureate Jean-Marie Lehn, "supramolecular chemistry may be defined as "the chemistry beyond the molecule", bearing on the organized entities of higher complexity that result from the association of two or more chemical species held together by intermolecular forces"[1] i.e. the properties of the system arise from the interaction of different molecules together through weak forces. Nowadays a broader definition identifies a supramolecular system with a complex organized system, obtained from the association of two or more species, where the electronic interaction energy between the different components is little in comparison with the other energetic parameters that characterise the system. In simple words, it means that the individual properties of the components are kept. Additional properties emerge from the interaction of the components.

As a minimal example one can think about Europium complexes, bearing ligands that are able to absorb light in the near UV region: irradiation of the metal or the ligand alone would not produce any emission of light, whereas the excitation of the complex (i.e. the supramolecular system, where ligands coordinate the metal centre) results in the emission of light, because the ligands are able to absorb light and transfer the electronic energy to the metal, that is able to emit a photon, producing the observed luminescence (figure 1.1).

This chapter is partially derived — with permission — from G. Ragazzon, *Master Thesis*: "Photoinduced unidirectional transit of a macrocycle through a molecular axle" **2013**.

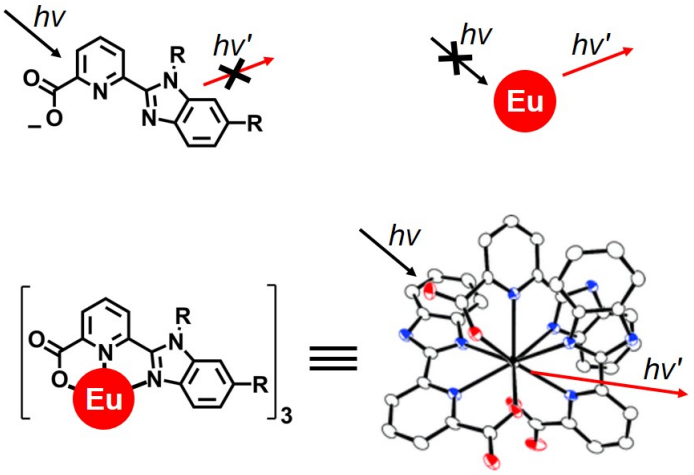

Figure 1.1: *The shown ligand (top left) is able to absorb near UV light, but not to emit. On the contrary Europium (III) is not able to absorb near UV light, thus is not emissive, even if the radiative de-excitation path is permitted. Combining the two entities together affords a luminescent metal complex, where light is absorbed by the ligand and transferred to the emissive metal centre. Adapted with permission from* Inorg. Chem., ***2009**, 48, 5611.*

In our daily life it is rather frequent to deal with objects engineered to perform a useful action, that is possible thanks to the joint action of its different parts. Nowadays mobile phones and computers are good examples of such devices, although my personal choice goes to a simpler light-bulb. Indeed an incandescent tungsten wire would not produce light for long, and neither would a glass bulb filled with an inert gas, but the well known shiny light bulbs are constituted by these two components, properly matched together. This being said, it becomes straightforward to think about supramolecular chemistry as the nanoscopic equivalent of engineering: as an engineer builds devices, so the chemist does with molecules. Indeed supramolecular chemistry is strongly connected with the development of nanotechnology, that is the field of science and technology focusing on the control of matter and energy at the nanometer scale, in order to build useful devices and machines.

It is commonly accepted by the scientific community that reducing the dimensions of objects and devices to the nanometre scale is not only a matter of miniaturization, indeed as an example, at such a tiny dimension concepts like friction and inertia can not be defined, as they strictly apply to the macroscopic world. Similarly the force of gravity can be neglected, and the electronic interactions become the predominant factor to influence the behaviour of a nanoscopic object. The set of principles on which nanotechnology relies is often referred to as nanoscience, and the work of

the chemists to build molecular devices and machines belongs to this field of science.

1.2 Molecular devices and machines

As highlighted by Goodsell in his book "Our Molecular Nature", we humans are made of the molecular devices and machines introduced in the previous section; these machines are naturally produced in our body and continuously renewed during our life. As an example of naturally occurring molecular machine, the reader can think about his own eyes, that are now moving to follow the text, driven by the action of a huge number of molecules, that are acting together in a concerted manner.

Many different kinds of action can be performed by our molecular devices: enzymes frequently use a change in their shape to become active or inactive; our muscles move under the action of myosins, that are advancing along an actin filament; Adenosine triphosphate (ATP) synthase, the enzyme responsible for the synthesis of ATP (that can be roughly defined as our fuel), works thanks to the rotation of one of its sub-units, whose motion is coupled to the ATP production; finally the transport of a chemical through a membrane against a concentration gradient is an energy-demanding action of key importance for the cell activity.

Scientists embraced long ago the challenge of designing, synthesizing and studying artificial molecular devices and machines. Their outstanding ingenuity and creativity has been recently recognized with the award of the Nobel Prize in Chemistry 2016 to Jean-Pierre Sauvage, Fraser Stoddart and Ben Feringa. Far from mimicking the sophistication of naturally occurring molecular machines, chemists had to start from a much lower complexity level and the first systems were able to perform very simple actions, e.g. one of the very first molecular devices was an azobenzene-based molecule, able to modify its affinity for potassium ions as a function of the azobenezene moiety isomerisation (figure 1.2).[2]

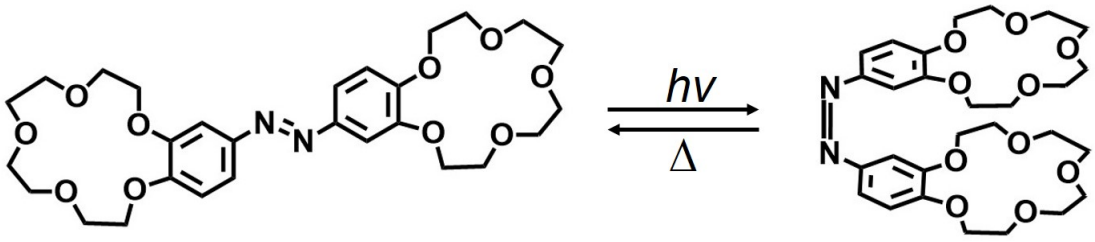

Figure 1.2: *One of the first molecular devices: K^+ has different affinities for the two shown isomers, thus it is possible to control the extent of potassium complexation with light.*

Widely studied structures are rotaxanes, the interlocked molecules whose cartoon representation is shown in figure 1.3 (bottom right), that were made available thanks to templated synthesis, that was developed by Sauvage.[3] Rotaxanes consist of a molecular axle threaded in a ring-like molecule. The dethreading of the axle is hampered by two bulky stoppers at the axle's end, therefore the two molecular components that constitute the rotaxane do not require a recognition motif to remain linked after the synthesis has been performed: they are mechanically interlocked. If the two entities are not mechanically interlocked and the axle is free to thread and dethread the system is called pseudo-rotaxane (figure 1.3 - top). Alternatively, when the two ends of the axle are joined together a catenane is obtained (figure 1.3 bottom right).

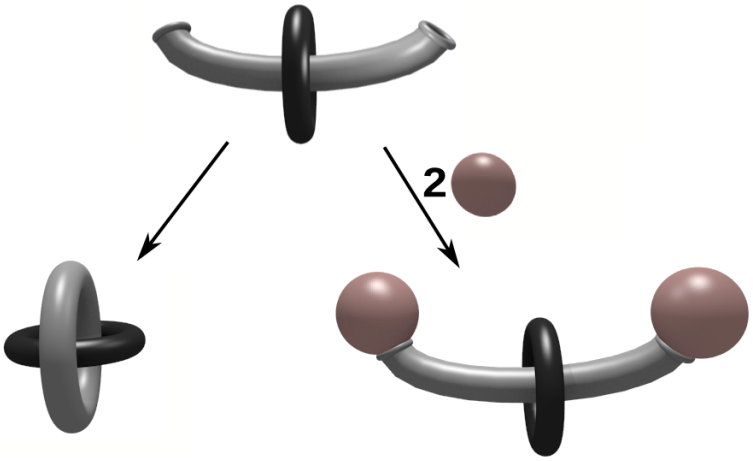

Figure 1.3: *A pseudo-rotaxane (top) can be chemically converted to a catenane if the two ends of the axle are joined (bottom left); otherwise it can become a rotaxane if two bulky stoppers that prevent the axle's dethreading are added (bottom right). [cartoon representation]*

If the axle of a rotaxane has two recognition sites for the ring, i.e. two different stations where the ring can reside, the statistical distribution of the ring between the two sites will depend on the relative strength of the ring-station interactions. Therefore favouring one of the two recognition sites over the other changes the statistical distribution of the ring between the two, causing a net mechanical movement at the molecular scale. The first controlled motion of a macrocycle in a rotaxane was demonstrated by Stoddart and coworkers in 1993.[4] Nowadays molecular-level shuttling can be easily achieved in a variety of ways, e.g. with a chemical, electrochemical or photochemical input, as a consequence of the deep scientific interest that guided the studies on such systems.

The third Nobel Laureate — Ben Feringa — developed the first example of an autonomous

molecular motor. The system consists of the bis-helicene reported in figure 1.4. The first of four steps required to perform a complete cycle is the photoisomerisation of the *E*-(P,P) to the *Z*-(M,M) form, where P and M indicate the right and left-handed helix. Intriguingly the isomerisation process also inverts the axial chirality, and the two axial methyl groups become equatorial. The equatorial conformation is less favoured than the axial one, therefore the system thermally and irreversibly converts to the more stable axial isomer (*Z*-(P,P)): the irreversibility of this step introduces a strong directional restriction in the system. A second photoisomerisation converts the motor to *E*-(M,M), again with its methyl groups in the unfavoured equatorial conformation and therefore the thermal isomerisation to the initial *E*-(P,P) form occurs. The very first molecular rotatory motor was then improved and many interesting results were obtained exploiting this type of molecular machine[5, 6], notably the photocontrolled motion of microscale objects[7] and the conversion of a rotary motion into linear motion, thanks to a car-like molecular architechture.[8]

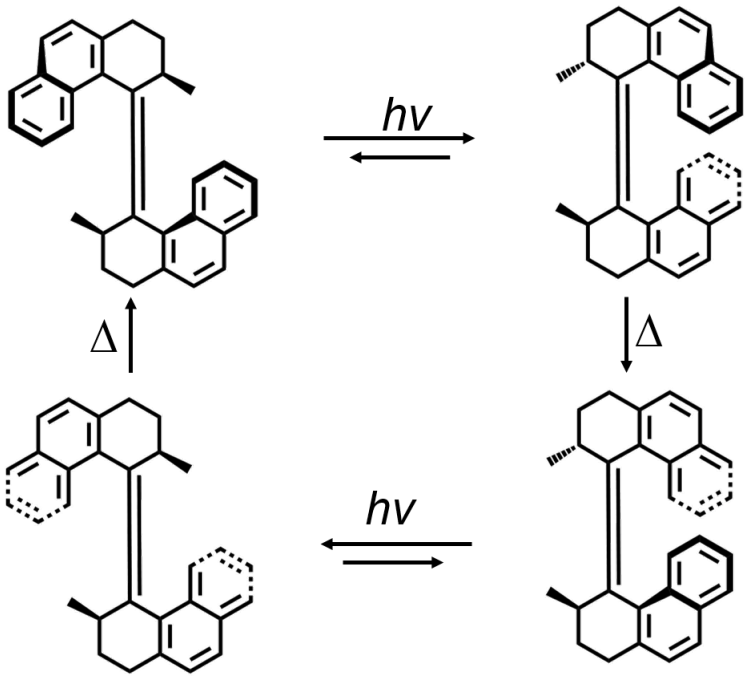

Figure 1.4: *Schematic operation of the rotary motor developed by Feringa, that rotates around the overcrowded double bond under light irradiation. Adapted with permission from reference [9].*

Despite the incredible progress of the field — that ultimately led to the award of the 2016 Nobel Prize — the field of molecular machines can still be considered in its infancy. To close the gap

between artificial and naturally occurring nanomachines, four main themes can be identified:[10–12]

1. Structural complexity. The structural complexity is likely the biggest difference between natural and artificial machines. With the current knowledge it does not seem possible to bridge this gap, however it can be noted that so far artificial molecular machines have often a high degree of symmetry. Two possible strategies to improve this aspect of molecular machines can be envisioned. One is to develop systems that can perform elaborated task but have a minimal architecture. The second strategy is to achieve a higher control on the machine operation upon reduction of the symmetry of the molecular system.[for selected examples see e.g.: 13–15] Both strategies should allow the future development of structurally more elaborated systems in which the higher structural complexity reflects in a higher control on the machine operation;

2. Functionality. Although proof-of-concept application of artificial machines have been reported, their ability to perform useful tasks is still unsatisfactory[12][for selected examples see e.g.: 7, 16, 17]. Possibly — to compete with existing technology — these machines should be designed to perform molecular-level tasks[for selected examples see e.g.: 18–21] and not just mimic macroscopic devices;

3. Ratcheting. What distinguishes a motor from a switch is its ability to perform work on the environment repetitively. In fact any work eventually performed by a switch is cancelled as the system returns to its initial state. What allows molecular motors to perform work is the appropriate engineering of the energy landscape (including its transition states, i.e., not only the thermodynamic but also the kinetic of the system) explored by the machine during its operation: its repetitive modulation allows the system to go back to the initial state through a kinetic path that is not the microscopic reverse of the initial switching process. This effect is described as ratcheting and implies the rectification of Brownian motion. Systems in which a ratchet mechanism operate are rare;[9, 18, 22–26]

4. Autonomous operation. Biomolecular machines have the outstanding ability of performing their functions under a constant energy supply, i.e., they work autonomously, away from equilibrium. On the contrary almost all the molecular machines reported to date exploit two (or more) external stimuli, that need to be alternated by an operator to induce the

switching of the machine between its states. The development of autonomous machines remains a challenge[9, 22, 24–26], and is expected to significantly contribute to the evolution of supramolecular chemistry as a whole, towards adaptive nonequilibrium systems.[27, 28]

In this thesis recent work performed in our lab, aimed at tackling these four challenges is presented. In particular, part II deals with the chemistry of nonsymmetric calix[6]arene wheels, in part III rotaxanes with a remarkable level of functionality are presented and in part IV an autonomous molecular pump based on a minimal architecture is presented and rationalized. Part V reports on the studies performed during my stay in the group of Prof. Aida at The University of Tokyo and RIKEN Centre, where the self-assembly of radical cations was investigated.

1.3 References

[1] J.-M. Lehn. *Nobel Lecture*, December 8th, 1987. 11

[2] S. Shinkai, T. Nakaji, T. Ogawa, K. Shigematsu, and O. Manabe. *J. Am. Chem. Soc.*, 103:111–115, 1981. 13

[3] C.O. Dietrich-Buchecker, J.P. Sauvage, and J.P Kintzinger. *Tetrahedron*, 24:5095–5098, 1983. 14

[4] R. A. Bissell, E. Cordova, A. E. Kaifer, and J. F. Stoddart. *Nature*, 369:133–137, 1994. 14

[5] R. A. van Delden, J. C. Mastergabin, M. K. J. ter Wiel, M. M. Pollard, J. Vicario, N. Koumura, and B. L. Feringa. *Nature*, 437:1337–1340, 2005. 15

[6] N. Ruangsupapichat, M. M. Pollard, S. R. Harutyunyan, and B. L. Feringa. *Nat. Chem.*, 3:53–60, 2011. 15

[7] R. Eelkema, M. M. Pollard, J. Vicario, N. Katsonis, B. S. Ramon, C. W. M Bastiaansen, D. J. Broer, and B. L. Feringa. *Nature*, 440:163, 2006. 15, 16

[8] T. Kudernac, N. Ruangsupapichat, M. Parschau, B. Maciá, N. Katsonis, S. R. Harutyunyan, K. Ernst, and B. L. Feringa. *Nature*, 479:208–2011. 15

[9] N. Koumura, R. W. J. Zijlstra, R. A. van Delden, N. Harada, and B. L. Feringa. *Nature*, 401:152–155, 1999. 15, 16, 17

[10] V. Balzani, A. Credi, and M. Venturi. *Molecular Devices and Machines, 2nd Ed.* Wiley-VCH, Weinheim, 2008. 16

[11] E. R. Kay, D. A. Leigh, and F. Zerbetto. *Angew. Chem. Int.Ed.*, 46:72–191, 2007.

[12] A. Coskun, M. Banaszak, R. D. Astumian, J. F. Stoddart, and B. A. Grzybowski. *Chem. Soc. Rev.*, 41:19–30, 2012. 16

[13] A. Arduini, R. Bussolati, A. Credi, A. Secchi, S. Silvi, M. Semeraro, and M. Venturi. *J. Am. Chem. Soc.*, 135:9924–9930, 2013. 16

[14] R. J. Bordoli and S. M. Goldup. *J. Am. Chem. Soc.*, 136:4817–4820, 2014.

[15] V. Blanco, D. A. Leigh, V. Marcos, J. A. Morales-Serna, and A. L. Nussbaumer. *J. Am. Chem. Soc.*, 136:4905–4908, 2014. 16

[16] T. J. Huang, B. Brough, C.-M. Ho, Y. Liu, A. H. Flood, P. A. Bonvallet, H.-R. Tseng, J. F. Stoddart, M. Baller, and S. Magonov. *Appl. Phys. Lett.*, 85(22):5391–5393, 2004. 16

[17] Q. Li, G. Fuks, E. Moulin, M. Maaloum, M. Rawiso, I. Kulic, J. T. Foy, and N. Giuseppone. *Nat. Nanotechnol.*, 10:161–165, 2015. 16

[18] C. Cheng, P. R. McGonigal, S. T. Schneebeli, H. Li, N. A. Vermeulen, C. Ke, and J. F. Stoddart. *Nat. Nanotechnol.*, 10:547–553, 2015. 16

[19] B. Lewandowski, G. De Bo, J. W. Ward, M. Papmeyer, S. Kuschel, M. J. Aldegunde, P. M. E. Gramlich, D. Heckmann, S. M. Goldup, D. D'Souza, A. E. Fernandes, and D. A. Leigh. *Science*, 339:189–193, 2013.

[20] J. Chen, S. J. Wezenberg, and B. L. Feringa. *Chem. Commun.*, 52:6765–6768, 2016.

[21] S. Kassem, A. T. L. Lee, D. A. Leigh, A. Markevicius, and J. Solá. *Nat. Chem.*, 8:138–143, 2016. 16

[22] V. Serreli, C.-F. Lee, E. R. Kay, and D. A. Leigh. *Nature*, 445:523–527, 2007. 16, 17

[23] M. N. Chatterjee, E. R. Kay, and D. A. Leigh. *J. Am. Chem. Soc.*, 128:4058–4073, 2006.

[24] D. A. Leigh, J. K. Y. Wong, F. Dehez, and F. Zerbetto. *Nature*, 424:174–179, 2003. 17

[25] M. R. Wilson, J. Solá, A. Carlone, S. M. Goldup, N. Lebrasseur, and D. A. Leigh. *Science*, 534:235–240, 2016.

[26] V. Balzani, M. Clemente-León, A. Credi, B. Ferrer, M. Venturi, A. H. Flood, , and J. F. Stoddart. *Proc. Nat. Acad. Sci. USA*, 103:1178–1183, 2006. 16, 17

[27] J.-M. Lehn. Toward complex matter: supramolecular chemistry and self-organization. *Proc. Nat. Acad. Sci. U. S. A.*, 99(8):4763–4768, 2002. 17

[28] E. Mattia and S. Otto. *Nat. Nanotechnol.*, 10:111–119, 2015. 17

2

Experimental part

2.0.1 General methods

Commercial compounds were used as received. Non-commercial compounds were synthesized by other group members or external collaborators. Dry solvents were bought dry and used directly.

2.0.2 UV-Visible Spectroscopy and Photochemistry

Absorption spectra were recorded with a Varian Cary 50Bio, Agilent Technologies Cary 300, Perkin Elmer Lambda 45 and Perkin Elmer Lambda 650 spectrophotometers, on air equilibrated solutions, if not otherwise stated at room temperature (ca. 20 °C), with concentrations ranging typically from 1×10^{-6} to 1×10^{-3} M. Circular dichroism spectra were recorded on a JASCO Type J-820 spectropolarimeter. Solutions were examined in 1 cm or 1 mm optical pathlength quartz cells. For the determination of absorption changes upon complex formation, dedicated spectrophotometric cells endowed with two compartments separated by a quartz wall were employed for a careful determination of the sum of the absorption spectra of the separated components (unmixed solutions) and the absorption spectrum of their complex (mixed solutions). The experimental error on the wavelength values was estimated to be ±1 nm. Emission spectra were recorded using Perkin-Elmer LS 50 and LS 55, Jobin Ivon FluoroMax-4 and Varian Cary Eclipse fluorometers. Luminescence lifetimes were measured with an Edinburgh Instruments FLS920 time-correlated single-photon counting spectrofluorimeter, exciting the sample with a pulsed diode laser. Emission spectra at 77 K were obtained from a frozen solution contained in a quartz tube immersed in a quartz Dewar filled with liquid nitrogen.

Photochemical reactions were performed at room temperature (ca. 20 °C), thoroughly stirred and eventually argon-purged (in particular when irradiate for long times, e.g. for more than typically 1

h), by using a Hanau Q400 or Helios Italquartz Polymer 125 medium pressure Hg lamp (respectively 150 and 125 W), or a 150 W tungsten halogen lamp equipped with a cutoff filter. Samples were irradiated either directly in a sealed cuvette or directly in the electrochemical cell.

The number of incident photons, determined by ferrioxalate actinometry in its micro version,[1] was typically 2.4×10^{-8} Einstein min^{-1} at 287 nm, 1.0×10^{-7} Einstein min^{-1} at 365 nm, and 2.4×10^{-7} Einstein min^{-1} at 436 nm. The $E\rightarrow Z$ photoisomerization quantum yield (λ_{irr}= 365 nm) was determined from the disappearance of the π-π^* absorption band of the azobenzene unit of the reactant at low conversion percentages (<10%; extrapolation to t = 0 was made). The fraction of light transmitted at the irradiation wavelength was taken into account in the calculation of the yields. The experimental error on the quantum yield values was estimated to be ±10%.

Reaction kinetic profiles were investigated by monitoring the time-dependent spectroscopic changes observed after addition of a concentrated (typically mM) solution of one component to a more diluted solution of the other component. Dethreading reactions were triggered by dilution and were studied by monitoring the time-dependent spectroscopic changes observed after rapid mixing of the investigated complex with the solvent. Thermal Z→E isomerization reactions were performed at room temperature (ca. 20 °C) in the dark, monitoring the time-dependent absorption changes. In all cases the data were elaborated by means of the SPECFIT fitting program.[2] Treading processes were modeled according to a mixed-order scheme, that is, second order (threading) and first order (dethreading) opposing reactions (equation 2.1)

$$Host + Guest \leftrightarrows [Host \supset Guest] \tag{2.1}$$

Dethreading processes and thermal $Z\rightarrow E$ isomerization reactions were modelled according to first-order kinetics. The values reported are typically an average of at least 2 independent experiments. The estimated experimental error is ±20%. Stability constants were determined from titration curves obtained by measuring the absorption or luminescence changes upon addition of small aliquots of a concentrated solution of the considered host/guest to a dilute solution of the respective guest/host. When monitoring luminescence, to minimize inner filter effects the emission detection was performed on an isosbestic point. The constants were calculated by means of the SPECFIT fitting program according to a 1:1 binding model (see eq. 2.1). The estimated experimental error is ±20%. Kinetic simulations were performed with SPECFIT software too.

2.0.3 Electrochemical measurements.

Cyclic voltammetry (CV) experiments were carried out at room temperature in argon-purged solutions with an Autolab 30 multipurpose instrument interfaced to a PC. The working electrode was a glassy carbon electrode (Amel; 0.07 cm^2); its surface was routinely polished with a 0.3 μm alumina-water slurry on a felt surface. The counter electrode was a Pt wire, separated from the solution by a frit; an Ag wire was employed as a quasi-reference electrode, and ferrocene was present as an internal standard. Ferrocene was added from a concentrated solution (typically 0.1 M). The concentration of the compounds examined was typically 2×10^{-4} M to 4×10^{-4} M; 0.04 M tetrabutylammonium hexafluorophosphate (for dichloromethane (DCM) or acetone solutions) or tetraethylammonum hexafluorophosphate (for acetonitrile (ACN) solutions) was added as supporting electrolyte. Cyclic voltammograms were obtained at sweep rates varying typically from 0.02 to 1 V s^{-1}. The IR compensation implemented within the Autolab 30 was used, and every effort was made throughout the experiments to minimize the resistance of the solution. In any instance, the full electrochemical reversibility of the voltammetric wave of ferrocene was taken as an indicator of the absence of uncompensated resistance effects. Differential pulse voltammograms (DPV) were performed with a scan rate of 20 mV s^{-1}, a pulse height of 75 mV, and a duration of 40 ms. For reversible processes the same halfwave potential values were obtained from the DPV peaks and from an average of the cathodic and anodic cyclic voltammetric peaks. The potential values for not fully reversible processes were estimated from the DPV peaks. The experimental error on the potential values for reversible and not fully reversible processes was estimated to be ±5 and ±10 mV, respectively. Spectroelectrochemical experiments were performed using the same experimental conditions (solvent, sample concentration, supporting electrolyte and reference) as for cyclic and pulsed voltammetry experiments. Prolonged and vigorous argon purging of the solution was performed to minimize the oxygen content in the investigated solution. Experiments were performed in a custom built optically transparent thin layer electrochemical cell, having Pt minigrids (ca. 0.3 cm^2) as the working and counter electrodes, and an Ag wire as a pseudo-reference electrode, all melt-sealed into a polyethylene spacer. The thickness of the layer, determined by spectrophotometry, was ca. 180 μm. The electrolysis was controlled by means of the above described Autolab 30 instrument, and the absorption spectra were recorded on an Agilent Technologies 8543 diode array spectrophotometer. The electrolysis times were determined on the basis of the spectral changes observed, i.e., the electrolysis was stopped when no further spectral variations occurred.

2.0.4 Other techniques

^{1}H-NMR spectra were recorded on a 400 MHz Varian spectrometer in deuterated acetone (unless otherwise noted).

Tapping-mode atomic force microscopy (AFM) images were recorded by an Asylum Research type CypherS AFM microscope, where all samples were prepared by dip-coating (dipping time ca. 1 s) on silicon wafer after 10-fold dilution (40 to 4 μM) and air-drying of the mother solution. The silicon wafer was pre-treated as follows: 5 minutes of sonication in acetone followed by 5 minutes of sonication in isopropanol, then the solvent was renewed and the solution was heated to reflux, finally, the wafer was ozone-treated for 5 minutes.

EPR spectra were recorded on Jeol X-320 spectrometer by using the following instrument settings: microwave power 32 mW, modulation width 0.2 mT, amplitude 30 and modulation frequency 100 kHz, scan time 30 s. Sample concentration was about 40 μM.

2.1 References

[1] M. Montalti, A. Credi, L. Prodi, and M. T. Gandolfi. *Handbook of photochemistry - Third Edition*. CRC Press, Boca Raton, USA, 2006. 22

[2] R. A. Binstead. *SPECFIT*. Spectrum Software Associates, Chapel Hill, USA, 1996. 22

Part II

Viologen-calix[6]arene based devices

3

Introduction

3.1 Calix[6]arene as nonsymmetric molecular wheels

A suitable selection and design of the molecular components are of paramount importance in determining the properties of molecular devices and allow a rational implementation of the mechanisms that govern their functions.[1–6] This is particularly true when these systems are supposed to perform a programmed task, such as, for example, sensing,[7, 8] switching[9–12] or nanoscale movements as in molecular machines.[13–15] When considering molecular machines based on interlocked structures, the number of available macrocycles is rather limited. In particular, the majority of macrocycles can be considered as symmetric with respect to the plane of the ring. The number of macrocycles with two chemically different rims is very limited. Cyclodestrins and calixarene are part of this very limited class of molecules.

In this context, in our lab it was demonstrated that calix[6]arene like those reported in figure 3.1 act as three-dimensional and heteroditopic wheels that, in apolar media, form oriented pseudorotaxanes and rotaxanes with dialkylviologen salts as axles.[16–18] Owing to the possibility of functionalizing the two chemically different rims, calix[6]arene wheels are also attractive as scaffold for the construction of multicomponent species bearing covalently linked molecular subunits. A study aimed at introducing molecular subunits at the upper or lower rim is the subject of chapter 4.

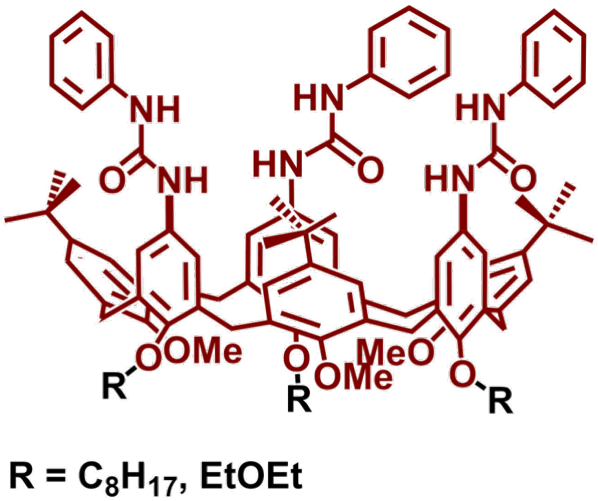

Figure 3.1: *Molecular structure of the calix[6]arene at study in our group.*

A peculiar property of such calix[6]arene macrocycles is that suitable bipyridinium axles can directionally pierce and transit through the calixarene annulus under the action of external stimulation.[19–22]. To date this remains — to the best of my knowledge — the sole example of unidirectional transit of a molecular axle through a nonsymmetric macrocycle. This is of particular interest because in order to exploit molecular-level movements to carry out some kind of task the first requisite that needs to be fulfilled is the directionality of motion,[3] that is, the components of the machine must move in a defined direction with respect to one another.[23, 24]. To achieve this goal an asymmetry needs to be introduced in the system, and this can be done by desymmetrizing the axle or the wheel. The latter strategy has never been exploited. Investigations devoted to this goal are the subject of chapters 5 and 6.

3.2 References

[1] T. Nakamura, T. Matsumoto, H. Tada, and K. Sugiura. *Chemistry of Nanomolecular Systems: Towards the Realization of Molecular Devices.* Springer-Verlag, Berlin, 2003. 27

[2] S. Saha and J. F. Stoddart. *Chem. Soc. Rev.*, 36:77–92, 2007.

[3] V. Balzani, A. Credi, and M. Venturi. *Molecular Devices and Machines, 2nd Ed.* Wiley-VCH, Weinheim, 2008. 28

[4] P. A. (Eds.) Steed, J.W. Gale. *Supramolecular Chemistry: From Molecules to Nanomaterials*. Wiley-VCH, Weinheim, 2012.

[5] S. F. M. van Dongen, S. Cantekin, J. A. A. W. Elemans, A. E. Rowan, and R. J. M. Nolte. *Chem. Soc. Rev.*, 43:99–122, 2014.

[6] P. Ceroni, A. Credi, and M. Venturi. *Chem. Soc. Rev.*, 43:4068–4083, 2014. 27

[7] L. Prodi. *New J. Chem.*, 29:20–31, 2005. 27

[8] B. Daly, J. Ling, and A. P. de Silva. *Chem. Soc. Rev.*, 44:4203–4211, 2015. 27

[9] B. L. Molecules 2001 6 1017-1018 Feringa. 27

[10] A. C. Benniston. *Chem. Soc. Rev.*, 33:573–578, 2004.

[11] H. Tian and Q. Wang. *Chem. Soc. Rev.*, 35:361–374, 2006.

[12] W. Yang, Y. Li, H. Liu, L. Chi, and Y. Li. *Small*, 8:504–516, 2012. 27

[13] V. Balzani, M. Gómez-López, and J. F. Stoddart. *Acc. Chem. Res.*, 31:405–414, 1998. 27

[14] V. Balzani, A. Credi, and M. Venturi. *Chem. Soc. Rev.*, 38:1542–1550, 2009.

[15] A. K. Mandal, M. Gangopadhyay, and A. Das. *Chem. Soc. Rev.*, 44:663–676, 2015. 27

[16] A. Arduini, R. Ferdani, A. Pochini, A. Secchi, and F. Ugozzoli. *Angew. Chem. Int. Ed.*, 39:3453–3456, 2000. 27

[17] F. Ugozzoli, C. Massera, A. Arduini, A. Pochini, and A. Secchi. *CrystEngComm*, 6:227–232, 2004.

[18] A. Credi, S. Dumas, S. Silvi, M. Venturi, A. Arduini, A. Pochini, and A. Secchi. *J. Org. Chem.*, 69:5881–5887, 2004. 27

[19] A. Arduini, R. Bussolati, A. Credi, G. Faimani, S. Garaudee, A. Pochini, A. Secchi, M. Semeraro, S. Silvi, and M. Venturi. *Chem. Eur. J.*, 15:3230–3242, 2009. 28

[20] A. Arduini, R. Bussolati, A. Credi, S. Monaco, A. Secchi, S. Silvi, and M. Venturi. *Chem. Eur. J.*, 18:16203–16213, 2012.

[21] A. Arduini, R. Bussolati, D. Masseroni, G. Royal, and A. Secchi. *Eur. J. Org. Chem.*, pages 1033–1038, 2012.

[22] A. Arduini, R. Bussolati, A. Credi, A. Secchi, S. Silvi, M. Semeraro, and M. Venturi. *J. Am. Chem. Soc.*, 135:9924–9930, 2013. 28

[23] D. A. Leigh, J. K. Y. Wong, F. Dehez, and F. Zerbetto. *Nature*, 424:174–179, 2003. 28

[24] G. Ragazzon, M. Baroncini, S. Silvi, M. Venturi, and A. Credi. *Nat. Nanotechnol.*, 10:70–75, 2015. 28

4

Calix[6]arene functionalized with naphthyl units

4.1 Introduction

In view of the current interest in the design and synthesis of calix[6]arene prototypes of molecular machines, it was envisaged that the incorporation of photoactive units in the calixarene skeleton could lead to the development of new systems whose working modes can be governed and monitored through a wider set of control tools. The naphthyl moiety, which is extensively employed in supramolecular chemistry because of its rich and well known photophysical behavior and its molecular recognition properties, [1–5], appears to be an ideal choice. This chapter describes the spectroscopic, photophysical and electrochemical behavior of two new calix[6]arene wheels decorated with three naphthyl groups anchored either to the upper or lower rim of the phenylureido calix[6]arene platform. Their ability to form pseudorotaxane complexes with a 1,1'-dioctyl-4,4'-bipyridinium ($\mathbf{DOV}^{2+}$) guest and the consequences of the complexation on their peculiar physico-chemical properties are also described. The studied compounds, including model compounds and $\mathbf{DOV}^{2+}$ guest are reported in figure 4.1.

This chapter is partially derived – with permission – from G. Orlandini, G. Ragazzon, V. Zanichelli, L. Degli Esposti, M. Baroncini, S.Silvi, M. Venturi, A. Credi, A. Secchi, A. Arduini, "Plugging a bipyridinium axle into multichromophoric calix[6]arene wheels bearing naphthyl units at different rims" *ChemistryOpen*, **2017**, 6, 64 - 72. I am particularly grateful to Lorenzo Degli Esposti, who collected part of the experimental data presented in this chapter.

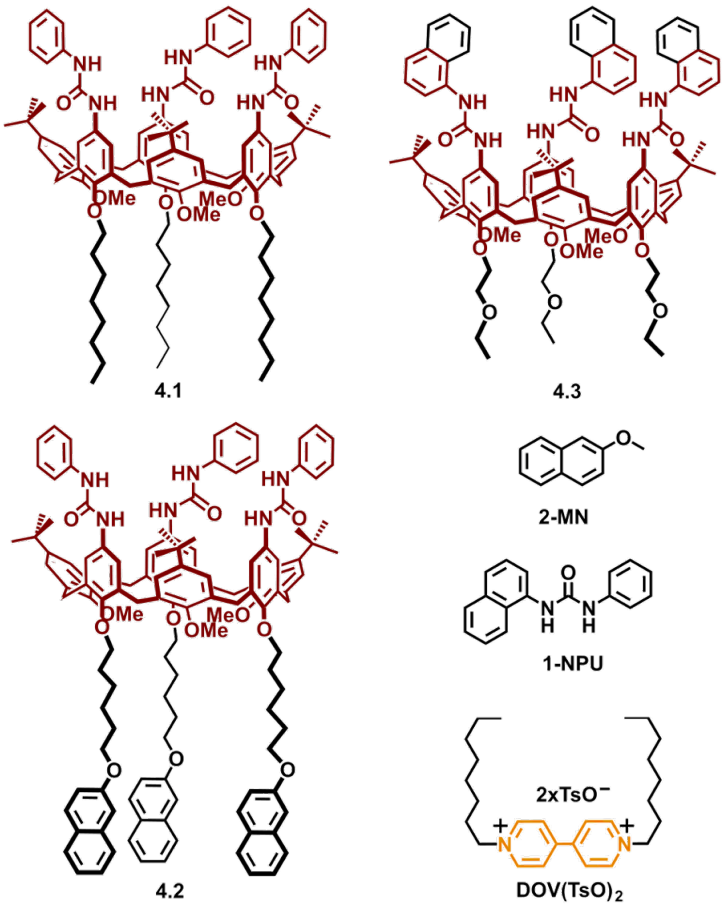

Figure 4.1: *Calix[6]arenes-based wheels* **4.1**, **4.2** *and* **4.3**, *model compounds* **2-MN** *and* **1-NPU** *and the viologen-based "axle"* $\mathbf{DOV}^{2+}$ *used in this study.*

The synthesis of the novel calix[6]arene hosts has been performed in the group of Prof. Arduini and Prof. Secchi, at the University of Parma. For the synthetic details and the structural characterization the interested reader can refer to [6].

4.2 Calix[6]arene bearing naphthalene units at its lower rim

The absorption and luminescence data for the calixarene host **4.2**, the guest $\mathbf{DOV}^{2+}$, their pseudorotaxane complex $\mathbf{4.2}\subset\mathbf{DOV}^{2+}$, and the model compounds for the calixarene scaffold (**4.1**) and for the naphthalene chromophore (2-methoxynaphthalene, **2-MN**) are reported in table 4.1.

Table 4.1: *Absorption and luminescence data for the calixarene host* **4.2**, *the guest* $\mathbf{DOV}^{2+}$, *their pseudorotaxane* $\mathbf{4.2}\subset\mathbf{DOV}^{2+}$, *and the model compounds for the chromophoric units (air equilibrated* CH_2Cl_2, *room temperature).*

	Absorption		Luminescence		
Compound	λ_{max} (nm)	ϵ (M^{-1} cm^{-1})	λ_{max} (nm)	Φ	τ (ns)
4.1[a]	250[b]	60000[b]	340	0.0025	<1[c]
2-MN	327	1900	348	0.12	4.8
4.2	327	5200	350	0.12	5.0
	250[b]	63000[b]			
$\mathbf{DOV}^{2+}$	270	24000	—	—	—
$\mathbf{4.2}\subset\mathbf{DOV}^{2+}$	460	600	350	0.006	<1[c]

[a] Data from ref. [7]. [b] Shoulder on the lower energy side of an intense band. [c] The lifetime value is shorter than the time resolution of the equipment

The UV-visible absorption spectrum of **4.2** in CH_2Cl_2 (figure 4.2) shows the typical bands of the aromatic system of the calixarene skeleton in the 240-300 nm region, while the features occurring between 280 and 340 nm are assigned to π-π^* transitions of the 2-alkoxynaphthalene units at the macrocycle lower rim. The absorption spectrum of **4.2** matches well with the sum of the absorption spectra of its chromophoric components (**4.1** plus 3×**2-MN**) in the 280-340 nm region, indicating the absence of interactions between the pendant naphthalene units in the ground state. On the other hand, the absorption of **4.2** is substantially more intense than the sum of its chromophoric components in the 240-280 nm region. As the naphthalene units and the wheel skeleton are electronically insulated by the long alkyl chains, we hypothesize that the change in the calixarene absorption bands arises from conformational effects exerted on the diphenylureido units of the wheel by the bulky substituents at the lower rim. In CH_2Cl_2 at room temperature, compound **4.2** shows a luminescence band (λ_{max} = 350 nm) that is safely assigned to the fluorescence of the alkoxynaphthalene units (table 4.1 and figure 4.2, inset). The emission quantum yield (Φ = 0.12) and lifetime (τ = 5.0 ns) values are identical within errors to those of the **2-MN** model. In rigid matrix at 77 K, **4.2** shows both the structured fluorescence (λ_{max} = 350 nm) and phosphorescence (λ_{max} = 465 nm) bands of the alkoxynaphthalene units.

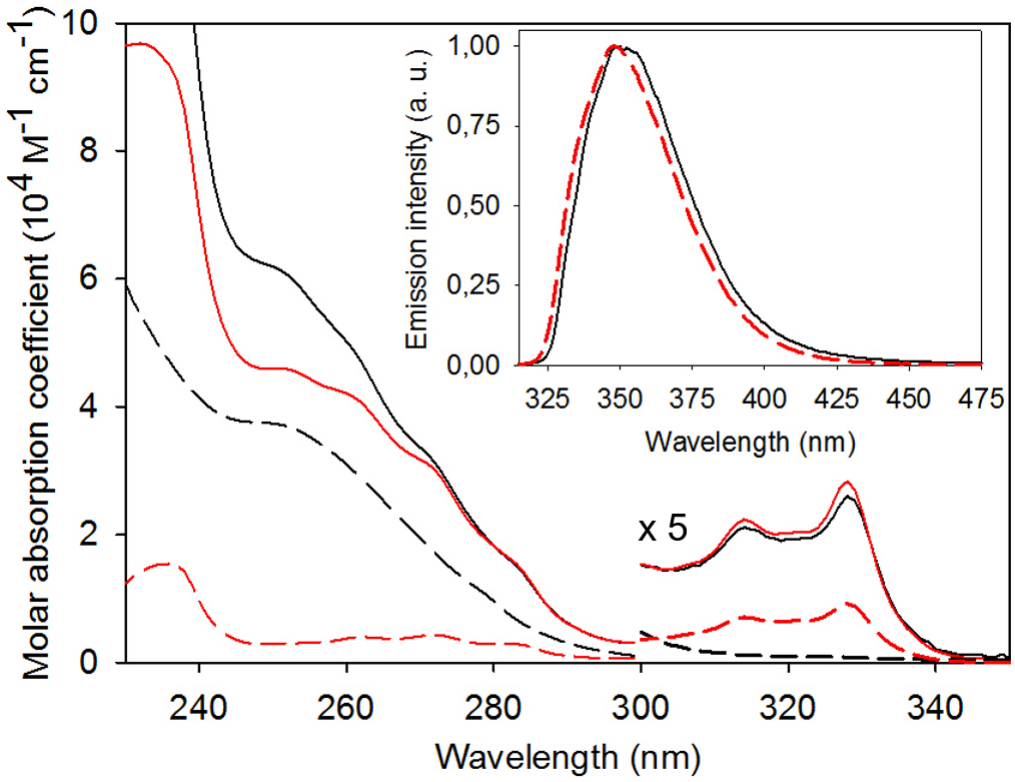

Figure 4.2: *Absorption spectra of multichromophoric calixarene* **4.2** *(black, full line), calix[6]arene* **4.1** *(black, dashed line), and* **2-MN** *(red, dashed line). The sum of the absorption spectra of the chromophoric components of* **4.2** *(red, full line) is also shown for comparison. Inset: normalized emission spectra (λ_{exc} = 315 nm) of* **4.2** *(black, full line) and* **2-MN** *(red, dashed line). Conditions: air equilibrated CH_2Cl_2, room temperature.*

The corrected excitation spectrum [8] of **4.2** (λ_{em} = 350 nm) at room temperature matches with the absorption spectrum of the same compound only between 310 and 340 nm, while it is significantly weaker in the 230-310 nm region. Conversely, the excitation spectrum of **4.2** exhibits a good overlap with the absorption spectrum of **2-MN** in the whole spectral region monitored. This observation indicates that the energy transfer from the excited states located on the calixarene skeleton to the excited singlet level of the pendant naphthalene units is inefficient. Unfortunately, an estimation of the residual fluorescence intensity arising from the calixarene annulus (λ_{max} = 340 nm, Table 4.1) is prevented because such an emission band is covered by the much more intense naphthalene-type fluorescence (λ_{max} = 350 nm). The application of the Förster model[9, 10] suggests that the

low energy-transfer efficiency is determined by the very poor overlap between the calixarene-type (donor) emission and the naphthalene-type (acceptor) absorption, together with the small quantum yield of the calixarene-type emission. In summary, the naphthalene units appended at the lower rim of the wheel as in **4.2** are photophysically independent both of one another and of the calixarene chromophore. The addition of $\mathbf{DOV}^{2+}$ to a solution of **4.2** causes changes in the UV absorption bands of the molecular components and the appearance of broad absorption features in the 350-600 nm region (λ_{max} = 460 nm, table 4.1), arising from charge-transfer (CT) interactions between the π-electron rich aromatic units of the calixarene and the π-electron poor 4,4'-bipyridinium moiety of the guest.[7, 11, 12] In the same experiment the fluorescence band of **4.2** is quenched as a function of the amount of $\mathbf{DOV}^{2+}$ added (figure 4.3). The absorption and luminescence data collected in the titration experiments could be satisfactorily fitted with a 1:1 binding model, yielding a value of the association constant logK = (7.0±0.2). These results are consistent with the NMR data and with previous observations on related compounds,[7, 11, 12] and confirm the formation of a pseudorotaxane in which $\mathbf{DOV}^{2+}$ is threaded into the cavity of **4.2** with its bipyridinium unit located close to the aromatic units of the calixarene.

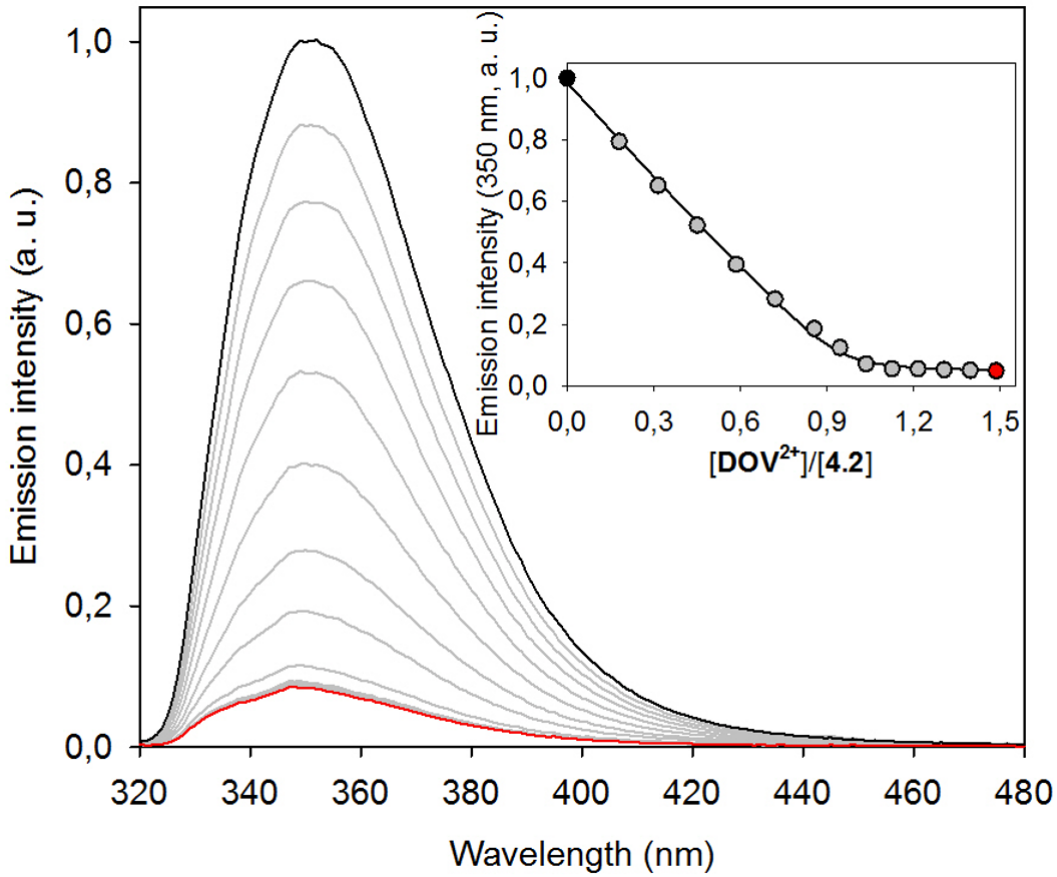

Figure 4.3: *Luminescence spectral changes (λ_{exc} = 315 nm) upon addition of increasing amounts of* $\mathbf{DOV}^{2+}$ *to a 3.0×10^{-5} M solution of* **4.2**. *The initial and final spectrum are shown in black and red, respectively. The inset shows the titration curve obtained by plotting the emission intensity at 350 nm as a function of the* $\mathbf{DOV}^{2+}$ *equivalents; the full line is the data fitting corresponding to a 1:1 binding model. Conditions: air equilibrated CH_2Cl_2, room temperature.*

In light of these observations, it is worth discussing the effect of the $\mathbf{DOV}^{2+}$ guest on the photophysics of the calixarene. From the residual emission intensity of **4.2** at the end of the titration one can calculate the quenching rate constant according to eq. 4.1:

$$k_q = \frac{1}{\tau_0}\left(\frac{\Phi_0}{\Phi - 1}\right) \tag{4.1}$$

where τ_0 and Φ_0 are the luminescence lifetime and quantum yields of **4.2** in the absence of $\mathbf{DOV}^{2+}$, and Φ is the luminescence quantum yield of the complex. According to the data listed in

table 4.1, $k_q = 3.8\times10^9$ s^{-1}. The quenching of the naphthalene-type emission of **4.2** by $\mathbf{DOV}^{2+}$ can involve two distinct mechanisms: (i) energy transfer from the singlet excited state localized on an alkoxynaphthalene unit to the lower lying charge-transfer levels due to the calixarene-bipyridinium interaction, and (ii) electron transfer from the alkoxynaphthalene singlet excited state to the encapsulated bipyridinium unit. Because of the good overlap between the naphthalene emission and the visibile charge-transfer absorption and the large luminescence quantum yield of the donor, the Förster radius (i.e. the donor-acceptor distance at which the energy-transfer efficiency is 50%) results to be as long as 5.4 nm. Considering that the maximum distance between the naphthalene substituents and the center of the calixarene cavity is 1.5 nm, the energy-transfer process (mechanism (i)) is expected to be very efficient. Moreover, from the available excited state energy and the potential values for oxidation of the donor and reduction of the acceptor (vide supra), one can estimate that the photoinduced electron transfer (mechanism (ii)) is highly exoergonic ($\Delta G^\circ < -1.8$ eV).[13] To gain more insight into the luminescence quenching mechanism we performed emission experiments in rigid matrix at 77 K. Under these conditions the solvent reorganization energy is small and highly exoergonic electron-transfer processes such as that mentioned above, that may fall into the Marcus inverted region, can become slow.[10, 14] Both the naphthalene-type fluorescence and phosphorescence bands observed for **4.2** in CH_2Cl_2:$CHCl_3$ 1:1 at 77 K are absent in the spectrum of the **4.2**⊂$\mathbf{DOV}^{2+}$ complex. The occurrence of such a strong quenching in a rigid medium at low temperature is consistent with an energy transfer from the naphthalene excited singlet to the CT levels. Laser flash photolysis experiments with ns excitation pulses, carried out in solution at room temperature, revealed no trace of the bipyridinium radical cation which would be a product of the electron-transfer reaction. It cannot be excluded, however, that a fast back-electron transfer process prevents the accumulation of the bipyridinium radical cation on the ns time scale.

4.3 Calix[6]arene bearing naphthalene units at its upper rim

The absorption and luminescence data for the calixarene host **4.3**, the guest $\mathbf{DOV}^{2+}$, their pseudorotaxane **4.3**⊂$\mathbf{DOV}^{2+}$, and the model chromophoric compound for the calixarene (N-1-naphthyl-N'-phenylurea, **1-NPU**) are reported in table 4.2. The absorption spectrum of **4.3** in CH_2Cl_2 (figure 4.4) shows the bands typical of the napthyl-phenylureido chromophore in the near UV region. The spectrum is very similar to the sum of the spectra of its chromophoric components (3×**1-NPU**), which suggests that the interactions between the pendant naphthalene units are negligible in the ground state.

Table 4.2: *Absorption and luminescence data for the calixarene host* **4.3**, *the guest* $\mathbf{DOV}^{2+}$, *their pseudorotaxane* $\mathbf{4.3}\subset\mathbf{DOV}^{2+}$, *and the model chromophoric compound* **1-NPU** *(air equilibrated* CH_2Cl_2, *r.t.).*

	Absorption		Luminescence		
Compound	λ_{max} (nm)	ϵ (M^{-1} cm^{-1})	λ_{max} (nm)	Φ	τ (ns)
1-NPU	290	6900	360	0.185	1.6
4.3	295	24000	410	0.11	2.8[a]
					18[a]
$\mathbf{DOV}^{2+}$	270	24000	—	—	—
$\mathbf{4.3}\subset\mathbf{DOV}^{2+}$	450[c]	200[c]	360	0.017	1.5[a]
					3.4[a]

[a] Biexponential decay. [b] Data from ref. [7]. [c] Shoulder on the lower energy side of an intense band.

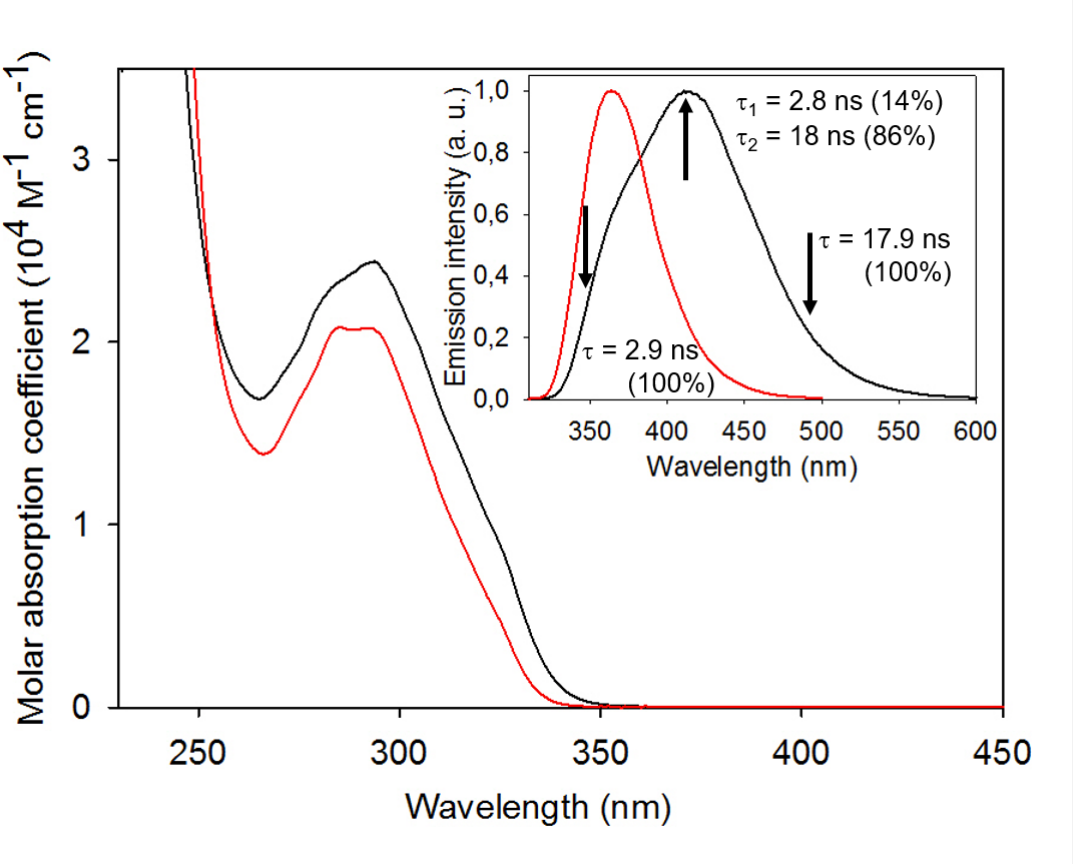

Figure 4.4: *Absorption spectrum of calixarene* **4.3** *(black) and sum of the absorption spectra of its chromophoric components (3×***1-NPU***, red). Inset: normalized emission spectra (λ_{exc} = 300 nm) of* **4.3** *(black) and* **1-NPU** *(red). Luminescence lifetime values measured at selected emission wavelengths, indicated by the arrows, are listed together with their respective contribution to the decay. Conditions: air equilibrated CH_2Cl_2, room temperature.*

The luminescence band of **4.3** in CH_2Cl_2 at room temperature is less intense, much broader and shifted to longer wavelengths in comparison with that of the **1-NPU** model (table 4.2 and figure 4.4, inset). The excitation spectrum of **4.3** (λ_{em} = 410 nm) is similar to its absorption spectrum. The emission band, however, shows a biexponential decay with τ_1 = 2.8 ns and τ_2 = 18 ns. The shorter lifetime is comparable with that of **1-NPU** (τ = 1.6 ns) and its contribution to the overall decay decreases as the monitored emission wavelength is moved towards the lower energy side (figure 4.4, inset). On the basis of these observations and in the light of the structure of **4.3**, it can be concluded that its emission has a dual nature: a higher energy and shorter lived component assigned to the individual naphthyl-phenylureido chromophores, and a lower energy and longer lived

component attributed to the formation of excimers between the pendant naphthalene moieties. This hypothesis is confirmed by the fact that in rigid matrix at 77 K, in which the formation of excimers is prevented, both the fluorescence (λ_{max} = 360 nm) and phosphorescence (λ_{max} = 540 nm) bands of **4.3** coincide with those of **1-NPU**.

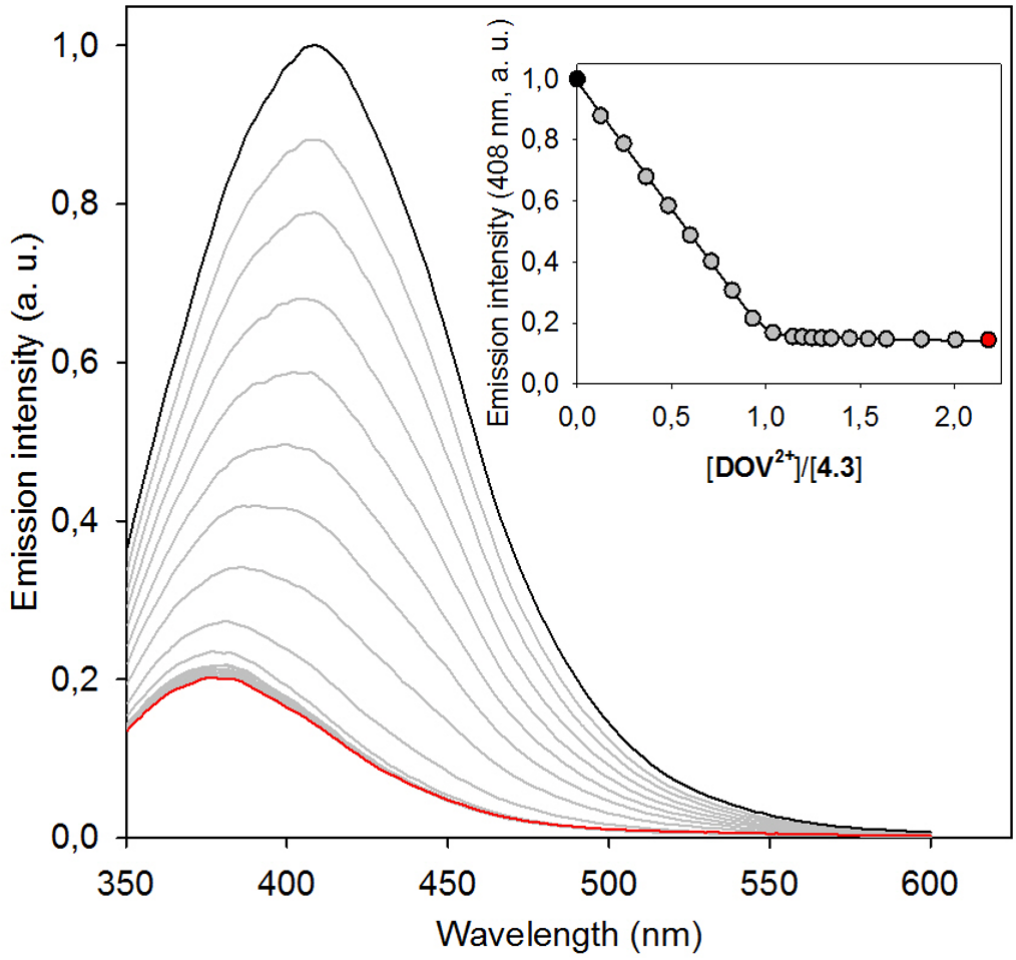

Figure 4.5: *Luminescence spectral changes (λ_{exc}= 330 nm) upon addition of increasing amounts of* $\mathbf{DOV}^{2+}$ *to a* 4.0×10^{-6} *M solution of* **4.3**. *The initial and final spectrum are shown in black and red, respectively. The inset shows the titration curve obtained by plotting the emission intensity at 408 nm as a function of the* $\mathbf{DOV}^{2+}$ *equivalents; the full line is the data fitting corresponding to a 1:1 binding model. Conditions: air equilibrated* CH_2Cl_2, *room temperature.*

The addition of $\mathbf{DOV}^{2+}$ to a solution of **4.3** causes absorption spectral changes consistent with the formation of a 1:1 complex, as discussed above for host **4.2**. In particular, a weak shoulder

on the lower energy side of the more intense UV bands, assigned to calixarene-bipyridinium CT interactions, is observed (Table 4.2). The emission changes of **4.3** upon titration with $\mathbf{DOV}^{2+}$ (figure 4.5) consist in a decrease of the band intensity accompanied by a change in shape; namely, the band becomes sharper and its maximum exhibits a blue shift. From the titration curves obtained from absorption and luminescence data and fitted with a 1:1 binding model, a lower limiting value of the association constant logK >7.5 was obtained. Once again, these findings are consistent with the NMR results and confirm that $\mathbf{DOV}^{2+}$ is threaded into wheel **4.3** in a pseudorotaxane fashion. Noteworthy, at the end of the titration the shape of the residual emission band of the calixarene is very similar to that of **1-NPU** but its decay is still described by a biexponential function (Table 4.2). As observed for the uncomplexed calixarene **4.3**, the contribution of the two lifetime components to the overall decay depends on the observation wavelength: the weight of the longer lifetime increases at longer wavelengths. On the basis of the discussion made for **4.3**, we assign τ_1 (1.5 ns) and τ_2 (3.4 ns) to emission from the naphthalene monomer and excimer species, respectively, in the complex. Both lifetimes are shorter than the corresponding values measured for **4.3** (table 4.2), indicating that both the excited monomer (singlet) and dimer (excimer) levels are quenched in the presence of $\mathbf{DOV}^{2+}$. The similarity of the luminescence band of the **4.3**⊂$\mathbf{DOV}^{2+}$ complex with that of the **1-NPU** model, which arises from a substantial disappearance of the contribution from the excimer emission, is consistent with the presence of a specific quenching pathway involving the excimers. It can also be hypothesized that the alkyl tail of the threaded $\mathbf{DOV}^{2+}$ guest can hinder the approach of two nearby naphthalene units by increasing the steric crowding at the upper rim of the calixarene, thus discouraging the formation of excimers. As previously discussed for **4.2**, the emission quenching mechanism of **4.3** upon complexation with $\mathbf{DOV}^{2+}$ can be an energy transfer from the excited naphthyl-type units (monomers or dimers) to lower lying charge-transfer states due to the calixarene-bipyridinium interaction, and/or an electron transfer from the excited naphthalenes to the bipyridinium guest, which is highly exoergonic also in the case of **4.3**. In contrast with the results obtained for host **4.2**, the emission spectra of the **4.3**⊂$\mathbf{DOV}^{2+}$ complex at 77 K exhibit the fluorescence and phosphorescence bands of **4.3**. Unfortunately, the luminescence intensities measured in the frozen solvent cannot be quantitatively compared and on the basis of our data we cannot extend the discussion any further.

4.4 Electrochemical pseudorotaxanes switching

The association of the calixarenes with $\mathbf{DOV}^{2+}$ can also be probed by electrochemical techniques. The voltammetric pattern of hosts **4.2** and **4.3** in CH_2Cl_2 exhibits no reduction processes and several chemically irreversible oxidation processes with onset at ca. +1.1 V, assigned to the oxidation of the naphthalene units and the alkoybenzene rings of the calixarene skeleton. Because of their irreversible nature, these processes will not be further discussed. $\mathbf{DOV}^{2+}$ shows the typical reversible monoelectronic reductions of the 4,4'-bipyridinium unit ($E_{1/2}$'= −0.27 V, $E_{1/2}$''= −0.81 V, see figure 4.6) and no oxidation.[15] The inclusion of $\mathbf{DOV}^{2+}$ into either **4.2** or **4.3** causes a large negative shift of the first reduction potential, while the second process occurs at the same potential as for the free guest (see figure 4.6). These results indicate that (i) the bipyridinium unit becomes more difficult to reduce because it is stabilized inside the calixarene wheel, and (ii) the one-electron reduction of $\mathbf{DOV}^{2+}$ promotes its dethreading from the host, in line with the behavior of several related bipyridinium-containing pseudorotaxanes.[7, 12, 16–18] The large peak-to-peak separation and the scan-rate dependence of the first reduction process of the **4.2**⊂$\mathbf{DOV}^{2+}$ and **4.3**⊂$\mathbf{DOV}^{2+}$ complexes indicate that the complexation/decomplexation reactions occur on the voltammetric time scale; these aspects have been discussed in detail elsewhere.[7]

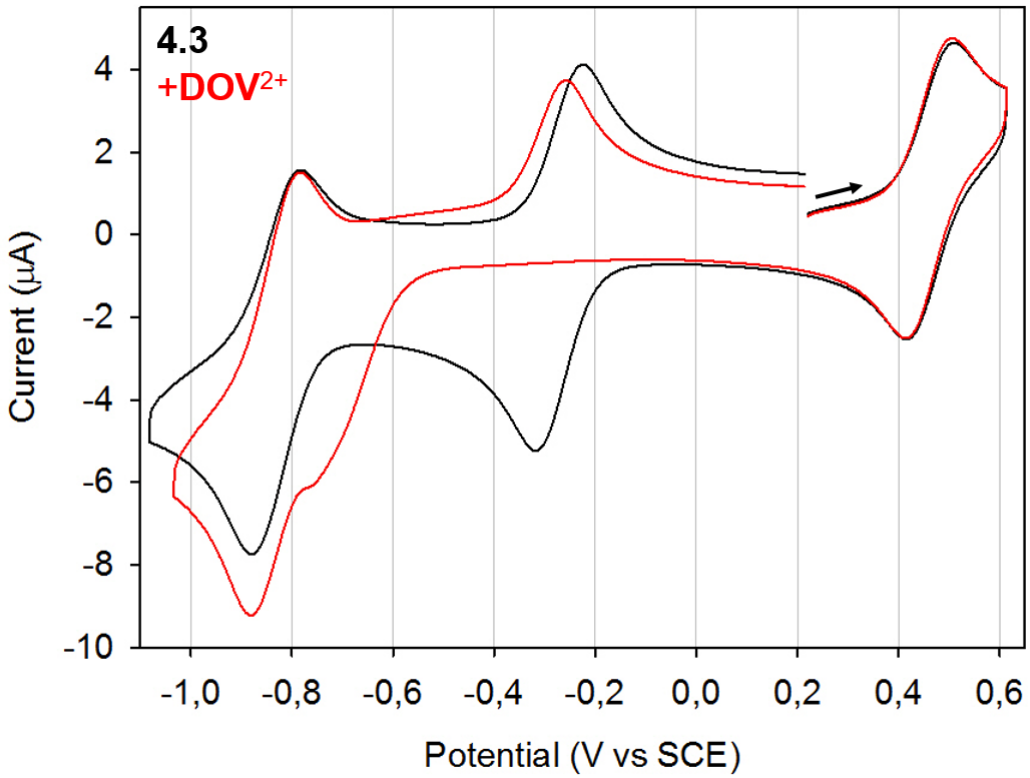

Figure 4.6: *Voltammetric pattern recorded upon reduction of* $\mathbf{DOV}^{2+}$ *(ca.* 4.0×10^{-4} *M) in the absence (black) and in the presence (red) of 1.5 equivalents of calixarene* **4.3** *to ensure full complexation of the electroactive guest. The wave at +0.460 V is due to ferrocene used as an internal standard. Conditions: argon-purged* CH_2Cl_2*, 0.04 M tetrabutylammonium hexafluorophosphate, scan rate 200 mV* s^{-1}*.*

4.5 Conclusions

In summary, in this chapter it has been reported the study of the spectroscopic, photophysical and electrochemical behavior of two new calix[6]arene wheels **4.2** and **4.3** decorated with three naphthyl groups anchored either to the upper or lower rim of the phenylureido calix[6]arene platform. Their ability to form pseudorotaxane complexes with a 4,4'-bipyridinium guest ($\mathbf{DOV}^{2+}$) and the consequences of the complexation on their peculiar physico-chemical properties were also reported. In particular, in the case of calixarene **4.2** the three naphthyl units connected to the lower rim do not interact with each other in the ground or excited states, and do not exchange electronic energy with the calixarene skeleton. The presence of a $\mathbf{DOV}^{2+}$ guest inside the wheel, however, enables

photoinduced energy and/or electron transfer processes from the peripheral chromophores to the cavity. The behavior of calixarene **4.3**, in which the three naphthalene moieties are linked to the ureidic moieties at the upper rim, is markedly different. The naphthyl units do not exhibit significant interactions in the ground state but they can form excimer species characterized by a red-shifted luminescence band and a longer lifetime. The threading of $\mathbf{DOV}^{2+}$ into the calixarene can activate energy- and/or electron-transfer pathways that cause the quenching of both the monomeric and, to a relatively higher extent, the excimeric naphthyl-type emission of **4.3**. For both calixarenes the bipyridinium guest can be reversibly dethreaded/rethreaded from the host by reduction/oxidation of $\mathbf{DOV}^{2+}$ in a potential region in which the host is not electroactive.

4.6 References

[1] P. Ceroni, A. Credi, and M. Venturi. *Chem. Soc. Rev.*, 43:4068–4083, 2014. 31

[2] A. K. Mandal, M. Gangopadhyay, and A. Das. *Chem. Soc. Rev.*, 44:663–676, 2015.

[3] J. S. Kim and D. T. Quang. *Chem. Rev.*, 107:3780–3799, 2007.

[4] M. Suresh, A. K. Mandal, M. K. Kesharwani, N. N. Adarsh, B. Ganguly, R. K. Kanaparthi, A. Samanta, and A. Das. *J. Org. Chem.*, 76:138–144, 2011.

[5] M. Suresh, A. K. Mandal, E. Suresh, and A. Das. *Chem. Sci.*, 4:2380–2386, 2013. 31

[6] G. Orlandini, G. Ragazzon, V. Zanichelli, L. Degli Esposti, M. Baroncini, S. Silvi, M. Venturi, A. Credi, A. Secchi, and A. Arduini. *ChemistryOpen*, 6:64–72, 2017. 32

[7] A. Credi, S. Dumas, S. Silvi, M. Venturi, A. Arduini, A. Pochini, and A. Secchi. *J. Org. Chem.*, 69:5881–5887, 2004. 33, 35, 38, 42

[8] A. Credi and L. Prodi. *J. Mol. Struct.*, 1077:30–39, 2014. 34

[9] J. R. Lakowicz. *Principles of Fluorescence Spectroscopy, 3rd Ed.* Springer, Berlin, 2006. 34

[10] V. Balzani, P. Ceroni, and Juris A. *Photochemistry and Photophysics: Concepts, Research Applications*. Wiley-VCH, Weinheim, 2014. 34, 37

[11] A. Arduini, R. Bussolati, A. Credi, G. Faimani, S. Garaudee, A. Pochini, A. Secchi, M. Semeraro, S. Silvi, and M. Venturi. *Chem. Eur. J.*, 15:3230–3242, 2009. 35

[12] A. Arduini, R. Bussolati, A. Credi, S. Monaco, A. Secchi, S. Silvi, and M. Venturi. *Chem. Eur. J.*, 18:16203–16213, 2012. 35, 42

[13] D. Rehm and A. Weller. *Isr. J. Chem.*, 8:259–263, 1970. 37

[14] V. Balzani (Ed.). *Electron transfer in Chemistry*. Wiley-VCH, Weinheim, 2008. 37

[15] A. Arduini, R. Bussolati, A. Credi, A. Pochini, A. Secchi, S. Silvi, and M. Venturi. *Tetrahedron*, 64:8279–8286, 2008. 42

[16] A. Arduini, A Credi, G Faimani, C Massera, A Pochini, A Secchi, M Semeraro, S Silvi, and F. Ugozzoli. *Chem. Eur. J.*, 14:98–106, 2008. 42

[17] V. Balzani, P. Ceroni, A. Credi, M. Gómez-López, C. Hamers, J. F. Stoddart, and R. Wolf. *New J. Chem.*, 25:25–31, 2001.

[18] H. Qian, D.-S. Guo, and Y. Liu. *Chem. Eur. J.*, 18:5087–5095, 2012. 42

5

Calix[6]arene based rotaxanes with one recognition site

5.1 Introduction and design

As anticipated in the first chapter of this part of the thesis, it was planned to investigate whether the asymmetry of the calix[6]arene wheel could induce a directional motion within a rotaxane architecture. To this aim the first requirement is to induce motion, in rotaxanes bearing a calix[6]arene wheel and a bipyridinium recognition site, therefore, it was planned to investigate a series of rotaxanes with the aim of understanding whether, on applying an appropriate stimulus, it is possible to induce a movement of the components and eventually to assess the direction of motion. A catenane with the same recognition motif was also investigated. The investigated rotaxanes and catenane are reported in figure 5.1. They are composed of a calix[6]arene wheel and a series of axles of different length comprising a bipyridinium core. The synthesis of the investigated compounds has been performed in the group of Prof. Arduini and Prof. Secchi at the University of Parma[1]. Moreover, since the monoreduced bipyridinium unit is an EPR-active species, the rotaxanes were also studied

This chapter is partially derived – with permission – from V. Zanichelli, G. Ragazzon, A. Arduini, A. Credi, P. Franchi, G. Orlandini, M. Venturi, M. Lucarini, A. Secchi, S. Silvi, "Synthesis and characterization of constitutionally isomeric oriented calix[6]arene-based rotaxanes" *Eur. J. Org. Chem.*, **2016**, 1033 - 1042 and G. Orlandini, V. Zanichelli, A. Secchi, A. Arduini, G. Ragazzon, A. Credi, M. Venturi, S. Silvi, "Synthesis by ring closing metathesis and properties of an electroactive calix[6]arene [2]catenane" *Supramol. Chem.*, **2016**, 28, 427 - 435.

[1]In this context the ability of this host to accelerate the alkylation of piridyl moieties to afford quaternary salts has also been proved.

with EPR in the group of Prof. Lucarini at the University of Bologna. The interested reader in the synthetic methods or the details of the EPR investigation can refer to [1].

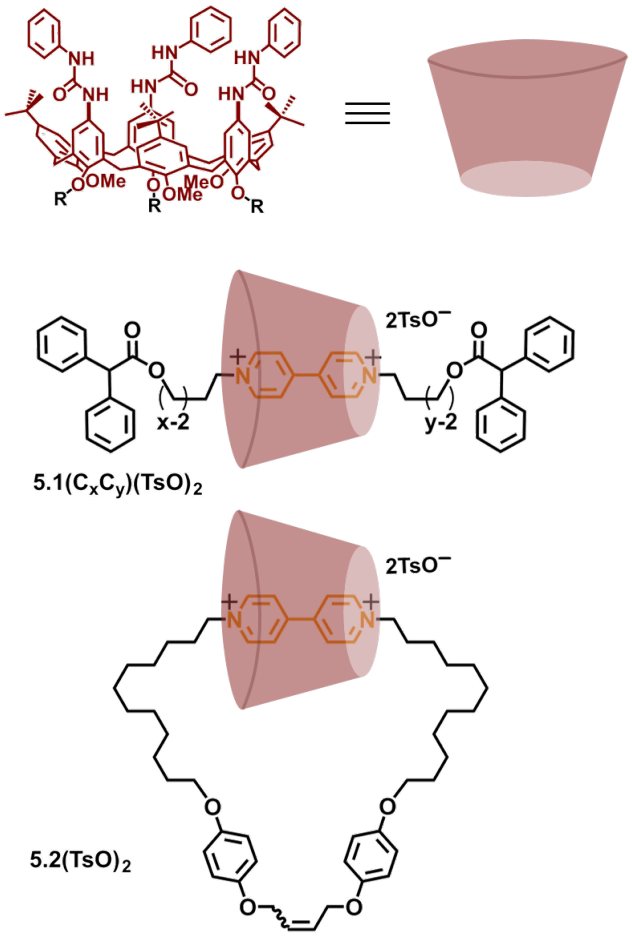

Figure 5.1: *Molecular structure of rotaxanes* $\mathbf{5.1}(C_xC_y)^{2+}$ *(*$R = C_8H_{17}$*) and catenane* $\mathbf{5.2}^{2+}$ *(*$R = EtOEt$*) used in this study. Subscripts x and y stand for the length of the alkyl chains bound to the bipyridinium core, with respect to the upper and lower rim of the wheel, respectively. Compounds of the* $\mathbf{5.1}^{2+}$ *class with the following descriptors have been studied:* (C_3C_3)*;* (C_6C_6)*;* $(C_{12}C_{12})$*;* $(C_{16}C_{16})$*;* (C_3C_{12})*;* (C_6C_{16})*;* $(C_{16}C_6)$*.*

It is known from previous studies[2] that the calix[6]arene and the bipyridinium axles strongly interact, mainly by virtue of charge transfer and solvophobic effects. The direction of the axle threading into the wheel in homologous pseudorotaxane systems can be controlled using appropriate substituents of the bipyridinum core in apolar solvents, thus allowing the preparation of orientational

isomers.[3] The interaction between the components is weakened upon reduction of the bipyridinium core, leading to the dethreading of the axle in parent pseudorotaxane systems.[2, 4] On combining spectroelectrochemical and EPR techniques we envisage to understand whether reduction of the bipyridinium core is a sufficient stimulus to cause the shuttling of the calixarene wheel away from the bipyridinium site even in the absence of an explicit secondary station. The investigations on the prepared rotaxanes should indeed reveal if the different length of the axles affects their stimuli-triggered rearrangement. Moreover the orientationally isomeric rotaxanes were designed to disclose a possible preference in the shuttling direction, dictated by the wheel orientation. To favour the establishment of a difference between different isomeric rotaxanes, it was necessary to build axles bearing two alkyl chains with an appropriate length difference. On this basis, isomers with one propyl and one dodecyl chain and with one hexyl and one hexadecyl chain were synthesized. In the following discussion rotaxanes will be named **5.1**$(C_xC_y)^{2+}$: subscripts x and y stand for the length of the alkyl chains at the upper and lower rim of the wheel, respectively. The studied catenane is named **5.2**$^{2+}$.

5.2 Spectroscopic and electrochemical investigation

In agreement with previous investigations,[5] all the rotaxanes exhibit two main absorption bands, regardless of the solvent (either dichloromethane or acetonitrile, figure 5.2). The intense band in the UV region, below 300 nm, is ascribed to the absorption of the phenylureido moieties and bipyridinium core, whereas the weaker absorption band in the visible region, around 460 nm, arises from a charge transfer interaction between the aromatic rings of the calixarene and the bipyridinium unit contained in the rotaxane axles. Both the energy and the absorption coefficient of this band are independent on the length of the alkyl chain, suggesting that the donor-acceptor electronic coupling is the same for all the rotaxanes. On the other hand the absorption coefficient of the band in the UV region depends on the length of the alkyl chain.

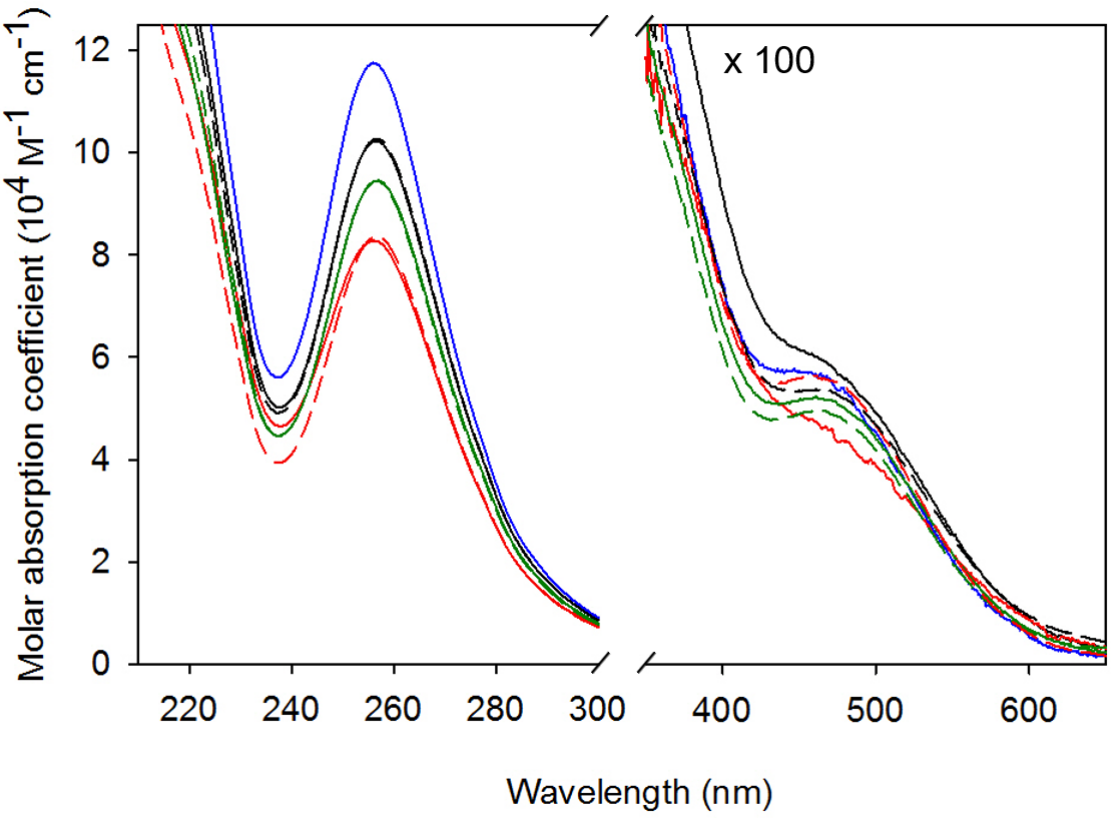

Figure 5.2: *Absorption spectra of the studied rotaxanes in ACN:* **5.1**$(C_3C_3)^{2+}$ *(black, full line);* **5.1**$(C_6C_6)^{2+}$ *(red, full line);* **5.1**$(C_{12}C_{12})^{2+}$ *(blue, full line);* **5.1**$(C_{16}C_{16})^{2+}$ *(green, full line);* **5.1**$(C_3C_{12})^{2+}$ *(black, dashed line);* **5.1**$(C_6C_{16})^{2+}$ *(red, dashed line);* **5.1**$(C_{16}C_6)^{2+}$ *(green, dashed line). Rotaxanes with the upper alkyl chain of the same length have the same color, rotaxanes bearing simmetric axles are plotted with a full line and rotaxanes bearing asimmetric axles are plotted with a dashed line (often overlapped with the corresponding full line spectrum).*

These results suggest that the extent of encapsulation of the bipyridinium core in the calixarene cavity is similar for all the rotaxanes (similar results were also obtained in the case of catenane **5.2**$^{2+}$), whereas the portion of alkyl chain that extrudes from the rims depends on the length of the chain. In particular, as the signal in the UV region is ascribed to the phenylureido moieties, it is expected that the chain at the upper rim of the calixarene cavity would affect their absorption. Apparently the absorption intensity is not directly related to the chain length; nevertheless it appears that rotaxanes with the same chain at the upper rim show comparable absorption (figure

5.2), thus supporting our hypothesis. In contrast with parent pseudorotaxane systems, in the studied rotaxanes the dethreading is prevented by the bulky stoppers and indeed previous investigations [5] on rotaxanes **5.1**$(C_3C_3)^{2+}$, **5.1**$(C_6C_6)^{2+}$ and **5.1**$(C_{12}C_{12})^{2+}$ suggest that the charge-transfer interaction is still present after monoreduction of the bipyridinium, regardless of the length of the alkyl chain and of the polarity of the solvent. After a preliminary screening in dichloromethane and acetonitrile, we restricted our investigation to the latter solvent, as electrochemical experiments in dichloromethane proved to be less reproducible. Moreover, beside the charge-transfer interaction, which appears to be unaffected by the solvent, other interactions contribute to the overall stability of the complex, like solvophobic effects and hydrogen bonds. These interactions are weaker in the more polar solvent, and we envisaged to exploit this difference to maximize the destabilization due to the electrochemical reduction, and cause some displacement of the components. The electrochemical investigation has been performed by CV and DPV on the rotaxanes and on DOV, used as the model compound for the bipyridinium unit of the axles. The model compound shows two reversible monoelectronic reduction processes at -0.42 V and -0.86 V. In presence of an equimolar amount of calix[6]arene a pseudorotaxane is formed with an association constant around 5×10^4 M^{-1} in CH_3CN. Therefore at the concentration of the electrochemical experiments about 25% of axles are not associated with the wheel. The first reduction process shows two cathodic peaks, related to the free and complexed axle, and one anodic peak, at the potential of the free axle. This behaviour suggests that the radical cation is not associated with the calix[6]arene. Indeed the second reduction process takes place at -0.86 V, confirming that the pseudorotaxane dissociates after the first reduction.

Table 5.1: *Halfwave potential values of the investigated compounds. Conditions: argon-purged ACN, 0.04 M tetraethylammonium hexafluorophospate, 300 μM analyte.*

	E_1 (V)	E_2 (V)
$\mathbf{DOV}^{2+}$	-0.42[a]	-0.86[a]
$\mathbf{5.1}(C_3C_3)^{2+}$	-0.64[b]	-1.15[b]
$\mathbf{5.1}(C_6C_6)^{2+}$	-0.62[a]	-1.14[a]
$\mathbf{5.1}(C_{12}C_{12})^{2+}$	-0.62[a]	-1.18[a]
$\mathbf{5.1}(C_{16}C_{16})^{2+}$	-0.62	-1.24[b]
$\mathbf{5.1}(C_3C_{12})^{2+}$	-0.60	-1.16
$\mathbf{5.1}(C_6C_{16})^{2+}$	-0.62	-1.22[b]
$\mathbf{5.1}(C_{16}C_6)^{2+}$	-0.61	-1.11
$\mathbf{5.2}^{2+}$	-0.60	-1.13

[a] From ref [5], [b] Poorly reversible process; value determined from DPV peak.

On the other hand, all the interlocked molecules show two reversible or quasi-reversible monoelectronic reduction processes at more negative potential values with respect to the free bipyridinium derivative (see table 5.1). The reversibility of the electrochemical waves suggests that either no conformational rearrangement takes place, or the rearrangement is fast on the timescale of the electrochemical experiment. The shift toward negative potential values of the second reduction potential shows that the reduced forms of the bipyridinium still interact with the calix[6]arene. It should be noted that the presence of a residual interaction does not exclude that minor rearrangements can occur. An inspection of the molecular models reveals that $\mathbf{5.1}(C_3C_3)^{2+}$, bearing two short alkyl side chains on the axle, is a rather constrained structure in which large scale relative movements of the wheel and axle are prevented. From a detailed investigation of the voltammogram, it can be noticed that the anodic to cathodic peak separation of the first reduction process in the CV of $\mathbf{5.1}(C_3C_3)^{2+}$ is larger with respect to the other rotaxanes for all the investigated scan rates. Such a quasi-reversible character suggests that the heterogeneous electron-transfer process is slowed down in $\mathbf{5.1}(C_3C_3)^{2+}$, possibly because of the constrained structure of this rotaxane and consequent effective encapsulation of the electroactive site.[6] In rotaxanes characterized by a larger distance between the bipyridinium unit and the stoppers, as well as in catenane $\mathbf{5.2}^{2+}$ a translation of the wheel along the axle could in principle take place, but the similarity of their voltammetric pattern with that of $\mathbf{5.1}(C_3C_3)^{2+}$ suggest that large conformational changes are not occurring upon

reduction.

In order to gain more information on the consequences of electrochemical reduction, we performed spectroelectrochemical experiments on the model compounds and on the rotaxanes. The discussion is restricted to the radical cation species, as the second reduction process is affected by reproducibility issues. The absorption spectra of $\mathbf{DOV}^{+\bullet}$, both in absence and in presence of calix[6]arene, match the typical absorption spectrum of the bipyridinium radical cation in acetonitrile (figure 5.3 red line).[7]

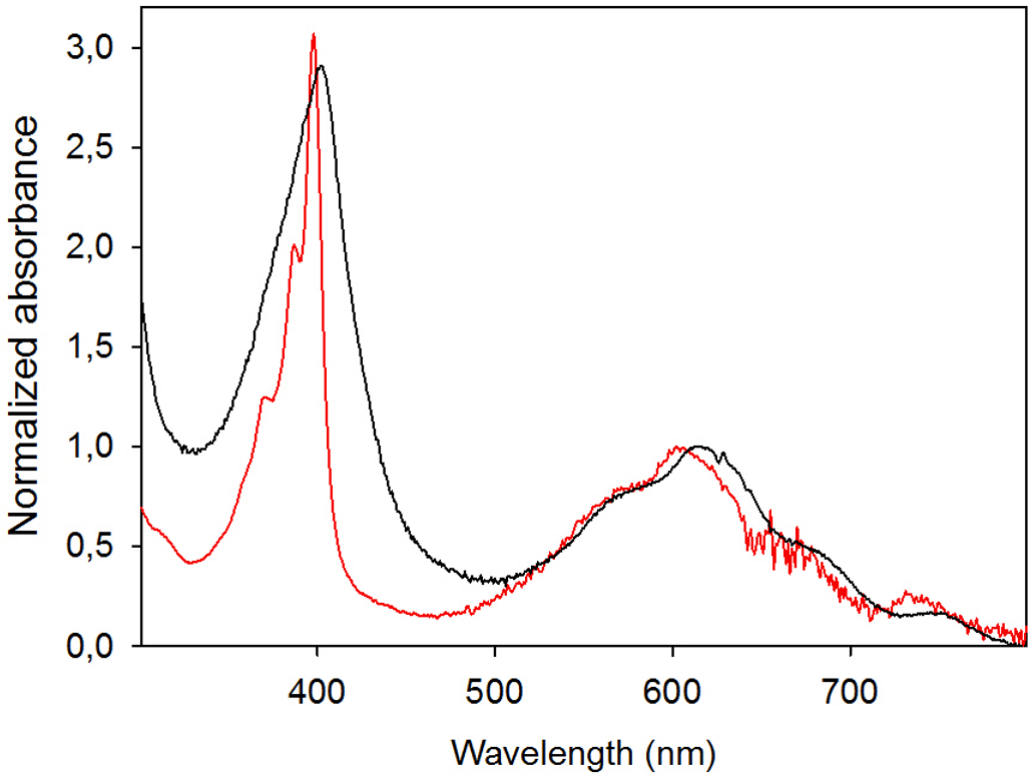

Figure 5.3: *Absorption spectra of* $\mathbf{5.1}(C_6C_6)^{+\bullet}$ *(black) and model compound* $\mathbf{DOV}^{+\bullet}$ *(red) obtained upon one-electron reduction of* $\mathbf{5.1}(C_6C_6)^{2+}$ *and* $\mathbf{DOV}^{2+}$*, respectively. Spectra are normalized at the maximum of the lower energy band.*

Two structured and intense absorption bands are present with λ_{max} = 398 and 602 nm. The energy, shape and intensity of the bands are not affected by the presence of the calixarene, thus confirming that the monoreduced bipyridinium axle dethreads from the wheel. Instead, in the case of $\mathbf{5.1}(C_xC_y)^{2+}$ compounds the spectra are characterized by the same absorption features, but with

some significant differences (figure 5.3 black line). The band at higher energy is less structured, whereas the band at lower energy is about 10 nm bathochromically shifted, with substantially no difference among the rotaxanes. These observations suggest that the bipyridinium radical cation in the rotaxanes experiences a different environment in comparison with the free axle, regardless of the length of the alkyl chains and their position with respect to the wheel. Analogous results were also obtained for catenane $\mathbf{5.2}^{2+}$ upon photoreduction in the presence of $Ru(bipy)_3{}^{2+}$ (bipy = 2,2'-bipyridine) as a photosensitizer and triethanolamine as a sacrificial reductant.[6] These observations suggest that, in such interlocked structures, after monoreduction of the bipyridinium unit the wheel is still located relatively close to it.

5.3 Conclusions

In summary we have designed and synthesized a series of rotaxanes containing bipyridinium-based axles and a calix[6]arene wheel. Our electrochemical investigation showed that, in sharp contrast with the behavior of the corresponding pseudorotaxane system, the monoelectronic reduction of the bipyridinium recognition site does not cause the shuttling of the wheel away from the bipyridinium unit. It seems indeed that, rather than residing on an alkyl chain, the calixarene prefers to remain on the bipyridinium radical cation. These conclusion are in agreement with the EPR data collected in the group of Prof. Lucarini.[for more details please refer to 1] Nevertheless, the combined use of EPR and spectroelectrochemistry enabled us to gain detailed information on the effect of the electrochemical stimulus, as both techniques can clearly distinguish between a free and a complexed bipyridinium radical. These results prompt us to improve the design of the rotaxanes, by inserting secondary recognition sites in the axle that can offer a stabilization to the wheel when the bipyridinium core has been reduced. This is the subject of the following chapter.

5.4 References

[1] V. Zanichelli, G. Ragazzon, A. Arduini, A. Credi, P. Franchi, G. Orlandini, M. Venturi, M. Lucarini, A. Secchi, and S. Silvi. *Eur. J. Org. Chem.*, pages 1033–1042, 2016. 48, 54

[2] A. Credi, S. Dumas, S. Silvi, M. Venturi, A. Arduini, A. Pochini, and A. Secchi. *J. Org. Chem.*, 69:5881–5887, 2004. 48, 49

[3] A. Arduini, R. Bussolati, A. Credi, A. Secchi, S. Silvi, M. Semeraro, and M. Venturi. *J. Am. Chem. Soc.*, 135:9924–9930, 2013. 49

[4] G. Orlandini, G. Ragazzon, V. Zanichelli, L. Degli Esposti, M. Baroncini, S. Silvi, M. Venturi, A. Credi, A. Secchi, and A. Arduini. *ChemistryOpen*, 6:64–72, 2017. 49

[5] A. Arduini, R. Bussolati, A. Credi, A. Pochini, A. Secchi, S. Silvi, and M. Venturi. *Tetrahedron*, 64:8279–8286, 2008. 49, 51, 52

[6] M. Semeraro, A. Secchi, S. Silvi, M. Venturi, A. Arduini, and A. Credi. *Inorg. Chim. Acta*, 417:258–262, 2014. 52, 54

[7] P. M. S. Monk. *The viologens —Physicochemical Properties, Synthesis and Applications of the Salt of 4,4'-Bipyridine*. John Wiley and Sons, Chichester, 1998. 53

6

Calix[6]arene based rotaxanes with two recognition sites

6.1 Introduction and design

In the previous chapter it was shown that in [2]rotaxanes bearing a bipyridinum (bpy) unit as the sole recognition site for calixarene wheels, upon reduction of the bpy unit the calixarene wheel does not move away from the $bpy^{+\bullet}$ station.[1] This phenomenon is observed most likely because locating the calix[6]arene ring along the alkyl chain is energetically demanding, in particular the results indicate that the monoreduced viologen is a better recognition site with respect to the alkyl chain. On the basis of these results novel rotaxanes bearing a dialkylamine station in addition to the bpy^{2+} one were synthesized in the lab of Prof. Arduini and Prof. Secchi at the University of Parma, and their electrochemical properties have been investigated. The amine should act as a secondary recognition site with much better affinity for the wheel with respect to the alkyl chain and hopefully also better than the reduced viologen unit. Moreover it is possible to protonate the amine to afford a possibly better recognition motif for the wheel. To widen the scope of the study it was decided to synthesize derivatives with different spacer length. The studied compounds are reported in figure 6.1. The two axles are named **6.1**$(Sh/Lo)^{2+}$ depending on the length of the alkyl spacers, meaning short (Sh) and long (Lo) respectively. Rotaxanes are named **6.2**$(Up/Do\text{-}Sh/Lo)^{2+}$ where Up and Do indicate whether the secondary station is located on the same side of the upper (Up) or lower (Down - Do) rim of the calix[6]arene.

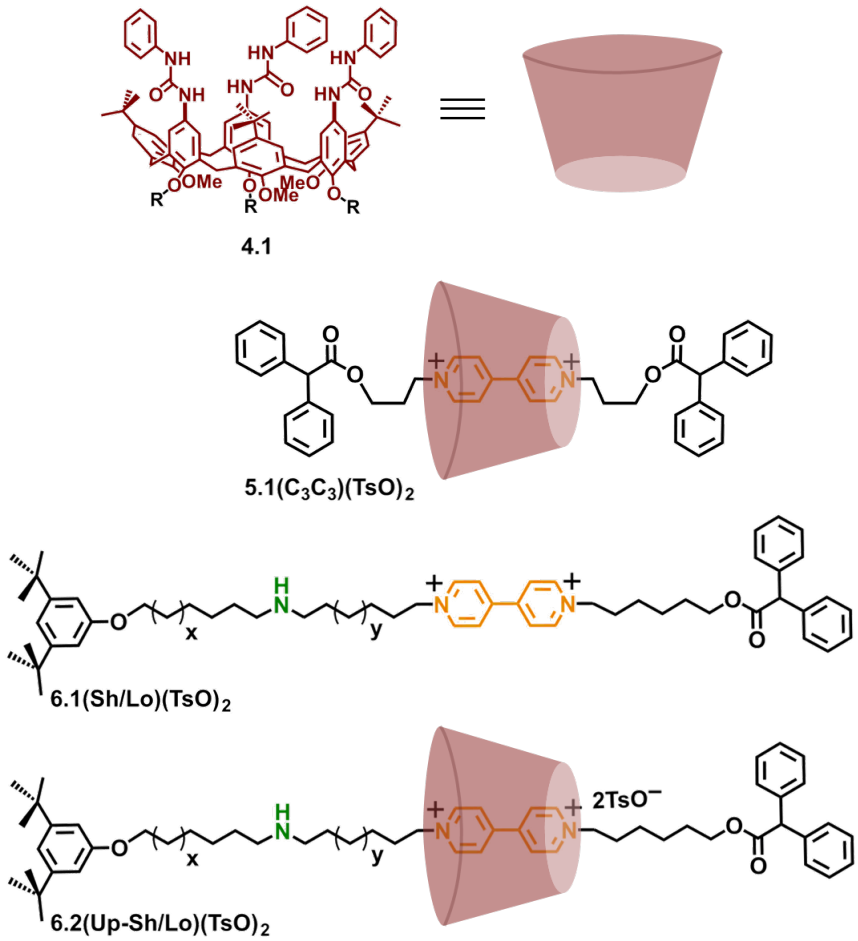

Figure 6.1: *Molecular structure of calixarene wheel* **4.1** *(R = C_8H_{17}), model compounds* **5.1**$(C_3C_3)^{2+}$ *and* **6.1**$^{2+}$ *and the two-station rotaxanes* **6.2**$^{2+}$. *Compounds* **6.1**$^{2+}$ *and* **6.2**$^{2+}$ *are labelled Sh-short for x = 1, y = 1 and Lo-long for x = 6, y = 7; in this figure the Up-isomer of compounds* **6.2**$^{2+}$ *is represented, in which the upper rim of the wheel is oriented toward the amine: the isomers in which the calixarene component has the opposite orientation are labelled Do-down in the text.*

6.2 Spectroscopic and electrochemical investigation

In agreement with previous investigations,[1, 2] all the rotaxanes exhibit two main absorption bands, regardless of the solvent (either dichloromethane or acetonitrile, figure 6.2). The intense band in the UV region, below 300 nm, is ascribed to the absorption of the phenylureido moieties and bipyridinium core, whereas the weaker absorption band in the visible region, around 460 nm, arises from a charge transfer interaction between the aromatic rings of the calixarene and the bipyridinium

unit contained in the axle. Both the energy and the absorption coefficient of this latter band are the same for the studied rotaxanes, suggesting that the donor-acceptor electronic coupling is the same for all the examined compounds. On the other hand the absorption coefficient of the band in the UV region shows a predominant dependance from the location of the secondary station with respect to the wheel, even if the difference is less pronounced with respect to what was observed for rotaxanes with one recognition site and different axle's length (see previous chapter).

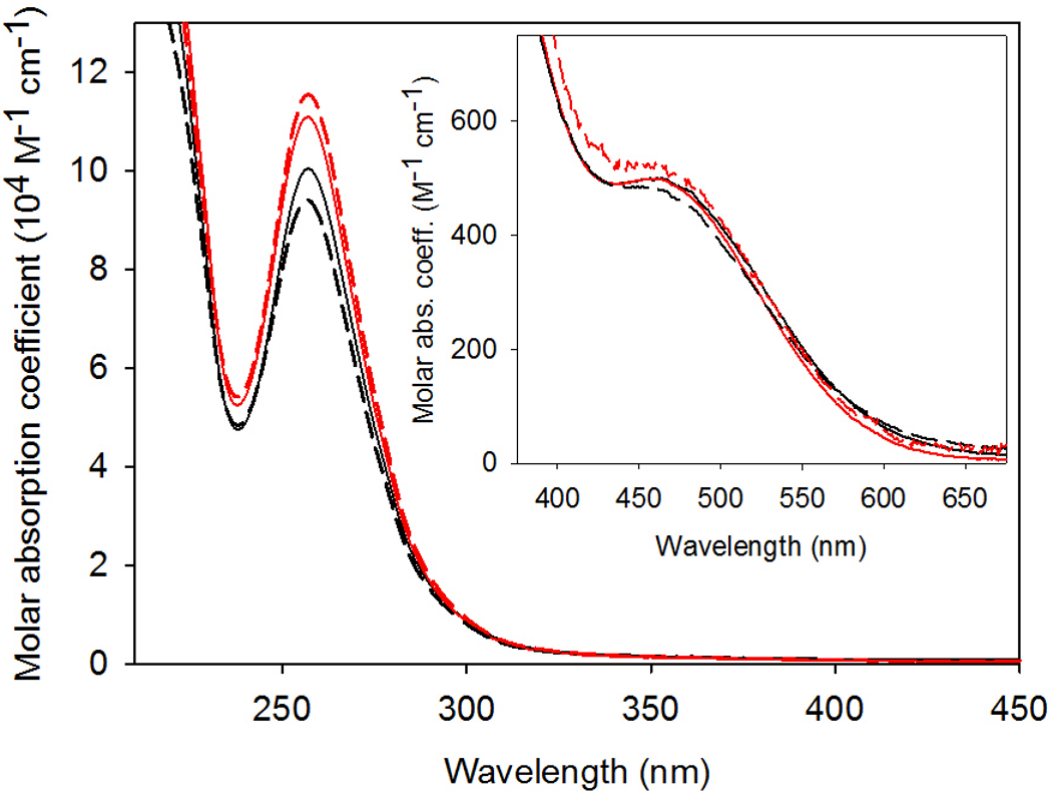

Figure 6.2: *Absorption spectra of the investigated isomeric rotaxanes in ACN:* **6.2***(Up-Sh)*$^{2+}$ *(black, full line),* **6.2***(Up-Lo)*$^{2+}$ *(black, dashed line),* **6.2***(Do-Sh)*$^{2+}$ *(red, full line),* **6.2***(Do-Lo)*$^{2+}$ *(red, dashed line). Up and Down isomers are shown in black and red, respectively, whereas Short and Long isomers are shown with full and dashed lines, respectively.*

Electrochemical experiments were performed to disclose the mechanochemical behaviour of the rotaxanes upon reduction of the viologen unit, i.e. upon destabilization of the viologen-calixarene interaction. Following previous studies the compounds were investigated in acetonitrile. All studied

compounds show two reversible or quasi-reversible monoelectronic reduction processes: electrochemical data are reported in table 6.1, where the reduction potential of the rotaxane **5.1**$(C_3C_3)^{2+}$ is also reported for comparison.

Table 6.1: *Halfwave potential values of the investigated compounds as dissolved and upon sequential addition of 1 eq. of triflic acid (TrH) and tributylamine (TBA). The reduction potential of model compound* **5.1***$(C_3C_3)^{2+}$ are also reported for comparison. Conditions: argon-purged ACN, 0.04 M tetraethylammonium hexafluorophospate, 300 μM analyte.*

	E_1 (V)	E_2 (V)
6.1$(Sh)^{2+}$	−0.41	−0.85
6.1$(Sh)^{2+}$ + TrH	−0.40	−0.84
6.1$(Sh)^{2+}$ + TrH + TBA	−0.40	−0.84
6.1$(Lo)^{2+}$	−0.40	−0.85
6.1$(Lo)^{2+}$ + TrH	−0.40	−0.85
6.1$(Lo)^{2+}$ + TrH + TBA	−0.40	−0.85
6.2$(Up\text{-}Sh)^{2+}$	−0.60	−0.94
6.2$(Up\text{-}Sh)^{2+}$ + TrH	−0.59	−0.90
6.2$(Up\text{-}Sh)^{2+}$ + TrH + TBA	−0.59	−0.93
6.2$(Up\text{-}Lo)^{2+}$	−0.61	−0.87
6.2$(Up\text{-}Lo)^{2+}$ + TrH	−0.59	−0.84
6.2$(Up\text{-}Lo)^{2+}$ + TrH + TBA	−0.61	−0.88
6.2$(Do\text{-}Sh)^{2+}$	−0.52	−0.93
6.2$(Do\text{-}Sh)^{2+}$ + TrH	−0.51	−0.89
6.2$(Do\text{-}Sh)^{2+}$ + TrH + TBA	−0.55	−0.93
6.2$(Do\text{-}Lo)^{2+}$	−0.60	−0.88
6.2$(Do\text{-}Lo)^{2+}$ + TrH	−0.58	−0.87
6.2$(Do\text{-}Lo)^{2+}$ + TrH + TBA	−0.60	−0.88
5.1$(C_3C_3)^{2+}$	−0.64[a]	−1.15[a]

[a] Poorly reversible process; value determined from DPV peak.[1]

Since the behaviour of the studied rotaxanes is similar, only **6.2**$(Up\text{-}Sh)^{2+}$ will be discussed in detail. The voltammetric pattern of **6.2**$(Up\text{-}Sh)^{2+}$ (figure 6.3) shows two quasi-reversible reduction processes at −0.60 and −0.94 V. The shape of the voltammetric trace does not change significantly upon changing the scan rate between 50 and 1000 mV s^{-1}.

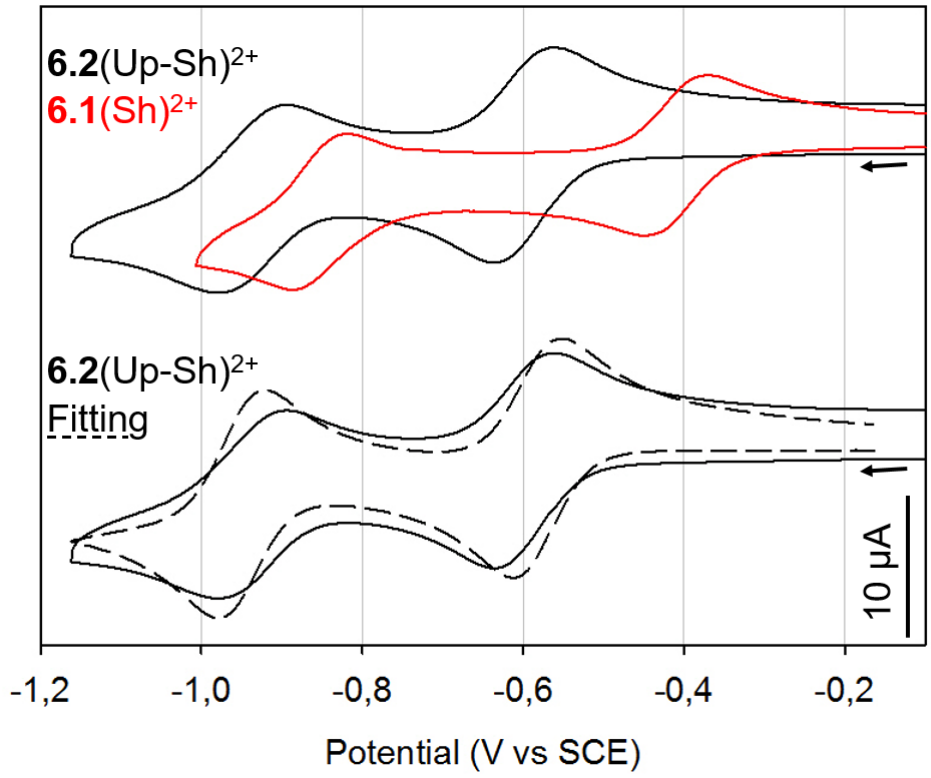

Figure 6.3: *Voltammetric pattern obtained for* **6.2***(Up-Sh)*$^{2+}$ *(top and bottom, black, full line) and* **6.1***(Sh)*$^{2+}$ *(top, red, full line). A numeric fitting of the voltammetric pattern of* **6.2***(Up-Sh)*$^{2+}$ *is also shown (bottom, black, dashed line). Conditions: argon-purged ACN, 0.04 M tetraethylammonium hexafluorophosphate, 300µM analyte, scan rate 200 mV s−1. See text for details regarding the fitting parameters. Corresponding reduction potentials for reference compound* **5.1***(C_3C_3)*$^{2+}$*, in which the viologen moiety remains included in the calixarene cavity upon reduction, are −0.64 V for the first reduction process and −1.15 V for the second reduction process.*

The first reduction process falls at almost the same potential as in model compound **5.1**$(C_3C_3)^{2+}$, in which the viologen moiety remains included in the calixarene cavity upon reduction, suggesting that this is happening also in the present case. On the contrary the second reduction process occurs at potentials that resemble that of the free axle **6.1**$(Sh)^{2+}$ (i.e. −0.85 vs −0.91 V respectively, see figure 6.3), whereas in model compound **5.1**$(C_3C_3)^{2+}$ the corresponding process occurs at −1.15 V. This suggests that the calixarene-based wheel moves away from the viologen upon reduction. EPR data collected in the group of Prof. Lucarini[1] indicated that when the viologen is monoreduced to

[1]Unpublished results.

its radical cation the wheel does not interact strongly any more with the primary station, meaning that the first reduction provides a destabilization energy that is sufficient to dislocate the wheel in proximity of the secondary amine. This can be consistent with a second reversible reduction process in the cyclic voltammetry if the shuttling equilibrium in the monoreduced state is fast with respect to the scanning speed. On the basis of this hypothesis a fitting has been performed on the cyclic voltammetry, to support the consistency of our data with the proposed scheme. The obtained cyclic voltammogram is reported in figure 6.3, and is in good qualitative agreement with the experimental data. The fitting was obtained fixing the reduction potentials equal to −0.64 and −1.18 for the encapsulated species and −0.41 and −0.945 for the free viologen unit. Chemical equilibrium constant for shuttling reactions were 1.2969×10^{-3} ($k_f = 1.0\times10^{-3}$ s^{-1}), 10 ($k_f = 1.0\times10^{5}$ s^{-1}) and 9.3668×10^{4} ($k_f = 3.0\times10^{7}$ s^{-1}) for the shuttling reaction in the oxidized, monoreduced and doubly reduced rotaxanes respectively (only constants related to thermal equilibria were optimized).
The complete reaction scheme, involving reduction and shuttling reactions are represented in figure 6.4.

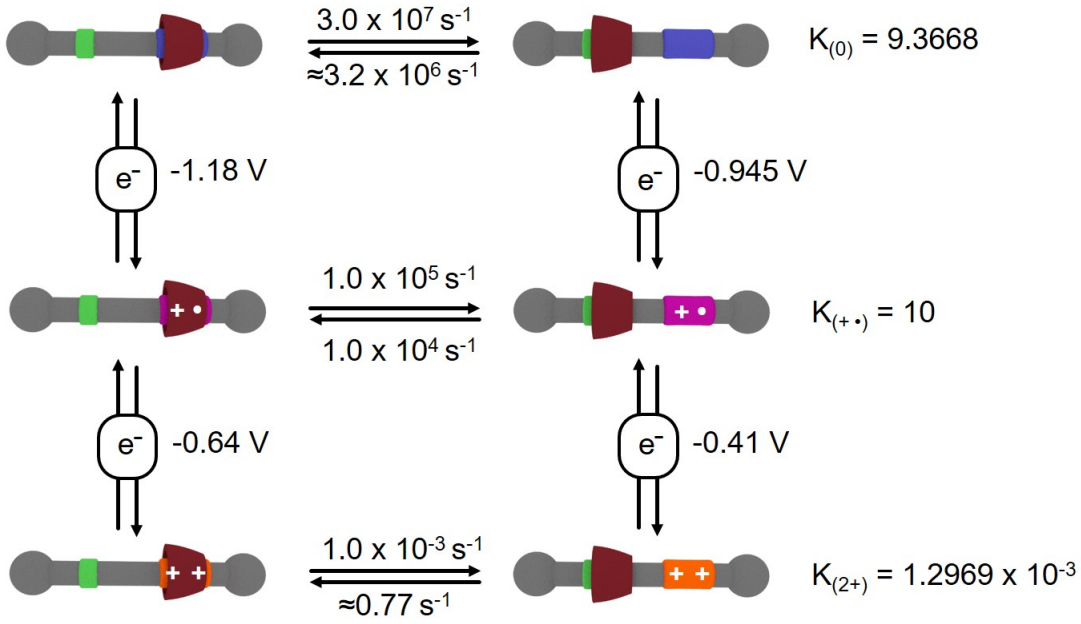

Figure 6.4: *Reaction scheme reporting the thermodinamic and kinetic data for the simulated voltammogram of* **6.2***(Up-Sh)*$^{2+}$ *reported in figure 6.3. The used colors follow the color-code of figure 6.1.*

Surprisingly, protonation of the amine with triflic acid does not affect significantly the cyclic

voltammogram of the studied compounds: small shifts to less negative potentials for both reductions are observed in the rotaxanes, but this does not affect significantly their mechanochemical behaviour.

To facilitate the comparison between different rotaxanes, the data collected in table 6.1 have been represented in the genetic diagram reported in figure 6.5.

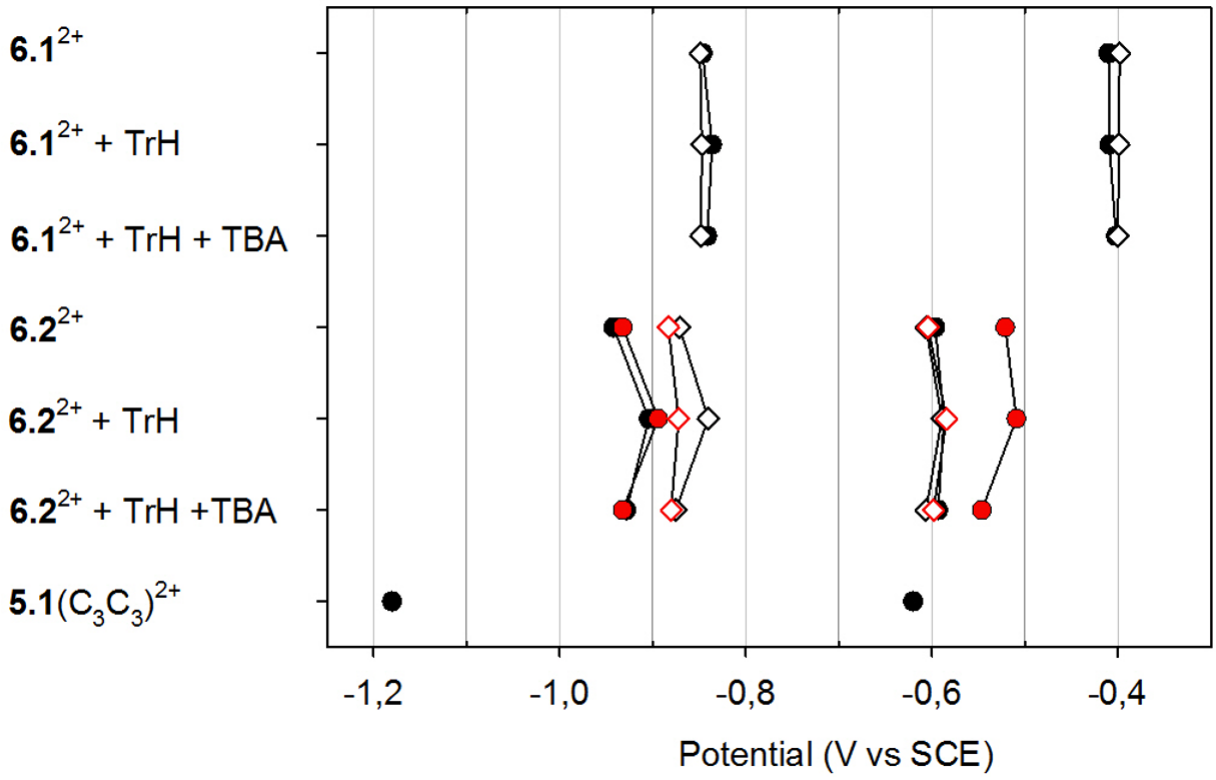

Figure 6.5: *Genetic diagram for the studied compounds* **6.1***(Sh)*$^{2+}$ *(black dots),* **6.1***(Lo)*$^{2+}$ *(white diamonds),* **6.2***(Up-Sh)*$^{2+}$ *(black dots),* **6.2***(Up-Lo)*$^{2+}$ *(white diamonds),* **6.2***(Do-Sh)*$^{2+}$ *(red dots),* **6.2***(Do-Lo)*$^{2+}$ *(red diamonds) upon subsequent addition of 1 eq. of triflic acid (TrH) and an equimolar amount of tributylamine (TBA). The first reduction process occurs almost at the same potential for* **6.2***(Up-Sh)*$^{2+}$, **6.2***(Up-Lo)*$^{2+}$ *and* **6.2***(Do-Lo)*$^{2+}$*. The reduction potentials of* **5.1***(C_3C_3)*$^{2+}$ *are also reported for comparison (black dots).*

From the diagram it is clear that the behaviour of **6.2**(Up-Sh)$^{2+}$ is very similar to that of the other two-stations rotaxanes. The second reduction occurs at potential values similar to that of model axle compounds. However it is noted that the reduction of rotaxanes bearing the amine unit closer to the calixarene are slightly more difficult to reduce (regardless of the calix[6]arene orientation), suggesting that a little but non-negligible interaction between the calixarene and monoreduced

viologen is still taking place. This also suggests that when the amine is close to the viologen, it is possible for the calixarene wheel to interact with both sites simultaneously and with similar energetics, regardless of the orientation of the axle. This observation is somehow surprising, because the two rims of the calix[6]arene are very different from a chemical point of view (e.g. the upper rim has hydrogen bond donor characteristics and the lower rim has a hydrogen bond acceptor character) and it is therefore not easy to imagine different interaction modes that result in very similar interaction energies. The observed difference becomes less pronounced upon protonation of the amine unit. The first reduction process occurs at the same potential within the experimental error for **6.2**(Up-Sh)$^{2+}$, **6.2**(Up-Lo)$^{2+}$ and **6.2**(Do-Lo)$^{2+}$, whereas **6.2**(Do-Sh)$^{2+}$ it is easier to reduce. In agreement with EPR data collected in the group of Prof. Lucarini, this result suggest that when the viologen is monoreduced, the wheel partially moves towards the amine, but still interacts with the monoreduced viologen unit. This is in contrast with the other derivatives, in particular with the isomer **6.2**(Up-Sh)$^{2+}$, suggesting that it is thermodynamically favoured for the macrocycle to move onto the amine in **6.2**(Do-Sh)$^{2+}$ rather than in **6.2**(Up-Sh)$^{2+}$. Protonation of the amine affects only minimally the first reduction potential of the viologen. This suggests that an ammionium ion is not a much better recognition site for the calix[6]arene wheel. The same behaviour is also observed in dichloromethane, a less polar solvent that has a lower ability to compete with hydrogen bonding interactions. To explain this effect it can be hypotesized that accommodation of the counterion in proximity of the calixarene cavity, or molecular rearrangements necessary to interact with the ammonium ion with several oxygen atoms located at the lower rim, may be too energetically demanding and counterbalance the establishment of more favoured interactions between the wheel and the ammonium with respect to the wheel-amine recognition motif.

6.3 Conclusions

As a follow-up to the work presented in the previous chapter, isomeric rotaxanes bearing a calix[6]arene wheel and a dumbbell component with two recognition sites for the wheel have been investigated. In this family of compounds reduction of the primary station (a viologen moiety) induces a shuttling motion of the wheel over the secondary station, a secondary amine. Surprisingly, protonation of the amine only minimally affects the electrochemical behaviour of the studied rotaxanes. Moreover, in the case of the second reduction process, the effect of the length of the axle seems to dominate over the location of the amine. On the contrary in the case of the first reduction process a clear difference is observed when the amine is located at the lower rim and the axle is short: in this

derivative the first reduction occurs at less negative potential with respect to the same process in the isomeric rotaxane bearing the secondary station at the upper rim of the calixarene wheel, implying that the process is thermodynamically favoured in **6.2**(Do-Sh)$^{2+}$. This suggests that in a rotaxane composed by a calix[6]arene wheel and a symmetric axle bearing a central viologen unit and two secondary amine stations, connected to the viologen unit by a short spacer, there could be a preference to move towards the amine located at the lower rim rather than to the upper rim. This asymmetric movement would be only dictated by the asymmetry of the wheel and not by the symmetry of the axle component. To the best of our knowledge this would be an unprecedent result, as directional movement within a rotaxane with a fully symmetric axle has never be demonstrated. The envisioned rotaxane has already been synthesized in the group of Prof. Arduini and Prof. Secchi at the University of Parma, and the behaviour of this system upon reduction is currently under investigation.

6.4 References

[1] V. Zanichelli, G. Ragazzon, A. Arduini, A. Credi, P. Franchi, G. Orlandini, M. Venturi, M. Lucarini, A. Secchi, and S. Silvi. *Eur. J. Org. Chem.*, pages 1033–1042, 2016. 57, 58, 60

[2] A. Arduini, R. Bussolati, A. Credi, A. Pochini, A. Secchi, S. Silvi, and M. Venturi. *Tetrahedron*, 64:8279–8286, 2008. 58

Part III

Acid-base switchable rotaxanes

7

Introduction

7.1 pH-switchable rotaxanes: from fundamentals to applications

Rotaxanes and related interlocked molecules are intriguing chemical architectures with high relevance for the development of artificial nanoscale machines and switches as well as functional materials.[1–6] The tremendous progresses for their synthesis have broadened the scope of their use.[7–12] In particular bistable pH-switchable [2]rotaxanes, consisting of a macrocycle threaded on a molecular dumbbell axle with two potential sites of interaction (the "stations"), of which one can be deactivated upon deprotonation or protonation, likely constitute the most studied class of rotaxanes. The operation of a bistable rotaxane as a switch relies on the ability of the external stimulus (here a pH change induced by acid or base addition) to reversibly modify the relative affinity of the ring for the two stations, leading to a drastic structural change in the molecule. A simplified view of the process pictures the ring moving from one station to the other as a consequence of the application of the stimulus. This view, however, does not represent the behavior of a statistically significant population of rotaxanes, because an equilibrium exists between the two translational isomers (or co-conformations) corresponding to the positioning of the ring on either site on the axle.[13] In line with proposed definitions,[14] the most abundant translational isomer is referred to as the stable co-conformation (SCC) while the second isomer is called the metastable co-conformation (MCC). Therefore the switching event is associated to a change in the relative population of SCC and MCC. In chapter 8 the development of two novel methods to determine the relative distribution of the ring between the two conformations will be introduced.

From the dynamic equilibrium of the ring between the two stations in rotaxanes novel phenomena can arise, in particular an increased basicity of some pH-sensitive moieties within catenanes and

rotaxanes has been recognized by Sauvage[15] and Takata[16]. This comes from the fact that the congested molecular environment of the base or the conjugated acid can be extremely different in comparison to that of the parent non-interlocked component. As an example, a secondary ammonium ion encircled by a crown ether will be very stable, thus increasing its basicity; however, if a good station for the ring is present in the rotaxane, the ring will spend less time on the ammonium ion, and its apparent basicity will decrease. This behaviour is reminiscent of allostery, in which a chemical interacting with a biomolecule at one site can cause a significant change at a different site still within the biomolecule, but far from it. Recently similar effects have also been recognized in catenanes[17]. In chapter 9 the reversible allosteric-like modulation of pKa within a rotaxane architecture will be demonstrated.

The aspects outlined so far deal with the very basic properties of pH-switchable rotaxanes. However, these architectures have also been used to explore possible application of molecular machines, indeed they proved effective in offering a wide range of functions including ion sensing,[18–21] catalysis[22–24] and polymers actuation[25, 26]. With the aim of expanding the functionality of rotaxane architectures, a system able to capture, transport and release a molecular cargo has been studied, using the same rotaxane architecture studied in chapter 9. Although other systems that perform the translocation of a molecular cargo at the nanoscale have been reported by Zhu[27], Leigh[28] and Feringa[29], the illustrated system remains — to the best of my knowledge — the sole able to pick-up a cargo from solution, while binding it with a stable covalent bond, that is a key requirement to be sure that the cargo remains bound to the rotaxane architechture while it is moved from one site to the other. This study is the subject of chapter 10.

7.2 References

[1] W. Browne and B. Feringa. *Nat. Nanotechnol.*, 1:25–35, 2006. 69

[2] E. R. Kay, D. A. Leigh, and F. Zerbetto. *Angew. Chem. Int. Ed.*, 46:72–196, 2007.

[3] V. Balzani, A. Credi, and M. Venturi. *Molecular Devices and Machines, 2nd Ed.* Wiley-VCH, Weinheim, 2008.

[4] A. Coskun, M. Banaszak, R. D. Astumian, J. F. Stoddart, and B. A. Grzybowski. *Chem. Soc. Rev.*, 41:19–30, 2012.

[5] S. Erbas-Cakmak, D. A. Leigh, C. T. McTernan, and A. L. Nussbaumer. *Chem. Rev.*, 115:10081–10206, 2015.

[6] M. Xue, Y. Yang, X. Chi, X. Yan, and F. Huang. *Chem. Rev.*, 115:7398–7501, 2015. 69

[7] F. Aric, J. D. Badjić, S. J. Cantrill, A. H. Flood, K. C. F. Leung, Y. Liu, and J. F. Stoddart. *Top. Curr. Chem.*, 249:203–259, 2005. 69

[8] J. D. Crowley, S. M. Goldup, A. L. Lee, D. A. Leigh, and R. T. McBurney. *Chem. Soc. Rev.*, 38:1530–1541, 2009.

[9] K. D. Hänni and D. A. Leigh. *Chem. Soc. Rev.*, 39:1240–1251, 2010.

[10] J. E. Beves, B. A. Blight, C. J. Campbell, D. A. Leigh, and R. T. McBurney. *Angew. Chem. Int. Ed.*, 50:9260–9327, 2011.

[11] D. Thibeault and J. F. Morin. *Molecules*, 15:3709–3730, 2010.

[12] R. J. Bordoli and S. M. Goldup. *J. Am. Chem. Soc.*, 136:4817–4820, 2014. 69

[13] M. N. Chatterjee, E. R. Kay, and D. A. Leigh. *J. Am. Chem. Soc.*, 128:4058–4073, 2006. 69

[14] A. H. Flood, A. J. Peters, S. A. Vignon, D. W. Steuerman, H. R. Tseng, S. Kang, J. R. Heath, and J. F. Stoddart. *Chem. Eur. J.*, 10:6558–6564, 2004. 69

[15] M. Cesario, C. O. Dietrich, A. Edel, J. Guilhem, J.-P. Kintzinger, C. Pascard, and J.-P. Sauvage. *J. Am. Chem. Soc.*, 108 (20):6250–6254, 1986. 70

[16] N. Kihara, Y. Tachibana, H. Kawasaki, and T. Takata. *Chem. Lett.*, pages 506–507, 2000. 70

[17] M.-K. Chung, P. S. White, S. J. Lee, M. R. Gagne, and M. L. Waters. *J. Am. Chem. Soc.*, 138:13344–13352, 2016. 70

[18] S. S. Zhu, P. J. Carroll, and T. M. Zwager. *J. Am. Chem. Soc.*, 118:8713–8714, 1996. 70

[19] N. H. Evans and P. D. Beer. *Angew. Chem. Int. Ed.*, 53:11716–11754, 2014.

[20] M. J. Langton and P. D. Beer. *Acc. Chem. Res.*, 47:1935–1949, 2014.

[21] Y. Tokunaga, T. Nakamura, M. Yoshioka, and Y. Shimomura. *Tetrahedron Lett.*, 47:5901–5904, 2006. 70

[22] D. A. Leigh, V. Marcos, and M. R. Wilson. *ACS Catalysis*, 4:4490–4497, 2014. 70

[23] E. A. Neal and S. M. Goldup. *Chem. Commun.*, 50:5128–5142, 2014.

[24] V. Blanco, D. A. Leigh, and V. Marcos. *Chem. Soc. Rev.*, 44:5341–5370, 2015. 70

[25] G. Du, E. Moulin, N. Jouault, E. Buhler, and N. Giuseppone. *Angew. Chem. Int. Ed.*, 51:12504–12508, 2012. 70

[26] A. Goujon, G. Du, E. Moulin, G. Fuks, M. Maaloum, E. Buhler, and N. Giuseppone. *Angew. Chem. Int. Ed.*, 55:703–707, 2016. 70

[27] J. Li, Y. Li, Y. Guo, J. Xu, J. Lv, Y. Li, H. Liu, S. Wang, and D. Zhu. *Chem. Asian J.*, 3:2091–2096, 2008. 70

[28] S. Kassem, A. T. L. Lee, D. A. Leigh, A. Markevicius, and J. Solá. *Nat. Chem.*, 8:138–143, 2016. 70

[29] J. Chen, S. J. Wezenberg, and B. L. Feringa. *Chem. Commun.*, 52:6765–6768, 2016. 70

8

Characterization of a bistable pH-switchable rotaxane

8.1 Introduction

A full characterization of the starting state of any bistable rotaxane — which in turn is important for understanding successive stimuli-induced switching processes — involves the measurement of the equilibrium constant K = $[SCC]_{eq}/[MCC]_{eq}$, where SCC = stable co-conformation and MCC = metastable co-conformation. This is a nontrivial task because K is an intramolecular quantity which reflects relative binding strengths within an individual molecular entity. Indeed, the free energy difference between the SCC and MCC can be accurately calculated from the value of K, thereby enabling correlations with the noncovalent intercomponent interactions. ^{1}H NMR spectroscopy can be used to measure $[SCC]_{eq}$ and $[MCC]_{eq}$ but, because of its inherent sensitivity, it provides reliable results only when K does not exceed ca. 20.[1, 2] Rotaxanes characterized by high values of K, however, are required to make efficient molecular shuttles. Thus, new assays that can yield information on bistable rotaxanes with highly shifted co-conformational equilibria need to be developed. Paolucci and coworkers used cyclic voltammetry (CV) experiments to evaluate K.[3, 4] Stoddart and coworkers also reported a method based on CV whose sensitivity was comparable

This chapter is partially derived — with permission — from G. Ragazzon, A. Credi, B. Colasson, "Thermodynamic insights on a bistable acid-base switchable molecular shuttle with strongly shifted co-conformational equilibria" *Chem. Eur. J.*, **2017**, 23, 2149 - 2156. I am particularly grateful to Dr. Benoit Colasson, who collected the experimental data that are presented in this chapter.

with that of ^{1}H NMR.[5] Later, by using variable scan rate CV, the sensitivity was dramatically increased,[6, 7] enabling the measurement of K values up to 104. These methods, however, can only be applied to rotaxanes having a well behaved electroactive unit (e.g. a redox-switchable ring recognition site). For pH-triggered bistable rotaxanes — the subject of this part of the thesis — a sensitive assay is still missing.

In this chapter it is described how it is possible to quantify the co-conformational equilibrium in a bistable interlocked molecule taking advantage of its acid-base properties. In particular the acid-base properties of rotaxane **8.1**H^{2+} shown in figure 8.1 are discussed. Another sensitive method based on luminescence lifetime measurement has also been developed in the course of this study and it is briefly described first, as it follows from the photophysical characterization of the studied compounds, that is required to discuss the acid-base titrations.

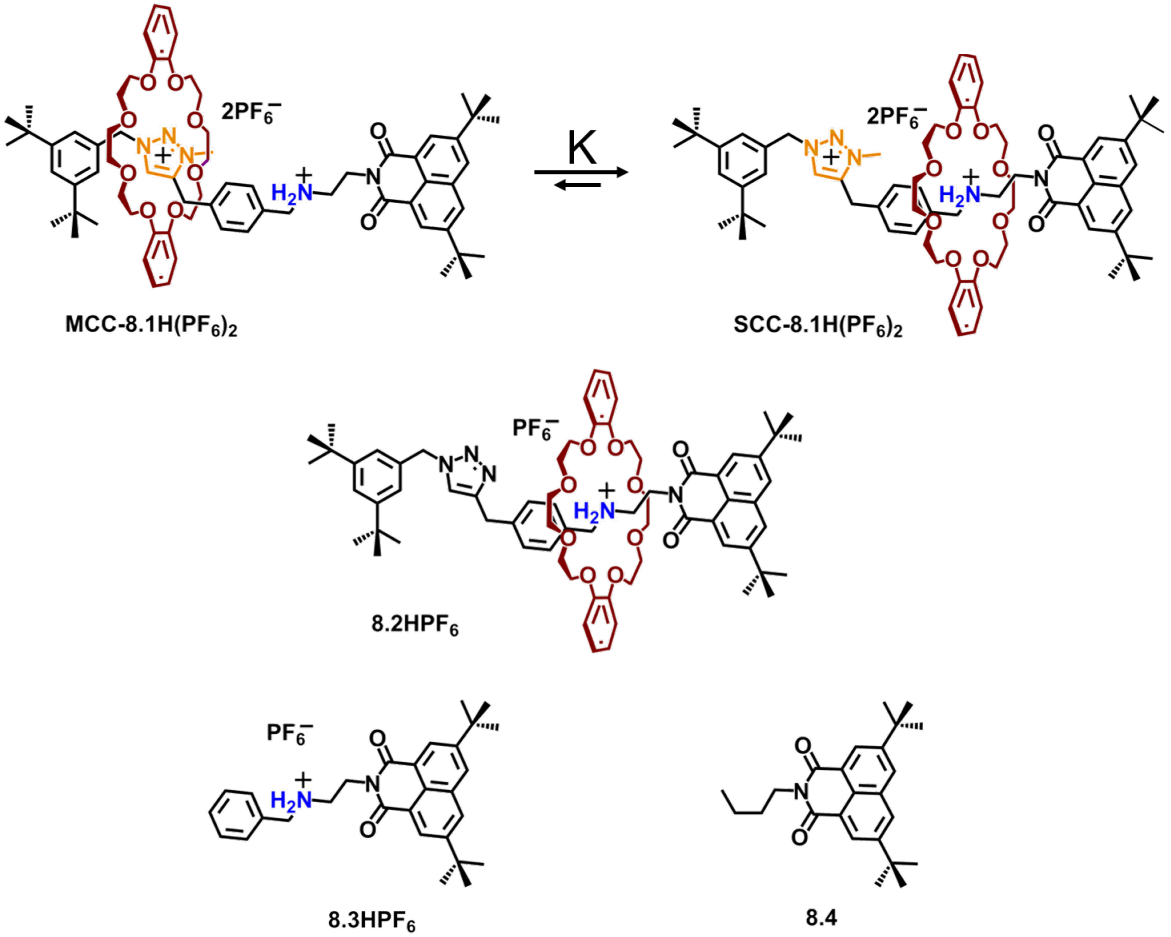

Figure 8.1: *Co-conformational equilibrium for the investigated switchable rotaxane* **8.1**H^{2+} *(top) and its model compounds* **8.2**H^{+}, **8.3**H^{+} *and* **8.4** *(middle and bottom).*

8.2 Design

Recently, the 1,2,3-triazolium unit (tria^{+}) has been identified as a convenient secondary station for a dibenzo[24]crown-8 ring (DB24C8) in rotaxanes in which a dialkylammonium unit (amH^{+}) plays the role of the primary station.[8, and references therein][9–20] The intermolecular apparent association constant between charged species is highly dependent on the concentration because the ionic strength has a strong effect on the ion pairing in the uncomplexed thread (for a complete discussion on this effect see [21, 22]). This is also the case for dialkylammonium guests and DB24C8. At low concentrations (ca. 50 μM), in an apolar solvent like CH_2Cl_2 the association constant for this

recognition motif is ca. 10^4 - 10^5 M^{-1}.[see e.g. 23, 24] This value has not yet been reported in the case of a triazolium axle, presumably because of the very inefficient complexation. Indeed, it was found that the triazolium moiety cannot be used as a template for rotaxane formation.[8] Consequently, the triazolium unit is considered to be a weak station within a rotaxane. Such a difference in the behavior of the two guests should ensure a largely unbalanced co-conformational distribution, and for this reason it was decided to synthesize and investigate a [2]rotaxane containing ammonium and triazolium stations in the axle, for the development of a sensitive method for measuring large values of K. Figure 8.1-top shows the bistable rotaxane studied in this work, **8.1**H^{2+}, and the equilibrium linking its SCC and MCC. A few model compounds necessary for the experiments are represented in figure 8.1-bottom. The interested reader can refer to [25] for details on the synthesis and characterization of the compounds. In particular, **8.2**H^+ is structurally identical to **8.1**H^{2+} except for the absence of the secondary triazolium station; thus, the only translational co-conformation of **8.2**H^+ is that shown in figure 8.1-bottom. The axle in both **8.1**H^{2+} and **8.2**H^+ possesses a fluorescent naphthalimide (NI) stopper placed in the vicinity of the ammonium station. Encouraged by the results obtained for many previously reported fluorescent rotaxanes,[26–29] we anticipated that the fluorescence properties of the naphthalimide group would be sensitive to the position of the ring on the axle and could be used to quantitatively report on its distribution.

8.3 Determination of the ring distribution from luminescence measurements

The UV-visible absorption and emission spectra of **8.3**H^+, **8.2**H^+ and **8.1**H^{2+} in CH_3CN are similar and are dominated by the bands of the NI chromophore (λ_{max} = 354 nm, ϵ = 14000 M^{-1} cm^{-1}). In the case of **8.1**H^{2+} and **8.2**H^+ the absorption band of the DB24C8 component (λ_{max} = 275 nm) is also present. All compounds show a luminescence band centered at ca. 390 nm, assigned to the NI fluorescence. The relevant fluorescence data are given in table 8.1.

Table 8.1: *Fluorescence data (quantum yields Φ, fluorescence lifetimes τ_i and pre-exponential factors β_i) for* **8.4**, **8.3**H^+, **8.2**H^+ *and* **8.1**H^{2+}

		τ_i (ps) / β_1 (a.u.) [a]		
	Φ	τ_1	τ_2	τ_3
8.1H^{2+}	1.8±0.2	2620/0.11	763/6	220/12.3
8.2H^+	1.0±0.1	-	621/5	186/20
8.3H^+	20±1	2660	-	-
8.4	18.4±1	1530	-	-

[a] In CH_3CN at room temperature.

The emission quantum yield of **8.3**H^+ is very close to that of the bare naphthalimide model NI. The presence of the ammonium is nevertheless testified by a longer lifetime (2.66 ns vs 1.53 ns), a 2 nm bathochromic shift of the absorption band, and a fluorescence maximum shifted to longer wavelengths. These observations are consistent with the presence of an intramolecular hydrogen bond between the ammonium unit and a carbonyl group of the naphthalimide both in the ground and excited states.[30, 31] The emission quantum yields in the two rotaxanes are significantly smaller because of photoinduced electron transfer quenching, as evidenced by transient absorption measurements. Insightful information about the co-conformational distribution of **8.1**H^{2+} can be obtained from a careful analysis of the time-correlated fluorescence decays. While **8.3**H^+ exhibits a monoexponential decay ($\tau = 2.66$ ns), the fluorescence decay of **8.2**H^+ is biexponential with $\tau_2 = 621$ ps and $\tau_3 = 186$ ps. In analogy with previous studies on the time-resolved luminescence properties of crown-ether ligands,[32] these two short lifetimes are tentatively ascribed to the decay of the NI excited singlet in two different conformations of the ring placed on the ammonium station.[33–35] Interestingly, in **8.1**H^{2+} a third longer lifetime ($\tau_1 = 2.62$ ns) similar to the lifetime determined for the ammonium model **8.3**$^+$ is present, while the two shorter lifetimes $\tau_2 = 763$ ps and $\tau_3 = 220$ ps) have values comparable to those found in **8.2**H^+ (table 8.1 and figure 8.2).[1] Since the emission decay (~ ns) is much faster than the ring shuttling (~ μs −ms),[36, 37] the NI fluorophores in the two co-conformations can be treated as two isolated fluorophores placed in different environments. By comparison with the behavior of the models, the lifetime τ_1 for **8.1**H^{2+} was therefore attributed

[1] A third lifetime component must be added to the exponential function to afford a reasonable fit of the fluorescence intensity decay. The fitting with a biexponential function clearly neglects the tail of the decay and the residuals are not randomly distributed.

to the MCC, in which the ring is far enough from the fluorophore to avoid any interaction with the NI excited state. Consequently we associated τ_2 and τ_3 with the SCC, in which the ring surrounds the amH$^+$ station. The remarkable correspondence between the lifetimes of the studied models and those found in **8.1**H^{2+} confirms that the two stations can be considered as spectroscopically independent and are appropriately described by the reference compounds. With this requirement satisfied, the pre-exponential factors β_i represent the fractions of SCC (α_{SCC}) and MCC (α_{MCC}), weighted for a factor F which takes into account the inherent photophysical differences (e.g. fast static quenching, radiative rates, absorption and emission spectra) of the NI fluorophore in the two situations.[38] The F factor can be measured with time-correlated fluorescence decay experiments by comparing the initial photon count accumulated during the same time under identical instrumental conditions for two solutions of **8.2**H$^+$ and **8.3**H$^+$ having the same concentration. From the ratio between the initial photon counts for **8.3**H$^+$ and **8.2**H$^+$ a value F = 9.82±0.04 was determined. Hence, K can be obtained from equation 8.1 where $\beta_{SCC} = \beta_2 + \beta_3$ and $\beta_{MCC} = \beta_1$:

$$K = (\alpha_{SCC}/\alpha_{MCC}) = F(\beta_{SCC}/\beta_{MCC}) \tag{8.1}$$

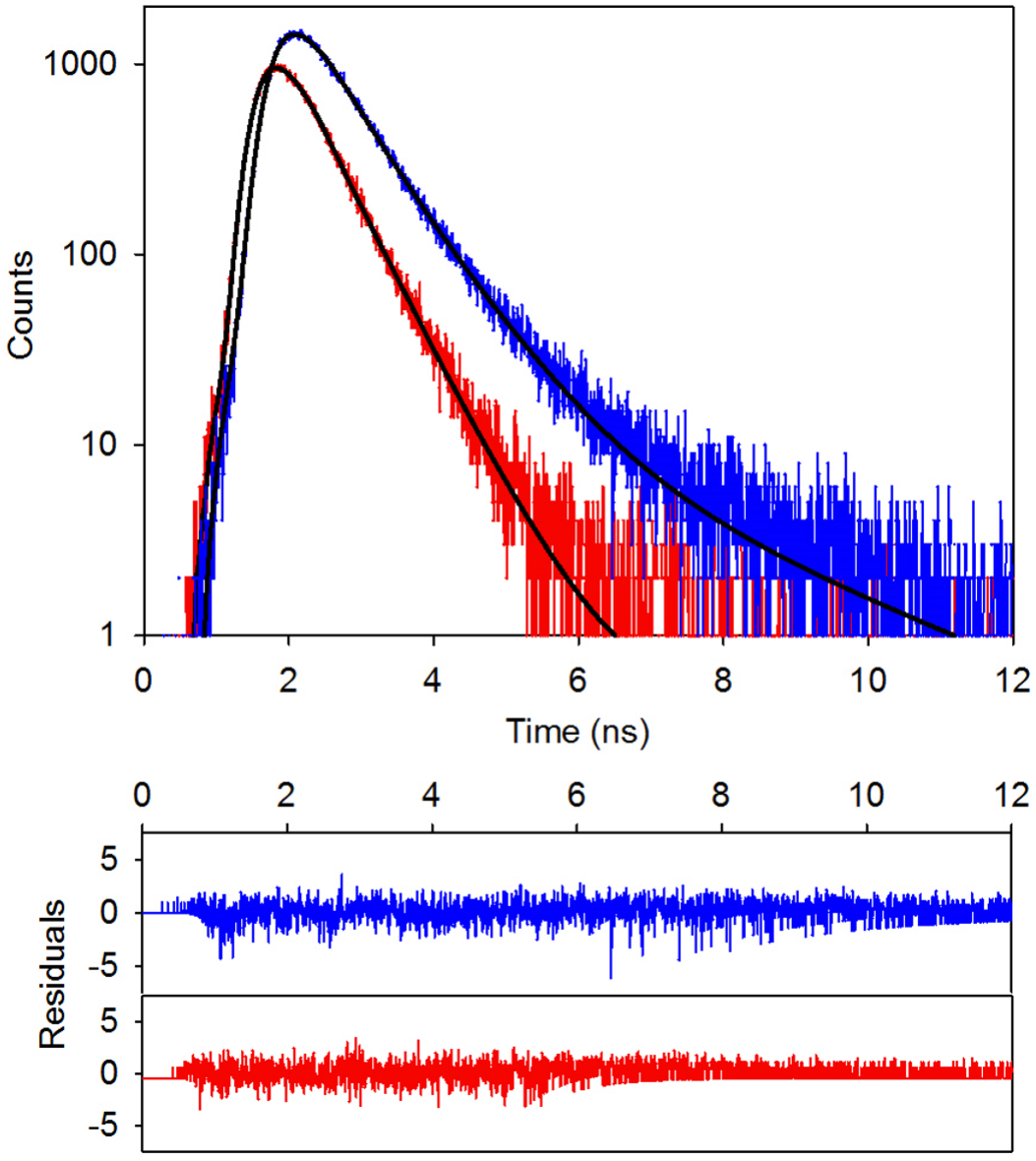

Figure 8.2: *Fluorescence intensity decays in CH_3CN at room temperature for* **8.1**H^{2+} *(blue, top) and* **8.2**H^{+} *(red, top) and their respective residuals (bottom). The black curves are the two best fit for both decays and correspond to the parameters listed in table 8.1. Conditions: λ_{exc} = 340 nm, λ_{em} = 415 nm, 10 μM analyte.*

By introducing the experimental values in equation 8.1 an equilibrium constant logK = 3.2±0.2 can be determined. This value is independent on the wavelength of observation. Time-resolved fluorescent measurements were also performed in CH_2Cl_2, where the emission of **8.1**H^{2+} exhibited

a biexponential decay with $\tau_2 = 781$ ps and $\tau_3 = 219$ ps. In line with the previous discussion, these two components are assigned to two different arrangements of the ring in the SCC. The absence of a third decay component with longer lifetime (τ_1), attributable to the metastable translational isomer, indicates that in this particular case the fluorescence-based method is not sensitive enough to detect the MCC in CH_2Cl_2. Such an observation points to a significantly higher value for K, in agreement with the prediction based on intermolecular association data obtained in the same solvent. Presumably, in CH_3CN the interaction of the ring with the amH^+ station is affected (destabilized) to a higher extent than with the $tria^+$ one, leading to a decrease in the K value in going from DCM to ACN.

8.4 Determination of the ring distribution from acid/base titrations

The operation of **8.1**H^{2+} as a pH-controlled molecular shuttle is shown in figure 8.3, wherein co-conformational and acid-base equilibria are represented as the horizontal and vertical processes, respectively. The reversible stimuli-induced shuttling is based on the fact that the SCC and MCC for **8.1**H^{2+} and its deprotonated counterpart **8.1**$^+$ correspond to opposite translational isomers. In fact, for **8.1**$^+$ only the isomer in which the ring encircles the $tria^+$ station was observed by ^{1}H NMR spectroscopy, in keeping with the fact that the amH^+ site is switched off upon deprotonation.[8, and references therein][9–20] Considering that deprotonation of SCC-**8.1**H^{2+} affords immediately and quantitatively SCC-**8.1**$^+$, the titration of **8.1**H^{2+} with a base enables the determination of an apparent acidity constant $K_{a,\mathbf{8.1}}$ linking these two forms (figure 8.3). On the other hand, it is reasonable to assume that **8.3**$^+$ is an appropriate model for measuring the acidity constant of the ammonium station of **8.1**H^{2+} when it is not surrounded by the ring ($K_{a,\mathbf{8.3}}$). A thermodynamic cycle can thus be established between the two co-conformations of the protonated rotaxane (**8.1**H^{2+}) and the deprotonated rotaxane (**8.1**$^+$), as shown by the full arrows in figure 8.3. The translational equilibrium constant K is then straightforwardly calculated from equation (2):

$$K = K_{a,\mathbf{8.3}}/K_{a,\mathbf{8.1}} \tag{8.2}$$

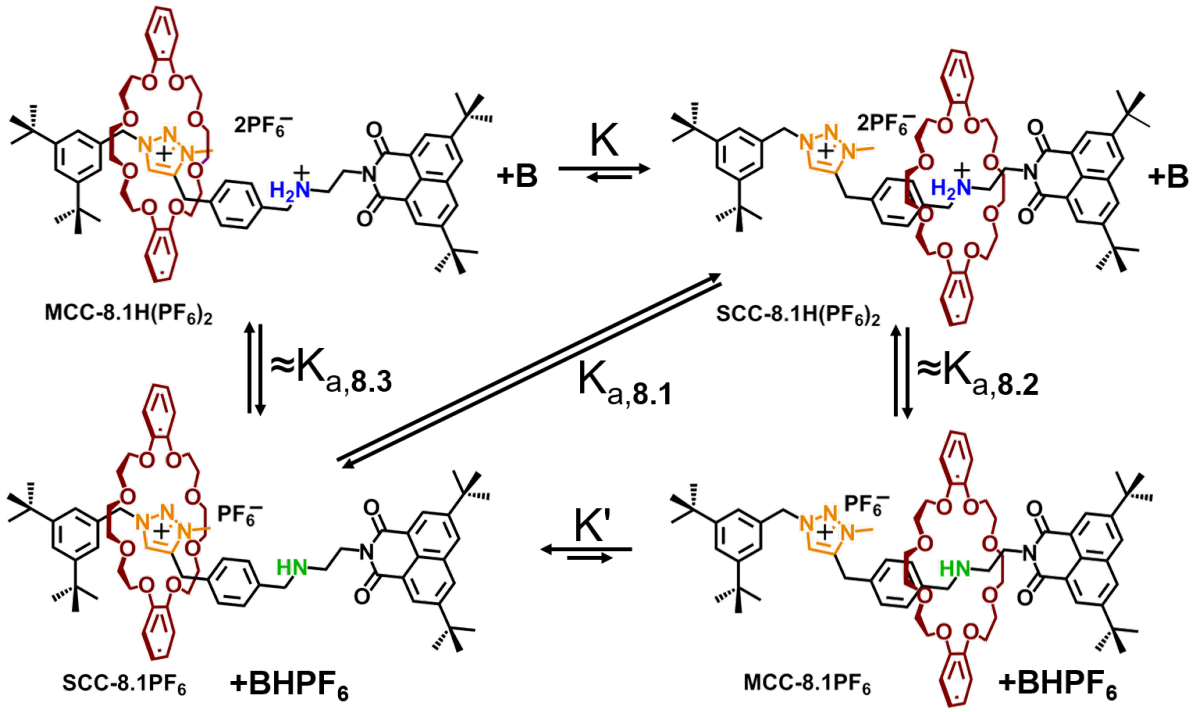

Figure 8.3: *Square scheme describing the switching between different co-conformations (horizontal processes) and protonated/deprotonated forms (vertical processes) for rotaxane* **8.1**. *The base employed in the titration and its conjugated acid are labelled respectively as B and BHPF$_6$. The thermodynamic cycle linking K and the acidity constants $K_{a,\mathbf{8.1}}$ and $K_{a,\mathbf{8.3}}$ is valid for B = CH$_3$CN. The translational isomer* **MCC-8.1**$^+$ *has never been experimentally observed. See the text for more details.*

In order to perform an accurate assay, the pK$_a$ of the bases used for the titration of the rotaxane and the axle model should be as close as possible to the pK$_a$ of the molecules under investigation. A search for bases compatible with our experiments (that is, operating in CH$_3$CN and spectroscopically silent) and known pK$_a$ was thus performed. The analysis of the absorption spectral changes observed upon titration of **8.1**H^{2+} by Et$_3$N (pK$_a$ = 18.82)[39] yielded a value of $pK_{a,\mathbf{8.1}}$ = 19.9±0.1 (figure 8.4 top). When the titration was performed on **8.3**H$^+$ using a weaker base (PhCH$_2$NH$_2$, pK$_a$ = 16.91),[39] a value of $pK_{a,\mathbf{8.3}}$ = 16.3±0.1 was obtained (figure 8.4 bottom). By introducing these values in equation 8.2, it was calculated that logK = 3.6±0.2. Within errors, this number is the same as that determined with the luminescence-based method. The titration of **8.2**H$^+$ with a base can provide information on the acid-base properties of the amH$^+$ site when it is surrounded by DB24C8 (vertical process in the right part of figure 8.3). Indeed, no spectroscopic modification could be observed when **8.2**H$^+$ was treated with a huge excess of 1,4-diazabicyclo[2.2.2]octane (DABCO,

pK_a = 18.2).[40] Since even in presence of 6000 equivalents of DABCO less than 10% of **8.2**H^+ is deprotonated, it followed that the pK_a of the amH^+ unit encircled by DB24C8 is larger than 23.9.

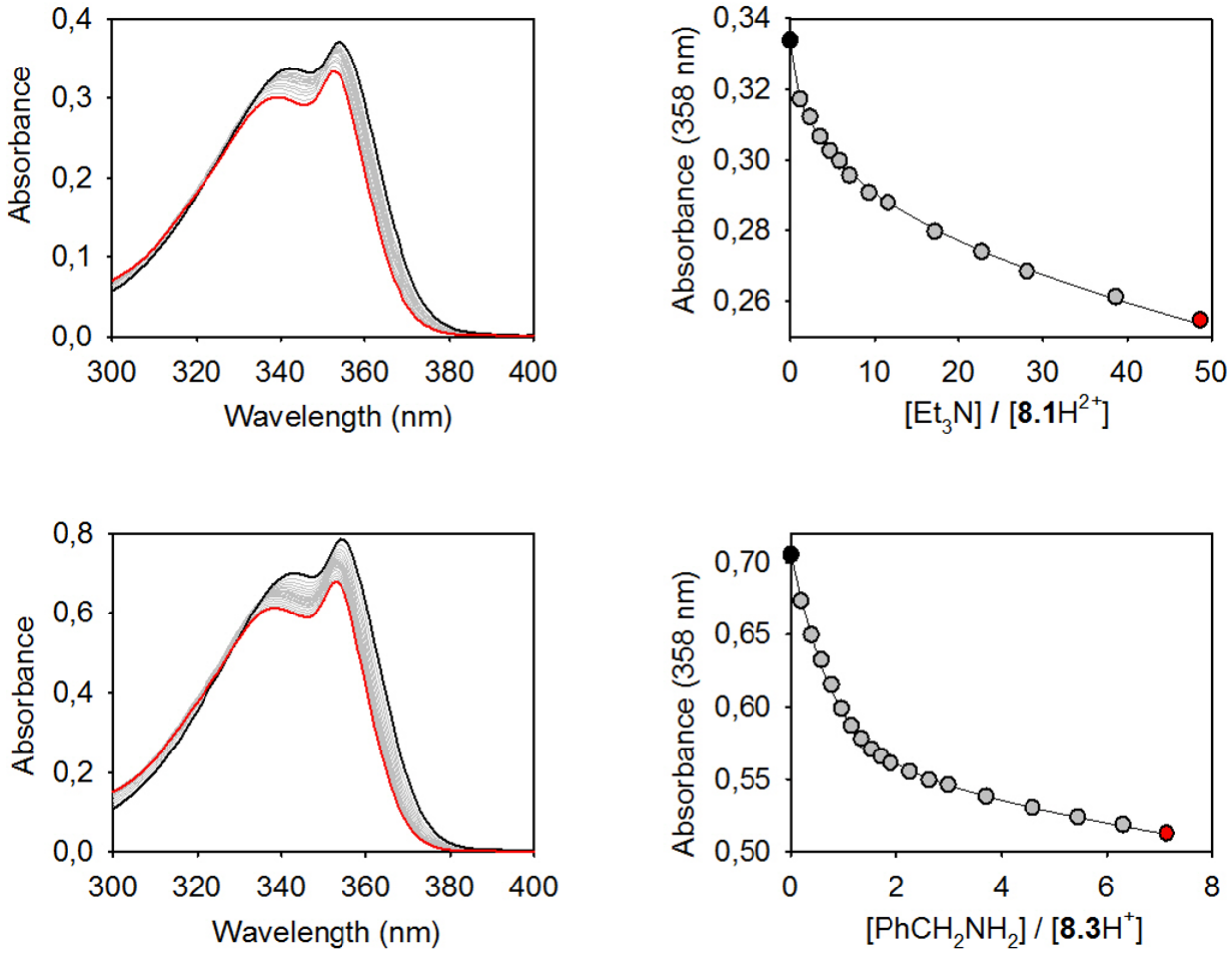

Figure 8.4: *UV-absorption spectral changes (left) and corresponding titration curves (right) in CH_3CN at room temperature upon titration of* **8.1**H^{2+} *(29 μM) by Et_3N (top) and (b)* **8.3**H^+ *(56 μM) by $PhCH_2NH_2$ (bottom). The initial and final spectra are shown in black and red, respectively. The dots in the right graphs correspond to the experimental points and the solid line is the curve fitting according to a proton exchange model.*

The free energy values associated with the processes displayed in figure 8.5 can be calculated from the corresponding equilibrium constants ($\Delta G° = -RT \ln K$) and an energy level diagram describing the acid-base induced co-conformational switching of **8.1**H^{2+} can be constructed (figure 8.5). The levels shown in figure 8.5 correspond to absolute (SCC) or relative (MCC) energy minima; the energy

maxima (i.e., the transition states) that separate the two minima in each curve are not known in the present case. However, these values could be measured from kinetic experiments performed by, e.g., stopped-flow spectrometry, as it was demonstrated for a related pH-responsive bistable rotaxane.[36] Indeed, an accurate knowledge of such an energy diagram implies that the switching properties of the device are fully characterized in terms of both thermodynamics and kinetics.

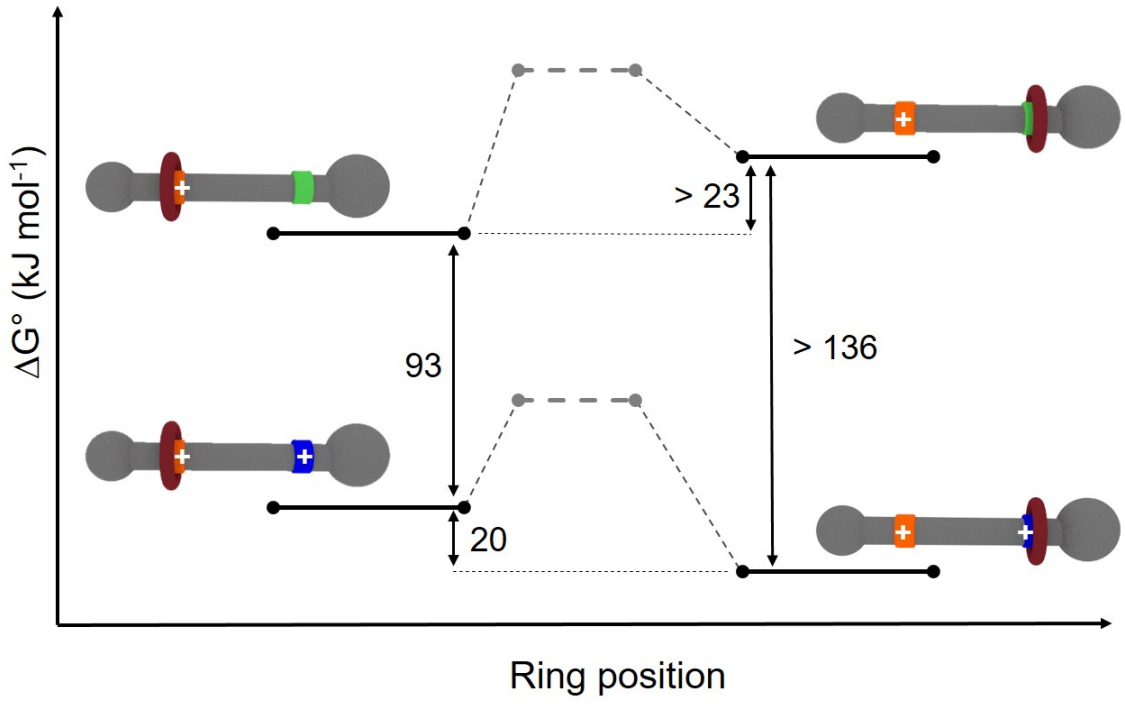

Figure 8.5: *Simplified energy level diagram as a function of the relative ring-axle position for rotaxane* **8.1** *in its protonated (bottom) and deprotonated (top) forms in CH_3CN. Transition states are representate with dashed lines, as no information on them is available in this specific case, the cartoon representation of the involved states follows the same color code used in figure 8.3 and energies are given in kJ mol^{-1} for B = CH_3CN).*

On the basis of the energy levels shown in Figure 8.5 we can evaluate the distribution constant in the deprotonated state to be K'= $[\text{MCC-}\mathbf{8.1}^+]_{eq}/[\text{SCC-}\mathbf{8.1}^+]_{eq}$ $<10^{-4}$. The knowledge of the values of K and K' enables us to make quantitative considerations about the shuttling efficiency of the rotaxane. A constant K = 4000 means that 99.97% of the rings in a population of rotaxanes are located on the primary station (amH^+). On the other hand, with a value of K' lower than 10^{-4}, more than 99.99% of the rings reside on the $tria^+$ station after deprotonation of the ammonium site.

Hence, in the hypothesis that the acid-base switching reactions are performed quantitatively (which can be done by adding a sufficiently strong base or acid in an appropriate excess), the overall yield of the device in a full shuttling cycle (base-induced forward and acid-induced backward movements) amounts to 99.92%.

This is indeed the highest yield reported to date for a stimuli-controlled molecular shuttle. It is worthwhile to note that a rotaxane capable of performing efficient shuttling cycles requires that the co-conformational equilibria in both states (in the present case, the protonated and deprotonated ones) are strongly shifted towards opposite co-conformations (figure 8.3); in other words, the system should be designed such that K is very large while K' is very small. The energy-level diagram shown in figure 8.5 is also interesting because it clearly shows that the acid strength of the pH-switchable site is affected by the position of the ring. Previous experiments indicate that deprotonation of the ammonium unit is extremely difficult to achieve in the absence of an alternative station for the crown ether macrocycle.[20, 41–46] The data collected on the present rotaxane show that the acidity of its ammonium unit changes by at least 7.6 pKa units upon switching the ring position. As a matter of fact, by adjusting the relative stabilities of the SCC and MCC in the protonated and deprotonated forms, one can modulate the acid-base properties of the pH-sensitive station. In principle, such a result could even be achieved by tuning the ring affinity of the sole pH-insensitive station. This observation enables the possibility of designing acid or basic sites with made-to-order pKa using the very same functional group (e.g. a secondary amine as in the present case). In other words, the acid-base properties of the site are determined by its dynamic molecular environment — a behavior which resembles that exhibited by many enzymes.[47–49]

8.5 Conclusions

The distribution between the two translational isomers (co-conformations) in a bistable [2]rotaxane containing DB24C8 as the ring, and ammonium and triazolium recognition sites in its axle, has been quantified with two novel and sensitive methodologies. The first one relies on time-correlated fluorescence measurements and the second one is based on appropriately designed acid-base titrations. The great difference of affinity of the ring for the two stations could be measured in the interlocked compound (logK = 3.6 in CH_3CN). The K values measured from the acid-base and the time-correlated fluorescence assays are the same within errors. While the lifetime-based assay requires a fluorescent rotaxane in which the emissive excited state of the fluorophore is influenced by the position of the ring, the acid-base approach seems more general because in principle it can be

applied to any pH-switchable rotaxane. The sensitivity of the fluorescence assay strongly depends on the spectroscopic differences of the fluorophore in the two different co-conformations. For instance, the higher the quantum yield ratio in favor of the minor (metastable) co-conformation, the more sensitive the measurement. Also, the deconvolution of the emission decay is facilitated if the difference between the lifetimes attributed to the two co-conformations is significant. For the case reported here, K values of ~ 10^3 with an upper limit estimated at ~ 10^4 could be measured. Last but not least, to gain information on the co-conformational equilibrium distribution the emission decay should be faster than the ring shuttling. This requirement is easily fulfilled with organic fluorophores, whose fluorescence lifetimes (~ ns) are much shorter than typical ring shuttling times (~ μs—ms).[36, 37] On the contrary, the acid-base assay does not rely on the photophysical properties of the system (as long as there is an analytical signal to be monitored in the titrations) and its sensitivity is limited only by experimental considerations, for instance, the availability of the suitable bases whose pKa values in the solvent of choice are reported. The results of these experiments, summarized in figure 8.5, not only show that the investigated rotaxane is a highly efficient molecular shuttle, but also indicate that the affinity of the (pH-insensitive) tria$^+$ station for the DB24C8 ring influences the acid-base behavior of the amH$^+$ station. This observation enables the use of programmed allosteric effects to bring about predetermined acid-base properties in artificial multicomponent systems: this is the topic of the following chapter of this thesis.

8.6 References

[1] E. Busseron, C. Romuald, and F. Coutrot. *Chem. Eur. J.*, 16(33):10062–10073, 2010. 73

[2] C. Romuald, E. Busseron, and F. Coutrot. *J. Org. Chem.*, 75:6516–6531, 2010. 73

[3] A. Altieri, F. G. Gatti, E. R. Kay, D. A. Leigh, D. Martel, F. Paolucci, A. M. Z. Slawin, and J. K. Y. Wong. *J. Am. Chem. Soc.*, 125:8644–8654, 2003. 73

[4] F. Scarel, G. Valenti, S. Gaikwad, M. Marcaccio, F. Paolucci, and A. Mateo-Alonso. *Chem. Eur. J.*, 18:14063–14068, 2012. 73

[5] J. W. Choi, A. H. Flood, D. W. Steuerman, S. Nygaard, A. B. Braunschweig, N. N. P. Moonen, B. W. Laursen, Y. Luo, E. Delonno, A. J. Peters, J. O. Jeppesen, K. Xe, J. F. Stoddart, and J. R. Heath. *Chem. Eur. J.*, 12:261–279, 2006. 74

[6] A. C. Fahrenbach, J. C. Barnes, H. Li, D. Benitez, A. N. Basuray, L. Fang, C. H. Sue, G. Barin, S. K. Dey, W. A. Goddard III, and J. F. Stoddart. *Proc. Natl. Acad. Sci. U. S. A.*, 108:20416–20421, 2011. 74

[7] A. C. Fahrenbach, C. J. Burns, D. Cao, and J. F. Stoddart. *Acc. Chem. Res.*, 45:1581–1592, 2012. 74

[8] F. Coutrot. *ChemistryOpen*, 4:556–576, 2015. 75, 76, 80

[9] F. Coutrot and E. Busseron. *Chem. Eur. J.*, 14:4784–4787, 2008. 75, 80

[10] F. Coutrot, C. Romuald, and E. Busseron. *Org. Lett.*, 10:3741–3744, 2010.

[11] C. Romuald, A. Arda, C. Clavel, J. Jimenez-Barbero, and F. Coutrot. *Chem. Sci.*, 3:1851–1857, 2012.

[12] V. Blanco, A. Carlone, K. D. Hänni, D. A. Leigh, and B. Lewandowski. *Angew. Chem., Int. Ed.*, 51:5166–5169, 2012.

[13] E. Busseron and F. Coutrot. *J. Org. Chem.*, 78:4099–4106, 2013.

[14] Z. J. Zhang, M. Han, H. Y. Zhang, and Y. Liu. *Org. Lett.*, 14:1698–1701, 2013.

[15] S. Chao, C. Romuald, K. Fournel-Marotte, C. Clavel, and F. Coutrot. *Angew. Chem. Int. Ed.*, 53:6914–6919, 2014.

[16] V. Blanco, D. A. Leigh, U. Lewandowska, B. Lewandowski, and V. Marcos. *J. Am. Chem. Soc.*, 136:15775–15780, 2014.

[17] V. Blanco, D. A. Leigh, V. Marcos, J. A. Morales-Serna, and A. L. Nussbaumer. *J. Am. Chem. Soc.*, 136:4905–4908, 2014.

[18] Z. Meng and C. F. Chen. *Chem. Commun.*, 51:8241–8244, 2015.

[19] Z. Meng, Y. Han, L. N. Wang, J. F. Xiang, S. G. He, and C. F. Chen. *J. Am. Chem. Soc.*, 137:9739–9745, 2015.

[20] P. Waelès, B. Riss-Yaw, and F. Coutrot. *Chem. Eur. J.*, 22:6837–6845, 2016. 75, 80, 84

[21] J. W. Jones and H. W. Gibson. *J. Am. Chem. Soc.*, 125:7001–7004, 2003. 75

[22] H. W. Gibson, J. W. Jones, L. N. Zakharov, A. L. Rheingold, and C. Slebodnick. *Chem. Eur. J.*, 17:3192–3206, 2011. 75

[23] M. Montalti, R. Ballardini, L. Prodi, and V. Balzani. *Chem. Commun.*, pages 2011–2012, 1996. 76

[24] G. Ragazzon, M. Baroncini, S. Silvi, M. Venturi, and A. Credi. *Nat. Nanotechnol.*, 10:70–75, 2015. 76

[25] G. Ragazzon, A. Credi, and B. Colasson. *Chem. Eur. J.*, 23:2149–2156, 2017. 76

[26] M. Xue, Y. Yang, X. Chi, X. Yan, and F. Huang. *Chem. Rev.*, 115:7398–7501, 2015. 76

[27] G. W. H. Wurpel, A. M. Brouwer, I. H. M. van Stokkum, A. Farran, and D. A. Leigh. *J. Am. Chem. Soc.*, 123:11327–11328, 2011.

[28] H. Zhang, J. Hu, and D. H. Qu. *Org. Lett.*, 14:2334–2337, 2012.

[29] H. Zhang, B. Zhou, H. Li, D. H. Qu, and H. Tian. *J. Org. Chem.*, 78:2091–2098, 2013. 76

[30] V. Wintgens, P. Valat, J. Kossanyi, L. Biczok, A. Demeter, and T. Bérces. *J. Chem. Soc. Faraday Trans.*, 90:411–421, 1994. 77

[31] D. W. Cho, M. Fujitsuka, U. C. Yoon, and T. Majima. *Phys. Chem. Chem. Phys.*, 10:4393–4399, 2008. 77

[32] M. T. Morgan, S. Sumalekshmy, M. Sarwar, H. Beck, S. Crooke, and C. J. Fahrni. *J. Phys. Chem. B*, 118:14196–14202, 2014. 77

[33] P. R. Ashton, I. Baxter, M. C. T. Fyfe, F. M. Raymo, N. Spencer, J. F. Stoddart, A. J. P. White, and D. J. Williams. *J. Am. Chem. Soc.*, 120:2297–2307, 1998. 77

[34] V. Bleve, C. Schäfer, P. Franchi, S. Silvi, E. Mezzina, A. Credi, and M. Lucarini. *ChemistryOpen*, 4:18–21, 2015.

[35] P. Franchi, V. Bleve, E. Mezzina, C. Schäfer, G. Ragazzon, M. Albertini, D. Carbonera, A. Credi, M. Di Valentin, and M. Lucarini. *Chem. Eur. J.*, 22:8745–8750, 2016. 77

[36] S. Garaudée, S. Silvi, M. Venturi, A. Credi, A. H. Flood, and J. F. Stoddart. *ChemPhysChem*, 6(10):2145–2152, 2005. 77, 83, 85

[37] A. M. Brouwer, C. Frochot, F. G. Gatti, D. A. Leigh, L. Mottier, F. Paolucci, S. Roffia, and G. W. H. Wurpel. *Science*, 291:2124–2128, 2001. 77, 85

[38] J. R. Lakowicz. *Principles of Fluorescence Spectroscopy, 3rd Ed.* Springer, Berlin, 2006. 78

[39] I. Kaljurand, A. Kütt, L. Sooväli, T. Rodima, V. Mäemets, I. Leito, and I. A. Koppel. *J. Org. Chem.*, 70:1019–1028, 2005. 81

[40] J. M. Darmon, N. Kumar, E. B. Hulley, C. J. Weiss, S. Raugei, R. M. Bullock, and M. L. Helm. *Chem. Sci.*, 6:2737–2745, 2015. 82

[41] C. Romuald, E. Busseron, and F. Coutrot. *J. Org. Chem.*, 75:6516–6531, 2010. 84

[42] N. Kihara, Y. Tachibana, H. Kawasaki, and T. Takata. *Chem. Lett.*, pages 506–507, 2000.

[43] K. Nakazono and T. Takata. *Chem. Eur. J.*, 16:13783–13794, 2010.

[44] D. A. Leigh and A. R. Thomson. *Tetrahedron*, 64:8411–8416, 2008.

[45] J. Cao, M. C. T. Fyfe, J. F. Stoddart, G. R. L. Cousins, and P. T. Glink. *J. Org. Chem.*, 65:1937–1946, 2000.

[46] J. D. Badjić, V. Balzani, A. Credi, J. N. Lowe, S. Silvi, and J. F. Stoddart. *Chem. Eur. J.*, 10:1926–1935, 2004. 84

[47] T. K. Harris and G. J. Turner. *IUBMB Life*, 53:85–98, 2002. 84

[48] C. N. Pace, G. R. Grimsley, and J. M. Scholtz. *J. Biol. Chem.*, 284:13285–13289, 2009.

[49] H. N. Motlagh, J. O. Wrabl, J. Li, and V. J. Hilser. *Nature*, 508:331–339, 2014. 84

9

Redox switching of pKa through mechanical allostery

9.1 Introduction

In the previous chapter it was shown that in acid-base switchable rotaxanes the pKa of the pH-sensitive station depends on the affinity of the ring component for the secondary station. In this chapter an acid/base switchable rotaxane at study in our group[see ref. 1, and chapter 10 of this thesis] is investigated to demonstrate that modulation of the affinity of the ring for the second station allows the reversible modulation of the pKa of the acid/base station, within the same system. The system at study (figure 9.1) takes advantage of a rotaxane architecture widely studied by us and others.[2–15] The dumbbell component bears a dibenzylammonium (amH^+) and a 4,4'-bipyridinium (bpy^{2+}) site, that serve as recognition sites for a functionalized dibenzo[24]crown[8] macrocycle (DB24C8R). In the protonated rotaxane (**9.1**H^{3+}) DB24C8R encircles almost exclusively amH^+. On the contrary in the presence of a suitable base the rotaxane is deprotonated and DB24C8R relocates over the bpy^{2+} unit, where it is engaged in charge-transfer interactions. The acid-base shuttling reaction is schematized in figure 9.1. Accordingly, since deprotonation and switching are thermodynamically coupled, **9.1**$^{2+}$ (DB24C8R⊂bpy^{2+}) is the apparent conjugate base of **9.1**H^{3+} (DB24C8R⊂amH^+).[16] In particular it is important to note that the DB24C8R-bpy^{2+} charge-transfer interaction is present only in the conjugated base. For this reason we hypotesized that reducing the bpy^{2+} unit could destabilize the intercomponent interaction in the conjugate base, while leaving unaffected the amH^+-DB24C8R interaction in the acid form **9.1**H^{3+}, since the macrocycle is far from the bpy unit. This would lead to an increase in the apparent pKa of the ammonium site.

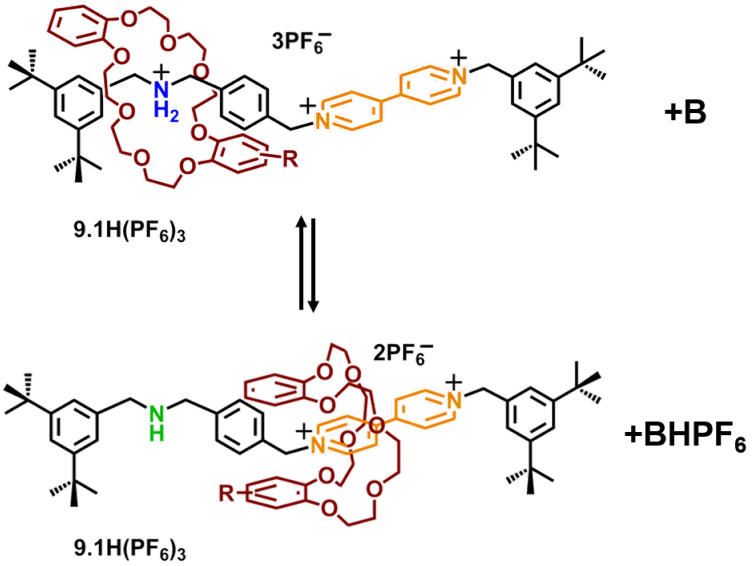

Figure 9.1: *Molecular structure of* $\mathbf{9.1}H^{3+}$ *(DB24C8R⊂amH*$^+$*) and its shuttling reaction upon deprotonation, to afford* $\mathbf{9.1}^{2+}$ *(DB24C8R⊂bpy*$^{2+}$*). R =* $CH_2O(CH_2)_3CN$*. Please refere to the following chapter of this thesis for details on the role of the residue R connected to the macrocycle.*

9.2 Electrochemical investigation

It has already been reported[1, 2] that in this rotaxane architecture when DB24C8R is located on bpy^{2+} the reduction of the latter occurs at more negative potentials. Cyclic voltammetry is therefore a powerful technique to assess the position of DB24C8R. For this reason, to investigate the ability to influence the ammonium apparent pKa upon bpy^{2+} reduction, the electrochemical properties of the rotaxane alone and in the presence of different bases were studied, and compared to that of the axle component. The reduction potentials of the axle are only minimally affected by the protonation state of the ammonium station, proving that the two sites are electronically decoupled and do not communicate. In the case of $\mathbf{9.1}H^{3+}$, the first and second reduction processes occur almost at the same potential as in the axle (figure 9.2 black curves), indicating that DB24C8R encircles amH^+. On the contrary in the presence of a strong base (phosphazene P_1-*t*Bu, pKa = 26.98[17]) both reduction processes are shifted to more negative potentials (figure 9.2 middle). This is consistent with the fact that DB24C8R resides on the bpy site regardless of its redox state[18, 19]. Instead when a milder base (tributhylamine, TBA, pKa = 18.26[20]) is used, the first reduction process of

bpy^{2+} becomes irreversible (figure 9.2 bottom), with a peak to peak separation of 263 mV. This observation is consistent with the reduction of bpy^{2+} while encircled by DB24C8R, followed by shuttling of DB24C8R away from $bpy^{+\bullet}$ and reoxidation of the "free" $bpy^{+\bullet}$. Since this behaviour is not observed in the presence of P_1-*t*Bu, the base must be involved in the backward shuttling process. Considering this, most likely the shuttling of DB24C8R occurs from $bpy^{+\bullet}$ to amH^+, that is formed as a consequence of coupled $TBAH^+$ deprotonation. Indeed the second reduction peak of the bpy^{2+} unit falls at the same potential (within error) of starting $\mathbf{9.1}H^{3+}$. This explanation implies that in the presence of TBA the state [$\mathbf{9.1}^{2+}$ (DB24C8R⊂bpy^{2+}) + $TBAH^+$] is more stable than [$\mathbf{9.1}H^{3+}$ (DB24C8R⊂amH^+) + TBA], however upon reduction the relative stabilities of these states are inverted and [$\mathbf{9.1}^{+\bullet}$ (DB24C8R⊂$bpy^{+\bullet}$) + $TBAH^+$] is less stable than [$\mathbf{9.1}H^{2+\bullet}$ (DB24C8R⊂amH^+) + TBA]. The processes are summarized in equations 9.1 and 9.2 where B = TBA.

$$\mathbf{9.1}H^{3+} + B \underset{\leftarrow}{\longrightarrow} \mathbf{9.1}^{2+} + BH^+ \tag{9.1}$$

$$\mathbf{9.1}H^{+\bullet} + B \overset{\rightarrow}{\longleftarrow} \mathbf{9.1}^{+\bullet} + BH^+ \tag{9.2}$$

This inversion of the relative stabilities occurs because of the presence of the macrocycle, as it can backshuttle on the ammonium site that is obtained upon coupled $TBAH^+$ deprotonation, thus restoring favourable hydrogen-bonding interactions, while avoiding being in an energetically less favoured situation (around $bpy^{+\bullet}$). Since in this process energy is spent to deprotonate the base, shuttling back is allowed in the presence of a mild base (TBA) but becomes energetically unfavourable when a much stronger base (P_1-*t*Bu) is used, consistently with our observations. A consequence of this mechanism is that the amine is more easy to protonate when bpy^{2+} is reduced, i.e., the apparent pKa of ammonium increases upon reduction of bpy^{2+}. Overall a redox input at the bpy^{2+} station modulates the basicity of the amine — the other station — thanks to the shuttling ability of the macrocycle. EPR measurements performed in the group of Prof. Lucarini[1] confirmed that when the bpy^{2+} unit is reduced to $bpy^{+\bullet}$, DB24C8R is located on $bpy^{+\bullet}$ only when (P_1-*t*Bu) is present, while in the presence of TBA it is located on amH^+.

[1] Unpublished results.

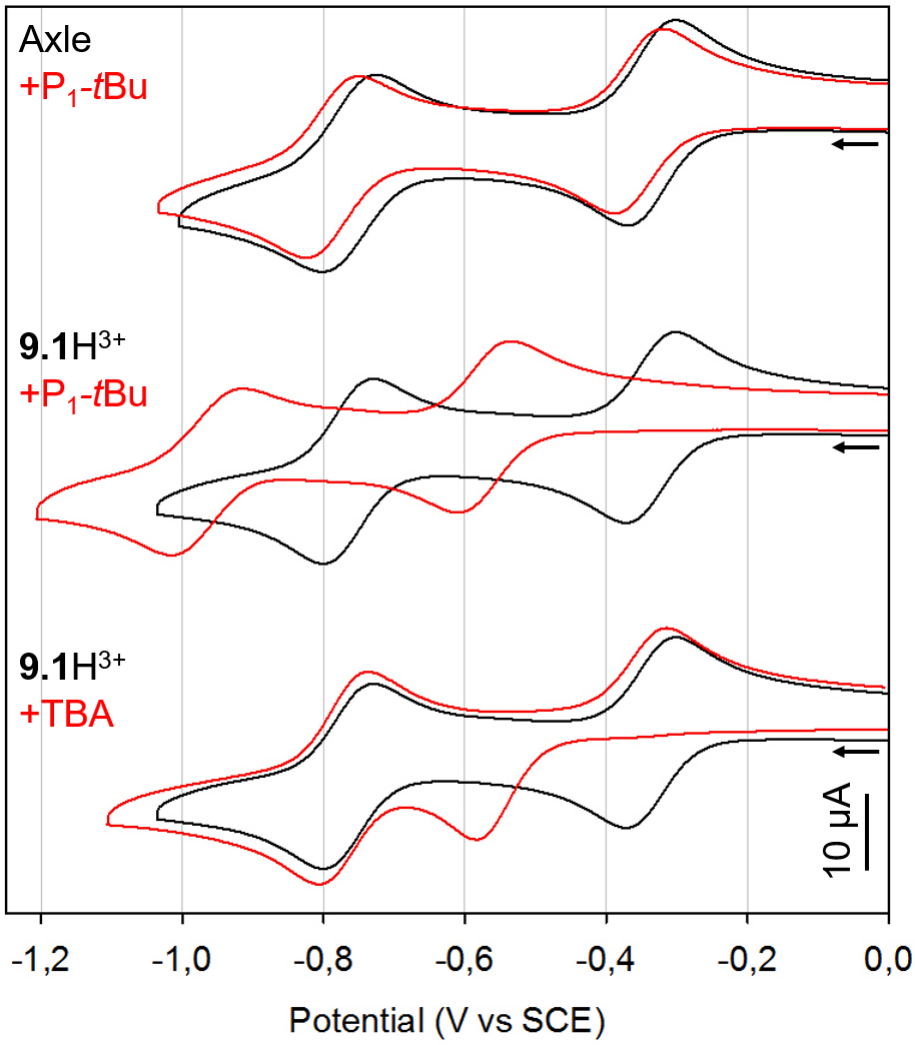

Figure 9.2: *Cyclic voltammogram of the axle component (top) and rotaxane* **9.1**H^{3+} *(middle and bottom) as dissolved (black curves) and upon addition of base (red curves, 1 eq. of* P_1-t*Bu or 22.4 eq. of TBA). Base-induced changes are fully reversible upon addition of an equimolar amount of triflic acid. Conditions: argon-purged ACN, 0.04 M tetraethylammonium hexafluorophosphate, 300 µM analyte, scan rate 300 mV* s^{-1}.

9.3 Energetic considerations

An energy level diagram can be associated to this system. The rotaxane explores states in which both the redox state of bpy^{2+} and the base change, besides the position of the ring. For this reason, instead of reporting $\Delta G°$, suitably chosen $\Delta(\Delta G°)$ are used, in order to afford a more informative

representation in which different bases and redox states can be compared in a useful manner: when comparing different bases, only the difference in their pKa is considered; when comparing different redox states, only the change induced in the energy of the charge-transfer interaction between DB24C8R and bpy is considered. The energy level diagram of the explored states is reported in figure 9.3.

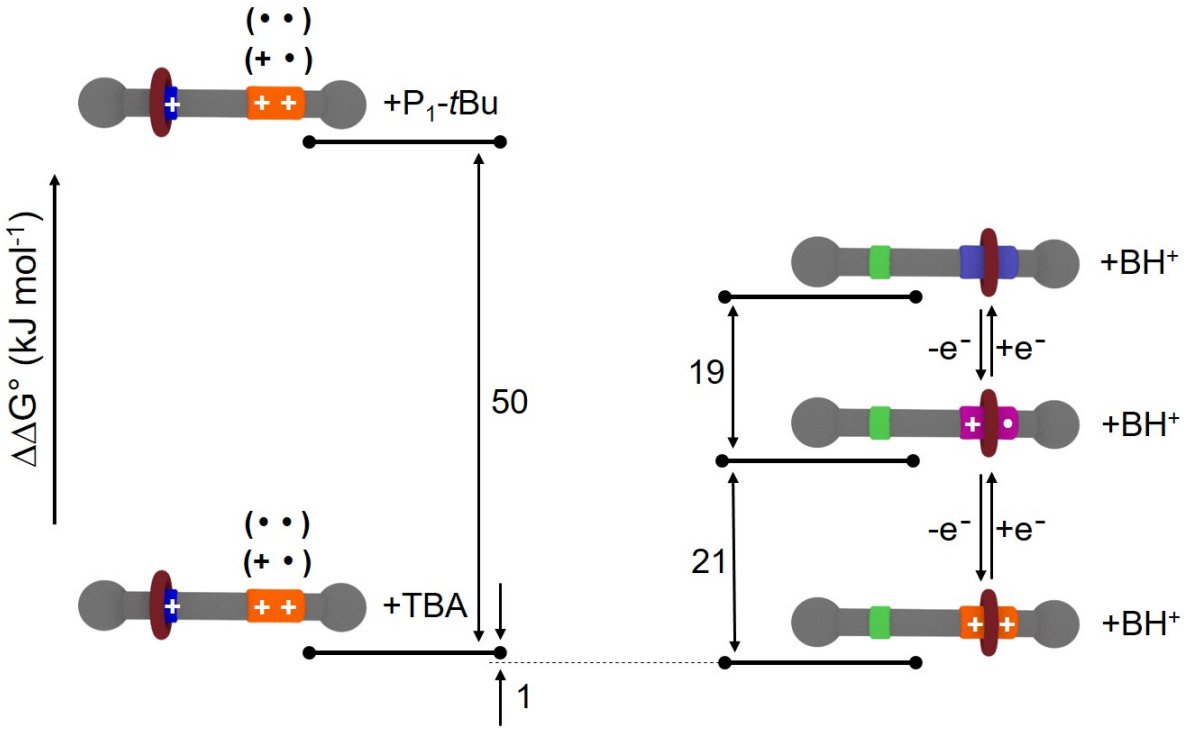

Figure 9.3: *Energy level diagram of the accessible states. The cartoon representation uses the color code introduced in figure 9.1. To compare different bases, the energy of the protonated form of different bases have been matched. To compare different redox states the energies of different redox states where DB24C8R is not engaged in charge-transfer interactions with bpy have been matched. For this reason the energy levels of the not shown* **9.1**$H^{2+\bullet}$*rad (DB24C8R⊂amH*$^+$*) and* **9.1**H^+ *(DB24C8R⊂amH*$^+$*) correspond to the energy levels associated to* **9.1**H^{3+} *(DB24C8R⊂amH*$^+$*)(see text for more details).*

Under the reasonable approximation that reducing bpy^{2+} only marginally affects the amH^+-DB24C8R interaction, the energies of the states with DB24C8R⊂amH^+ do not depend from the redox state of bpy^{2+}. In this representation the energy difference of 50 kJ mol^{-1} between [**9.1**H^{3+} + TBA] and [**9.1**H^{3+} + P_1-*t*Bu] corresponds to the difference of pKa between the two bases. The energy dfference of 1 kJ mol^{-1} between [**9.1**H^{3+} + TBA] and [**9.1**$^{2+}$ + $TBAH^+$] is obtained upon

titration of **9.1**H^{3+} with TBA and it follows that the pKa of **9.1**H^{3+} is 18.1.

The energy increase of 21 kJ mol^{-1} in going from [**9.1**$^{2+}$ (DB24C8R⊂bpy^{2+}) + BH^{+}] to [**9.1**H$^{+\bullet}$ (DB24C8R⊂bpy$^{+\bullet}$) + BH^{+}] corresponds to the destabilization of the charge-transfer interaction between bpy^{2+} and DB24C8R occurring upon reduction. This value is estimated from the square thermodynamic cycle reported in figure 9.4 based on acid-base and redox reactions, that connect the two mentioned states and the corresponding ones in which DB24C8R is located on amH^{+}.

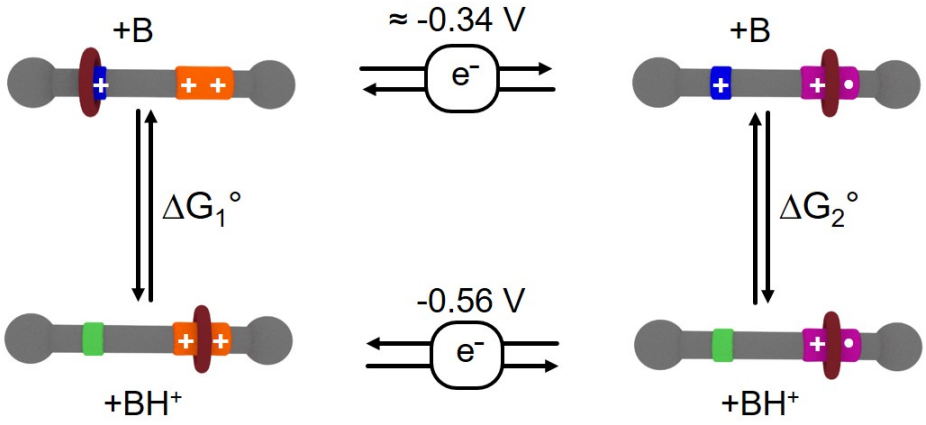

Figure 9.4: *Thermodynamic cycle involving redox and acid-base induced shuttling reactions, by which it is possible to gain informations on the pKa of the singly-reduced state. Potential values are referred to B = P$_1$-t*Bu*. The same color code of figure 9.1 and 9.3 has been used.*

The reduction potential of [**9.1**$^{2+}$ (DB24C8R⊂bpy^{2+}) + P$_1$-*t*BuH^{+}] is experimentally available and the reduction potential of [**9.1**H^{3+} (DB24C8R⊂amH^{+}) + P$_1$-*t*Bu] is reasonably assumed to be equal to that of the rotaxane in the absence of P$_1$-*t*Bu. The difference in the reduction potentials $\Delta E = 0.22$ V = 21 kJ mol^{-1} must reflect the difference between the interaction energies of DB24C8R with bpy^{2+} and bpy$^{+\bullet}$ unit. Indeed the environment of DB24C8R is the same before shuttling for both vertical reactions (DB24C8R⊂amH^{+}), therefore the difference in energy for the two redox reactions arises only from the different charge-transfer interaction in the bottom states. Moreover, it is important to note that $\Delta G_1°$ is related to the pKa's of **9.1**H^{3+} and P$_1$-*t*BuH^{+}, that are both known, therefore of the four steps of the thermodynamic cycle only $\Delta G_2°$ is not known. Its value is related to the pKa values of **9.1**H$^{2+\bullet}$ and P$_1$-*t*BuH^{+}, the latter of which is known, therefore by combining the available data, a pKa of 21.9 is obtained for **9.1**H$^{2+\bullet}$. Analogue considerations led to estimate a destabilization energy of 19 kJ mol^{-1} for the charge transfer interaction in going

from $bpy^{+\bullet}$ to bpy and a pKa of 25.2 for **9.1**H. The resulting energy diagram is fully consistent with all the available experimental evidences. Indeed the pKa of TBA (18.26) is intermediate between those of **9.1**H^{3+} and **9.1**$H^{2+\bullet}$ (18.1 and 21.9 respectively); moreover the pKa of P_1-*t*Bu (26.98)is always higher than the pKa of the rotaxane, regardless of its redox state. In going from [**9.1**H^{3+}] to [**9.1**H] an increase in pKa as large as 7.1 units is observed.
The obtained energy diagram rationalizes the behaviour of the system in the presence of TBA. Upon addition of base to a solution of **9.1**H^{3+}(DB24C8R⊂amH^{+}), **9.1**$^{2+}$(DB24C8R⊂bpy^{2+}) is formed (shuttling-coupled deprotonation). Then reduction of the electroactive bpy^{2+} unit affords **9.1**$^{+\bullet}$(DB24C8R⊂$bpy^{+\bullet}$), that relaxes to the more stable **9.1**$H^{+\bullet}$(DB24C8R⊂amH^{+}) upon proton abstraction from $TBAH^{+}$ (electrochemically induced shuttling-coupled protonation).

9.4 Conclusions

In conclusion it was demonstrated that, in a pH-switchable bistable rotaxane, a redox input at one site can be converted into a pKa change at a distant site, thanks to the shuttling motion of the macrocyclic component. Remarkably, reduction of the secondary station induces a fully reversible change of 7.1 pKa units in the basicity of the pH-sensitive station. This process conceptually mimicks protein complex I operation in a minimal synthetic system and there are no theoretical limitations to extend this strategy to other types of inputs or outputs.

9.5 References

[1] C. Schäfer, G. Ragazzon, B. Colasson, M. La Rosa, S. Silvi, and A. Credi. *ChemistryOpen*, 5:120–124, 2016. 89, 90

[2] P. R. Ashton, R. Ballardini, V. Balzani, I. Baxter, A. Credi, M. C. T. Fyfe, M. T. Gandolfi, M. Gómez–López, M. V. Martinez–Dìaz, A. Piersanti, N. Spencer, J. F. Stoddart, M. Venturi, A. J. P. White, and D. J. Williams. *J. Am. Chem. Soc.*, 120:11932–11942, 1998. 89, 90

[3] P. R. Ashton, V. Baldoni, V. Balzani, A. Credi, H. D. A. Hoffmann, M. Martínez–Dìaz, F. M. Raymo, J. F. Stoddart, and M. Venturi. *Chem. Eur. J.*, 7:3482–3493, 2001.

[4] L. Frankfort and K. Sohlberg. *J. Mol. Struct. Theochem*, 621:253–260, 2003.

[5] J. D. Badjic, V. Balzani, A. Credi, S. Silvi, and J. F. Stoddart. *Science*, 303:1845–1849, 2004.

[6] S. Garaudée, S. Silvi, M. Venturi, A. Credi, A. H. Flood, and J. F. Stoddart. *ChemPhysChem*, 6(10):2145–2152, 2005.

[7] K.-W. Cheng, C.-C. Lai, P.-T. Chiang, and S.-H. Chiu. *Chem. Commun.*, pages 2854–2856, 2006.

[8] J. D. Badjić, C. M. Ronconi, J. F. Stoddart, V. Balzani, S. Silvi, and A. Credi. *J. Am. Chem. Soc.*, 128:1489–1499, 2006.

[9] J. Wu, K. C. Leung, D. Benítez, J. Han, S. J. Cantrill, L. Fang, and J. F. Stoddart. *Angew. Chem. Int. Ed.*, 47:7470–7474, 2008.

[10] J. Li, Y. Li, Y. Guo, J. Xu, J. Lv, Y. Li, H. Liu, S. Wang, and D. Zhu. *Chem. Asian J.*, 3:2091–2096, 2008.

[11] M. Hmadeh, L. Fang, A. Trabolsi, M. Elhabiri, A. Albrecht-Gary, and J. F. Stoddart. *J. Mater. Chem.*, 20:3422–3430, 2010.

[12] W. Zhou, Y. Wu, B. Zhai, Q. Wang, and D. Qu. *RSC Adv.*, 4:5148–5151, 2014.

[13] V. Bleve, C. Schäfer, P. Franchi, S. Silvi, E. Mezzina, A. Credi, and M. Lucarini. *ChemistryOpen*, 4:18–21, 2015.

[14] P. Franchi, V. Bleve, E. Mezzina, C. Schäfer, G. Ragazzon, M. Albertini, D. Carbonera, A. Credi, M. Di Valentin, and M. Lucarini. *Chem. Eur. J.*, 22:8745–8750, 2016.

[15] X. Ma, J. Zhang, J. Cao, X. Yao, T. Cao, Y. Gong, C. Zhao, and H. Tian. *Chem. Sci.*, 7:4582–4588, 2016. 89

[16] G. Ragazzon, A. Credi, and B. Colasson. *Chem. Eur. J.*, 23:2149–2156, 2017. 89

[17] I. Kaljurand, A. Kütt, L. Sooväli, T. Rodima, V. Mäemets, I. Leito, and I. A. Koppel. *J. Org. Chem.*, 70:1019–1028, 2005. 90

[18] B. Long, K. Nikitin, and D. Fitzmaurice. *J. Am. Chem. Soc.*, 125:15490–15498, 2003. 90

[19] S. Altobello, K. Nikitin, J. K. Stolarczyk, E. Lestini, and D. Fitzmaurice. *Chem. Eur. J.*, 14:1107–1116, 2008. 90

[20] G. R. Padmanabhan J. F. Coetzee. *J. Am. Chem. Soc.*, 87:5005–5010, 1965. 90

10

A molecular transporter

10.1 Introducition

A key biological function of molecular machines is the controlled and directed transport of substrates within cells.[1, 2] While small molecules and ions diffuse to where they are needed, entities such as vesicles or organelles are too large to diffuse through the cytosol and need to be transported by motor proteins. These devices contain a motor domain that moves directionally along a track by consuming ATP as a fuel, and an extremity to which appropriate cargos can be attached and detached on demand. Indeed, the development of synthetic nanoscale machines [3–5] that can actively transport molecular or ionic substrates [6, 7] along specific directions[8–10] is a stimulating task in nanoscience and can open up unconventional routes in catalysis, smart materials, energy conversion and storage, and medical therapy.[11–17] In this chapter, the rotaxane that was introduced in the previous chapter is operated as a molecular device able to carry out controlled and directed transport of a nanometer-scale cargo.

10.2 Design and individual components

The designed strategy (figure 10.1) relies on the use of a bistable molecular shuttle[18, 19] in which the macrocyclic component can selectively bind and release a cargo. For rotaxanes with functional units attached to the ring component, see [12, 20–22]. From a functional point of view the design

This chapter is partially derived — with permission — from C. Schäefer, G. Ragazzon, B. Colasson, M. La Rosa, S. Silvi, A. Credi, "An artificial molecular transporter" *ChemistryOpen*, **2016**, 5, 120 - 124.

of such a device must consider the following requirements: (i) the cargo loading/unloading and ring transfer/return processes should be independent from one another, and controlled by orthogonal stimuli, (ii) they should be reversible, and (iii) the cargo should remain bound to the machine during the shuttling. Examples of reversible switching among more than two structurally different (supra)molecular states in response to distinct non-interfering stimuli (points (i) and (ii)), as shown in figure 10.1, are rare.[23–28] Point (iii) is also very challenging, especially in combination with the first two requirements, as it calls for the use of kinetically inert bonds for the cargo-transporter link rather than dynamic supramolecular interactions.[29]

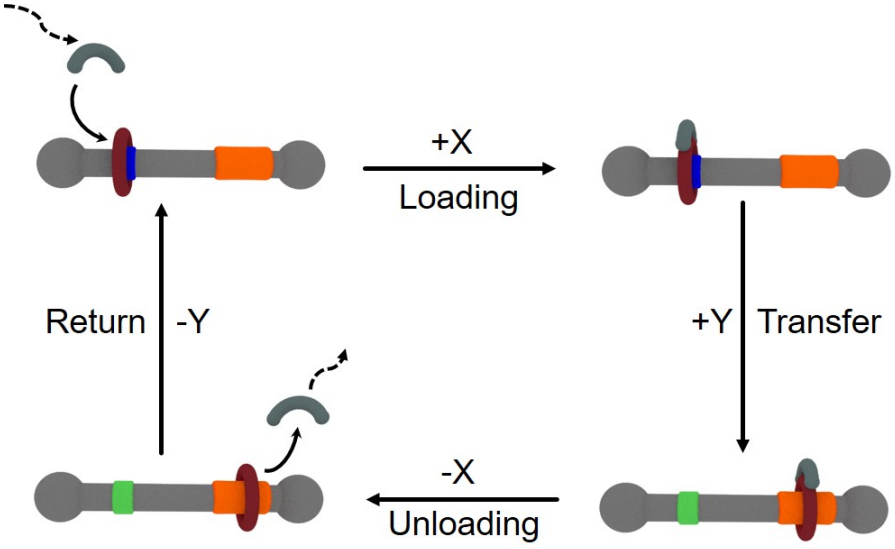

Figure 10.1: *Design of a molecular transporter based on a bistable rotaxane shuttle and operated by two independent external stimuli X and Y.*

The rotaxane architecture introduced in the previous chapter of this thesis satisfies the outlined requirements. In particular the structure of **9.1**H^{3+} was designed endowing the DB24C8R ring with a short tether ending with a nitrile unit that can serve as an anchor for the cargo (figure 10.2a). Similarly as discussed in chapter 9, where the experiments were performed in acetonitrile, also in acetone the molecular ring in **9.1**H^{3+} occupies the amH^{+} site in the as-dissolved rotaxane; the addition of 1 equivalent of a phosphazene base (P$_1$-*t*Bu) affords quantitatively **9.1**$^{2+}$in which the ring encircles the bpy site. The addition of a stoichiometric amount of triflic acid to **9.1**$^{2+}$, with respect to the previously added base, regenerates **9.1**H^{3+} and the ring returns to the amH^{+} site. In addition to ^{1}H NMR and UV-visible spectroscopies, the mechanical switching process schematized in

figure 10.2 can be conveniently observed by voltammetry also in acetone. The cyclic voltammogram of **9.1**H^{3+} (figure 10.2, top, full trace) exhibits two reversible monoelectronic reduction processes with $E_{1/2}$ values at −0.35 and −0.75 V, clearly assigned to the bipyridinium unit. These values are consistent with a co-conformation in which the ring is located on the amH$^+$ site and does not interact with the bpy site. The addition of base to **9.1**H^{3+} affords **9.1**$^{2+}$, whose reduction processes (figure 10.2, bottom trace) are both significantly shifted to more negative potentials. Such an observation clearly indicates that the bipyridinium site is now surrounded by the ring and is involved in charge-transfer interactions.[see 30, and previous chapter of this thesis] The initial voltammetric pattern is restored upon successive addition of acid that regenerates **9.1**H^{3+} (figure 10.2, top, dashed trace).

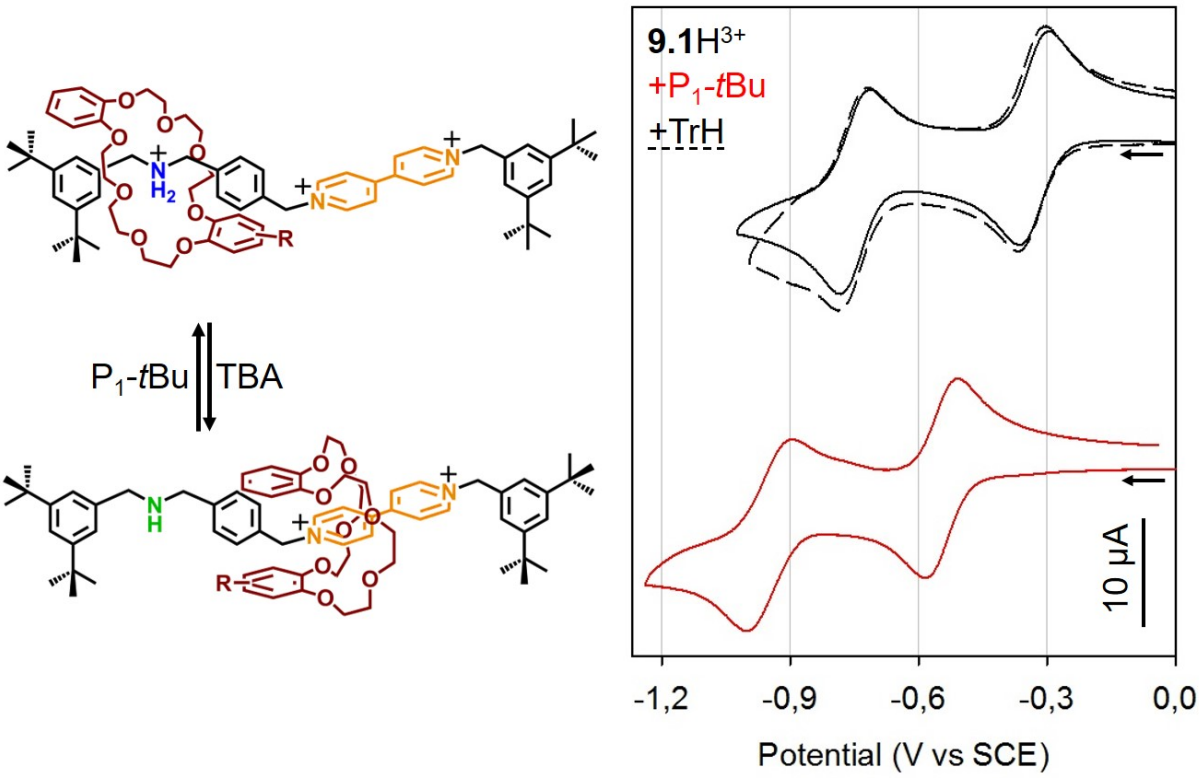

Figure 10.2: *Acid-base controlled ring shuttling in the bistable rotaxane* **9.1***H*$^{3+}$/**9.1**$^{2+}$ *(left). Cyclic voltammogram of* **9.1***H*$^{3+}$ *(black, full line) and of its deprotonated form* **9.1**$^{2+}$ *(red), obtained upon addition of one equivalent of* P_1-t*Bu. The successive addition of triflic acid (TrH) in stoichiometric amount regenerates* **9.1***H*$^{3+}$ *(black, dashed line) Conditions: argon-purged acetone, 0.04 M tetrabutylammonium hexafluorophosphate, 400 µM analyte, scan rate 300 mV* s^{-1}*).*

For the cargo loading/unloading reaction the photochemical decoordination and thermal recoordination of ligands in appropriately designed ruthenium(II) diimine complexes was exploited (figure 10.3).[31, 32] If the complex is sufficiently distorted from the octahedral geometry, such as $[Ru(tpy)(bipy)L]^{2+}$-type species (tpy = 2,2';6',2''-terpyridine, bipy = 2,2'-bipyridine, L = generic monodentate neutral ligand; denoted as $[\mathbf{10.1}\bullet L]^{2+}$), the metal-centered (d-d) excited state (^{3}MC) is lowered in energy such that it can be thermally populated from the lowest metal-to-ligand charge-transfer state (^{3}MLCT) which, in turn, is efficiently obtained by excitation with visible light. As the ^{3}MC state is strongly dissociative, light excitation in this kind of complexes results in the selective expulsion of the monodentate ligand and its replacement by solvent molecules or other entering ligands; successively, the thermally driven recoordination of the expelled ligand may take place in the dark. In recent years the combination of this kind of reaction with cleverly designed molecular and supramolecular species has led to the construction of interesting photoactive systems.[33–38] The behavior of the Ru complex was investigated by monitoring the resonance of the bpy proton in the α-position and close to the monodentate ligand (H^a in figure 10.3). Such a signal is observed as a doublet centered at 9.92 ppm in the ^{1}H NMR spectrum of $[\mathbf{10.1}\bullet CH_3CN]^{2+}$ (figure 10.3, top trace). After 2 h of visible light irradiation this doublet disappears and another signal, assigned to $[\mathbf{10.1}\bullet(CH_3)_2CO]^{2+}$, shows up at 9.73 ppm, indicating that the acetonitrile ligand has been quantitatively dissociated (figure 10.3, middle trace). Another less intense doublet at 9.84 ppm is observed, tentatively attributed to the $[\mathbf{10.1}\bullet H_2O]^{2+}$ species, in which the coordination position left vacant by the leaving CH_3CN ligand is occupied by an adventitious water molecule. If the irradiated solution is left in the dark, the signal corresponding to $[\mathbf{10.1}\bullet(CH_3)_2CO]^{2+}$ decreases and those related to $[\mathbf{10.1}\bullet L]^{2+}$ (L = CH_3CN and L = H_2O) are both enhanced (figure 10.3, bottom trace). The integration of the NMR signals shows that after 7 days, when the equilibrium is reached, the initial $[10.1\bullet CH_3CN]^{2+}$ complex is regenerated with 35% yield. The changes in the coordination sphere of the cargo $\mathbf{10.1}^{2+}$ can also be followed by voltammetric methods. The complex $[\mathbf{10.1}\bullet CH_3CN]^{2+}$ shows a metal-centered reversible oxidation process at +1.35 V. This signal disappears upon irradiation with visible light and another irreversible process with a peak potential of ca. +1.07 V is observed. In agreement with the NMR results, we assign this new peak to the Ru^{II}-Ru^{III} oxidation in the $[\mathbf{10.1}\bullet(CH_3)_2CO]^{2+}$ species. The peak broadens and shifts further to less positive potentials upon aging in the dark. Presumably, under the conditions employed for the voltammetric experiments, the weakly bound acetone molecules are replaced by more effective ligands, such as water molecules, anions, or other impurities.

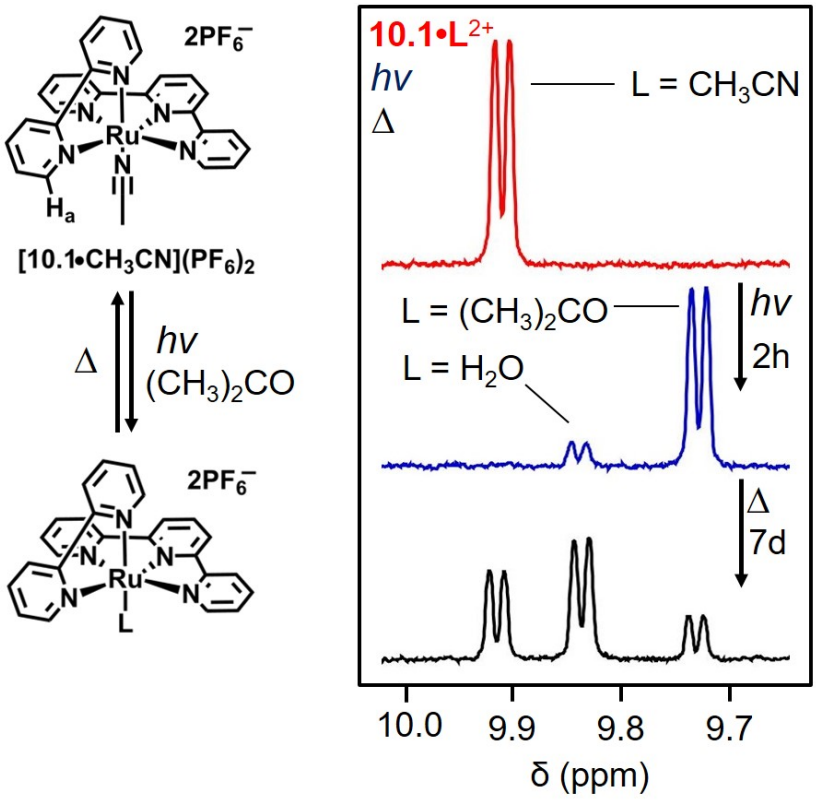

Figure 10.3: *Photoinduced decoordination and thermal recoordination of a monodentate ACN ligand in the Ru^{II} complex [**10.1**•CH_3CN]$^{2+}$ (left). Partial ^{1}H NMR spectra (Acetone-d_6, 400 MHz) of [**10.1**•CH_3CN]$^{2+}$ as dissolved (red) and after irradiation at λ >400 nm for 2 hours (blue); the bottom trace (black) was recorded on the irradiated solution (red) after 7 days in the dark at room temperature.*

It is worth noting that [**10.1**•CH_3CN]$^{2+}$ is insensitive to the addition of the base used to operate the molecular shuttle, and its photoproduct is insensitive to the presence of triflic acid. Both **9.1**H^{3+} and **9.1**$^{2+}$are not affected by visible light irradiation. Considering that the coordination bond linking the cargo to the transporter is kinetically inert at room temperature in the dark, we anticipated that our system could fulfill the functional requirements discussed above.

10.3 Transporter operation

The cargo-loaded transporter [**9.1**H•**10.1**]$^{5+}$ was obtained by visible light irradiation of an acetone solution of [**10.1**•CH_3CN]$^{2+}$ in the presence of 7 equivalents of **9.1**H^{3+} for 10 hours at room temperature (figure 10.4). As discussed above, voltammetric techniques are particularly useful to monitor

the in situ operation of the molecular transporter: the two reversible monoelectronic reduction processes of the bipyridinium unit of the rotaxane are diagnostic for the position of the DB24C8R-type ring along the axle (figure 10.2), whereas the position of the Ru^{II}-Ru^{III} oxidation peak can be used to determine whether the cargo is attached to the rotaxane or not.

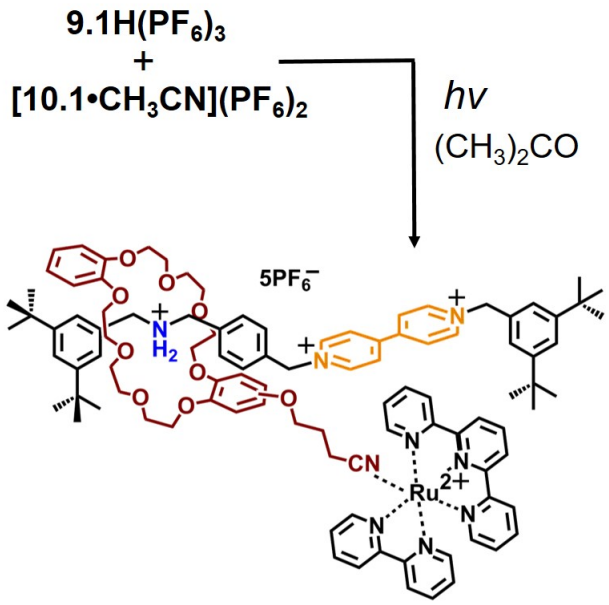

Figure 10.4: *Photochemical synthesis of the cargo-loaded transporter* $[\mathbf{9.1}H\bullet\mathbf{10.1}]^{5+}$.

Figure 10.5 shows a comparison of the differential pulse voltammetric (DPV) peaks measured in the potential window comprised between −0.7 and +1.5 V for the transporter-cargo system during its stimuli controlled switching cycle. The DPV trace of the loaded transporter $[\mathbf{9.1}H\bullet\mathbf{10.1}]^{5+}$ exhibits the expected bipyridinium reduction and the Ru-centered oxidation (figure 10.5, trace I); the corresponding potential values are consistent with the ring being located on the amH^+ site and the cargo being coordinated to the nitrile moiety of the transporter. The addition of the base causes a negative shift of the reduction process and no significant change in the oxidation peak, indicating the displacement of the ring from amH^+ to bpy with the Ru complex attached to it (figure 10.5, trace II). Successive irradiation in the visible (λ >400 nm) causes the complete detachment of the cargo, as witnessed by the disappearance of the oxidation peak at +1.34 V and the growth of signals at less positive potentials (figure 10.5, trace III). The invariance of the reduction peak at −0.53 V indicates that the ring is still occupying the bpy site. The DPV scan obtained after

acidification of the solution (figure 10.5, trace IV) shows that the unloaded ring goes back to the amH^+ site. At this point, in principle, the transporter would be ready to be reloaded with another cargo molecule. Practically, however, the thermally driven reloading in situ after the electrochemical experiments described in figure 10.5 was not obtained, most likely because the weakly bound solvent molecule that occupies the coordination position made free in the $[Ru(tpy)(bipy)]^{2+}$ complex after photodissociation is replaced by a stronger ligand and is no longer available for recoordination to the molecular transporter (see above), which is present in stoichiometric amount.

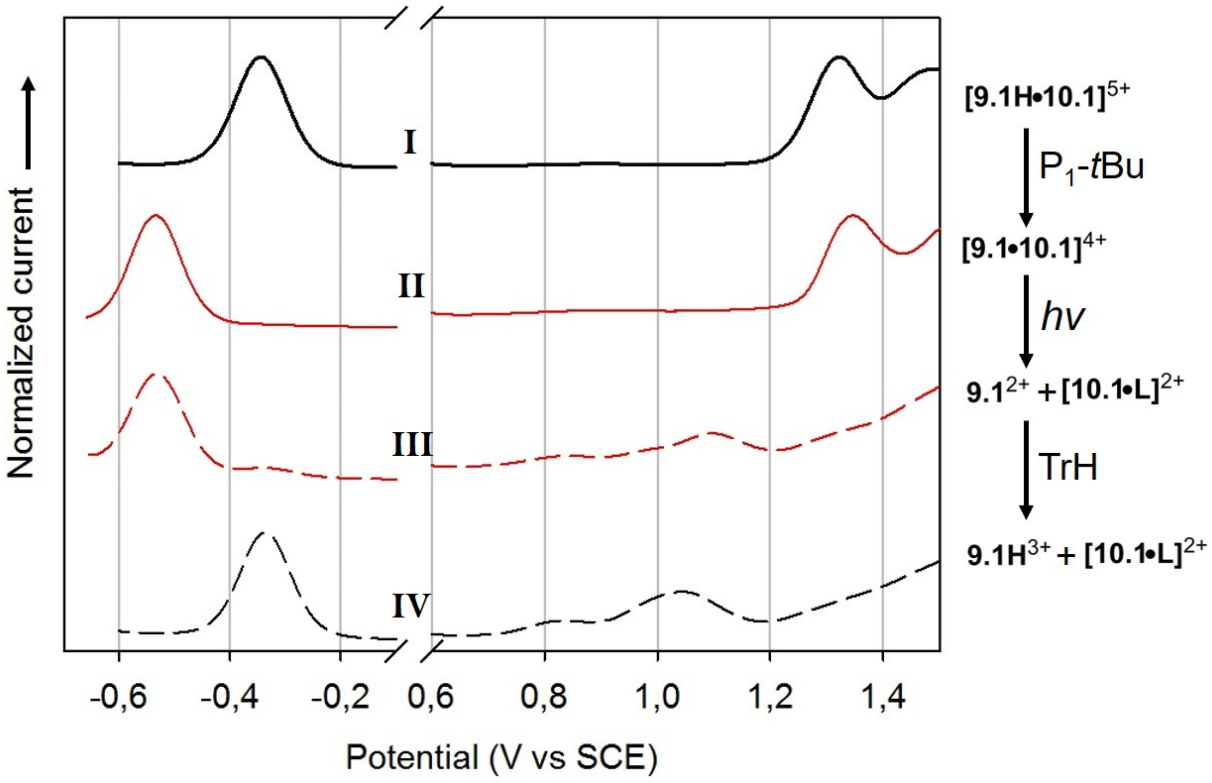

Figure 10.5: *Differential pulse voltammograms of a solution of the loaded transporter* $[\mathbf{9.1}H\bullet\mathbf{10.1}]^{5+}$ *(I) subjected to the following sequence of stimuli: addition of 1 eq. of the* P_1-tBu *base (II), irradiation at* λ *>400 nm for 1h (III), and addition of 1 eq. of triflic acid (TrH, IV). Black and re traces correspond to protonated and deprotonated states, respectively; full and dashed traces correspond to loaded and unloaded states, respectively. Conditions: argon-purged acetone, 0.04M tetrabutylammoinium hexafluorophosphate,* $400\mu M$ *anlyte, 20 mV* s^{-1}*).*

To investigate further the coupled operation of the switching processes in our system, we generated the unloaded transporter $\mathbf{9.1}H^{3+}$ and the $[\mathbf{10.1}\bullet L]^{2+}$ cargo in a 1:1 ratio by visible light

irradiation of $[\mathbf{9.1}H\bullet\mathbf{10.1}]^{5+}$, and we successively left the solution in the dark at room temperature. The analysis of the DPV peak intensity indicates that the thermally driven recoordination of the Ru complex to obtain the $[\mathbf{9.1}H\bullet\mathbf{10.1}]^{5+}$ species takes place with a yield of about 30%, in agreement with the results obtained for the $[\mathbf{10.1}\bullet L]^{2+}$ complex. Thereafter, electrochemical measurements revealed that the so-produced reloaded transporter can be displaced by addition of base and unloaded photochemically. In this experiment, however, the addition of acid to complete the cycle (figure 10.1) caused a degradation of the system, presumably because the products arising from thermal recoordination of the photodissociated $\mathbf{10.1}^{2+}$ complex undergo a decomposition reaction in the presence of acid.

10.4 Conclusions

In summary, a strategy for capturing, transporting and releasing a molecular substrate with a synthetic molecular machine in solution under control of external signals has been realized. Owing to the orthogonality of the reactions and the stimuli at the basis of the working mechanism, the loading/unloading and transfer/return processes can be controlled independently. The robust coordination bond ensures that the cargo remains attached to the transporter during the displacement. The shuttling process is fully reversible both for the loaded and unloaded transporters, and the photochemical unloading of the cargo proceeds with high yields; the thermally driven in situ reloading, however, is not completely efficient and generates byproducts that interfere with the operation of the machine. An important feature of the transporter approach is that the transport direction is fixed and dictated with nanoscale precision by the orientation of the track. Such a gain in directionality is balanced by the slow transport rate: on the basis of kinetic data obtained on a parent rotaxane under similar conditions,[39] the shuttling is expected to need hundreds of milliseconds at room temperature, while the cargo would cover the same distance (ca. 0.7 nm)[30, 39, 40] in less than 1 ns by diffusion.[1] In the present prototype the travelled distance is quite short, however it has been demonstrated that in similar rotaxane architectures with much longer spacers, shuttling occurs on the same timescale,[42] therefore other rotaxanes based on the same architecture but bearig longer spacers should work in analogous manner. Interestingly, although other systems that perform the translocation of a molecular cargo at the nanoscale have been reported[43–45], the illustrated system remains — to the best of my knowledge — the sole able to pick-up a cargo from solution, while

[1] The diffusion time can be estimated with the equation expressing the mean-square displacement for a three-dimensional random walk, $<r^2> = 6Dt$, taking $<r^2> = 1\ nm^2$ and $D = 1\times10^{-5}\ cm^2/s$. See [41]

binding it with a stable covalent bond, that is a key requirement to be sure that the cargo remains bound to the rotaxane architechture while it is moved from one site to the other.

10.5 References

[1] D.S. Goodsell. *Bionanotechnology.* Wiley, Hoboken, 2004. 97

[2] *Molecular Motors, Ed.: M. Schliwa.* Wiley-VCH, Weinheim, 2003. 97

[3] V. Balzani, A. Credi, and M. Venturi. *Molecular Devices and Machines, 2nd Ed.* Wiley-VCH, Weinheim, 2008. 97

[4] E. R. Kay, D. A. Leigh, and F. Zerbetto. *Angew. Chem. Int. Ed.*, 46:72–196, 2007.

[5] S. Erbas-Cakmak, D. A. Leigh, C. T. McTernan, and A. L. Nussbaumer. *Chem. Rev.*, 115:10081–10206, 2015. 97

[6] G. Ragazzon, M. Baroncini, S. Silvi, M. Venturi, and A. Credi. *Nat. Nanotechnol.*, 10:70–75, 2015. 97

[7] C. Cheng, P. R. McGonigal, S. T. Schneebeli, H. Li, N. A. Vermeulen, C. Ke, and J. F. Stoddart. *Nat. Nanotechnol.*, 10:547–553, 2015. 97

[8] F. C. Simmel. *ChemPhysChem*, 10:2593–2597, 2009. 97

[9] M. von Delius, E. M. Geertsema, and D. A. Leigh. *Nat. Chem.*, 2:96–101, 2010.

[10] R. A. Muscat, J. Bath, and A. J. Turberfield. *Nano Lett.*, 11:982–987, 2011. 97

[11] H. Gu, S.-J. Kiao, and N. C. Seeman. *Nature*, 465:202–205, 2010. 97

[12] J. Wang and B. L. Feringa. *Science*, 331:1429–1432, 2011. 97

[13] B. Lewandowski, G. De Bo, J. W. Ward, M. Papmeyer, S. Kuschel, M. J. Aldegunde, P. M. E. Gramlich, D. Heckmann, S. M. Goldup, D. D'Souza, A. E. Fernandes, and D. A. Leigh. *Science*, 339:189–193, 2013.

[14] M. Xue and J. I. Zink. *J. Am. Chem. Soc.*, 135:17659–17662, 2013.

[15] S. Chao, C. Romuald, K. Fournel-Marotte, C. Clavel, and F. Coutrot. *Angew. Chem. Int. Ed.*, 53:6914–6919, 2014.

[16] Q. Li, G. Fuks, E. Moulin, M. Maaloum, M. Rawiso, I. Kulic, J. T. Foy, and N. Giuseppone. *Nat. Nanotechnol.*, 10:161–165, 2015.

[17] A. Martinez-Cuezva, S. Valero-Moya, M. Alajarin, and J. Berna. *Chem. Commun.*, 51:15401–15404, 2015. 97

[18] R. A. Bissell, E. Cordova, A. E. Kaifer, and J. F. Stoddart. *Nature*, 369:133–137, 1994. 97

[19] S. Silvi, M. Venturi, and A. Credi. *J. Mater. Chem.*, 19:2279–2294, 2009. 97

[20] A. Mateo-Alonso, C. Ehli, G. M. A. Rahman, D. M. Guldi, G. Fioravanti, M. Marcaccio, F. Paolucci, and M. Prato. *Angew. Chem. Int. Ed.*, 46:3521–3525, 2007. 97

[21] H. Zhang, B. Zhou, H. Li, D.-H. Qu, and H. Tian. *J. Org. Chem.*, 78:2091–2098, 2013.

[22] V. Bleve, C. Schäfer, P. Franchi, S. Silvi, E. Mezzina, A. Credi, and M. Lucarini. *ChemistryOpen*, 4:18–21, 2015. 97

[23] R. Ballardini, V. Balzani, M. Clemente-León, A. Credi, M. T. Gandolfi, E. Ishow, J. Perkins, J. F. Stoddart, H.-R. Tseng, and S. Wenger. *J. Am. Chem. Soc.*, 124:12786–12795, 2002. 98

[24] J. V. Hernandez, E. R. Kay, and D. A. Leigh. *Science*, 306:1532–1537, 2004.

[25] D. Qu, Q. Wang, and H. Tian. *Angew. Chem. Int. Ed.*, 44:5296–5299, 2005.

[26] V. Balzani, M. Clemente-León, A. Credi, B. Ferrer, M. Venturi, A. H. Flood, , and J. F. Stoddart. *Proc. Nat. Acad. Sci. USA*, 103:1178–1183, 2006.

[27] T. Avellini, H. Li, A. Coskun, G. Barin, A. Trabolsi, A. N. Basuray, S. K. Dey, A. Credi, S. Silvi, J. F. Stoddart, and M. Venturi. *Angew. Chem. Int. Ed.*, 51:1611–1615, 2012.

[28] H. Cheng, H. Zhang, and Y. Liu. *J. Am. Chem. Soc.*, 135:10190–10193, 2013. 98

[29] J. Li, Y. Li, Y. Guo, J. Xu, J. Lv, Y. Li, H. Liu, S. Wang, and D. Zhu. *Chem. Asian J.*, 3:2091–2096, 2008. 98

[30] P. R. Ashton, R. Ballardini, V. Balzani, I. Baxter, A. Credi, M. C. T. Fyfe, M. T. Gandolfi, M. Gómez–López, M. V. Martinez–Dìaz, A. Piersanti, N. Spencer, J. F. Stoddart, M. Venturi, A. J. P. White, and D. J. Williams. *J. Am. Chem. Soc.*, 120:11932–11942, 1998. 99, 104

[31] J. Van Houten and R. J. Watts. *Inorg. Chem.*, 17:3381–3385, 1978. 100

[32] A. Juris, V. Balzani, F. Barigelletti, S. Campagna, P. Belser, and A. von Zelewsky. *Coord. Chem. Rev.*, 84:85−−277, 1988. 100

[33] E. R. Schofield, J.-P. Collin, N. Gruber, and J.-P. Sauvage. *Chem. Commun.*, pages 188–189, 2003. 100

[34] P. Mobian, J.-M. Kern, and J.-P. Sauvage. *Angew. Chem. Int. Ed.*, 43:2392–2395, 2004.

[35] S. Bonnet, J.-P. Collin, and J.-P. Sauvage. *Inorg. Chem.*, 45:4024–4034, 2006.

[36] S. Bonnet, B. Limburg, J. D. Meeldijk, R. J. M. Klein Gebbink, and J. A. Killian. *J. Am. Chem. Soc.*, 133:252–261, 2011.

[37] M. Frasconi, Z. Liu, J. Lei, Y. Wu, E. Strekalova, D. Malin, M. W. Ambrogio, X. Chen, Y. Y. Botros, V. L. Cryns, J.-P. Sauvage, and J. F. Stoddart. *J. Am. Chem. Soc.*, 135:11603–11613, 2013.

[38] B. A. Albani, B. Pena, N. A. Leed, N. A. B. G. de Paula, C. Pavani, M. S. Baptista, K. R. Dunbar, and C. Turro. *J. Am. Chem. Soc.*, 136:17095—-17101, 2014. 100

[39] S. Garaudée, S. Silvi, M. Venturi, A. Credi, A. H. Flood, and J. F. Stoddart. *ChemPhysChem*, 6(10):2145–2152, 2005. 104

[40] J. D. Badjić, C. M. Ronconi, J. F. Stoddart, V. Balzani, S. Silvi, and A. Credi. *J. Am. Chem. Soc.*, 128:1489–1499, 2006. 104

[41] H. C. Berg. *Random walks in biology.* Princeton University Press, Princeton, 1993. 104

[42] P. G. Young, K. Hirose, and Y. Tobe. *J. Am. Chem. Soc.*, 136:7899–7906, 2014. 104

[43] J. Li, Y. Li, Y. Guo, J. Xu, J. Lv, Y. Li, H. Liu, S. Wang, and D. Zhu. *Chem. Asian J.*, 3:2091–2096, 2008. 104

[44] S. Kassem, A. T. L. Lee, D. A. Leigh, A. Markevicius, and J. Solá. *Nat. Chem.*, 8:138–143, 2016.

[45] J. Chen, S. J. Wezenberg, and B. L. Feringa. *Chem. Commun.*, 52:6765–6768, 2016. 104

Part IV

A photochemically driven dissipative system

11

Introduction

11.1 Introduction

In this part of the thesis a molecular pump will be presented. This project tackles all the main themes that seem crucial for the development of artificial molecular machines. These themes have been outlined in the introduction of the thesis and are (1) structural complexity, (2) functionality, (3) ratcheting and (4) autonomous operation. In relation to structural complexity the studied system exploits a minimal design. This is important to envision any real-world application of such systems. In terms of functionality, pumping — intended as the unidirectional transit of a molecular entity through a macrocycle — is one of the most sophisticated tasks that can be performed at the molecular level. Moreover, it is a task that can be at the basis of even more elaborated functions e.g. creating a concentration gradient. The first example of a molecular pump was reported by our group[1] and the system described in this section is based on the same conceptual strategy. In recent years another pump module has been developed by the group of Prof. Stoddart.[2, 3] That molecular pump module has so far demonstrated greater capabilities in terms of functionality, indeed two macrocycles could be pumped into a high energy state, however definite proof of the ability of the pump to operate in an autonomous fashion is still missing to date. The ratcheting mechanism, the structural features of the pump module and its functionality have been discussed in detail,[4–6] and will be presented in the next chapter as well. Less attention has been devoted to the pump as a dissipative system, i.e. a system that operates upon continuous fuel consumption under constant environmental conditions. For this reason in this thesis this aspect will be discussed in grater detail.

11.2 Dissipative systems

Dissipative systems are systems that require a constant consumption of energy to maintain a steady-state. Great interest in such system roots into the assignment of the 1977 Nobel Prize in chemistry to Prof. Prigogine, "for his contributions to non-equilibrium thermodynamics, particularly the theory of dissipative structures". About 40 years after that recognition, extreme caution seems advisable in relating current work in the field of supramolecular chemistry to the work of Prigogine. Indeed there are controversy about the implications of its work. As an example 1977 Nobel laureate in Physics Prof. Anderson and Prof. Stein wrote: "Is there a theory of dissipative structures comparable to that of equilibrium structures, explaining the existence of new, stable properties and entities in such systems? [...] Contrary to statements in a number of books and articles in this field, we believe that there is no such theory, and it even may be that there are no such structures as they are implied to exist by Prigogine, Haken, and their collaborators. What does exist in this field is rather different from Prigogine's speculations and is the subject of intense experimental and theoretical investigation at this time.".[7] For this reason in this thesis the relation of the present work with nonequilibrium thermodynamic principles studied by Prigogine and coworkers will not be discussed. However, supramolecular chemists have an interest in dissipative structures that may be considered unrelated to the work of Prigogine, even if they may have taken inspiration from it. Indeed supramolecular chemistry has been developed taking advantage of the properties of equilibrium states (i.e. engineering the minimum of the potential energy surface), but it is clear that working away from equilibrium opens new possibilities. In particular one can distinguish between kinetically trapped systems and dissipative ones. The former have been widely studied, however some examples of dissipative systems have been also investigated. In these systems a continuous supply of energy is required to maintain a target steady state. Examples of kinetic schemes driven by different stimuli are represented in figure 11.1. In all these systems cycling in the clockwise direction is preferred over the opposite anticlockwise direction. In particular the probability of a microtrajectory to occur $\pi(\gamma)$ with respect to its microscopic reverse $\pi^*(\gamma^*)$ depends exponentially on the heat $\Delta Q(\gamma)$ that is dissipated in the surroundings while the forward path is traversed. This is a well known result for thermally evolving systems, but the relation holds even when an arbitrarily time-varying external field is being used to drive the system over the course of the whole trajectory.[8]

$$\frac{\pi(\gamma)}{\pi^*(\gamma^*)} = exp\left[\frac{\Delta Q(\gamma)}{k_B T}\right] \tag{11.1}$$

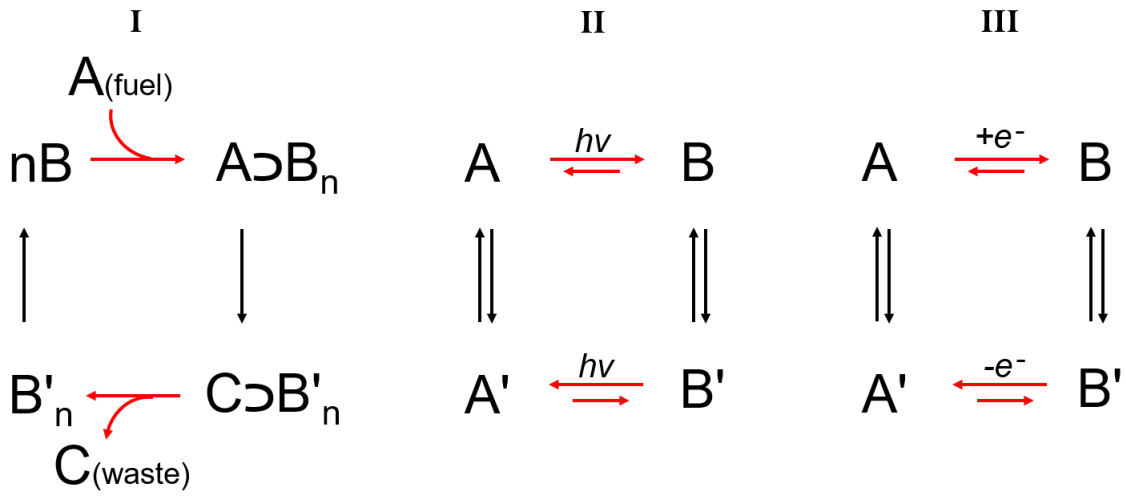

Figure 11.1: *Examples of dissipative reaction networks that are chemically (I), photochemically (II), and electrochemically (III) driven. In (III) the reduction reaction is electrochemically driven at a different potential with respect to the bottom oxidation, as two different redox couples must operate in an electrochemically driven dissipative system. Red arrows highlight the steps that power the cycling of the system.*

Each of these three categories has its own peculiarities. Chemically driven systems exploit the basic operation principles of naturally occurring enzymes: indeed when a chemical reagent is used as the energy source, the kinetic and thermodynamic properties of the system need to be suitably engineered to obtain the desired effect. Materials[9, 10], vescicles[11] and molecular motors[12] that exist or operate under dissipative conditions have been developed. For what concerns redox-driven systems, dissipative operation seems to be possible only exploiting two electrodes at fixed potentials (or two redox couples) and this poses some experimental difficulties, however the creation of a gradient has been demonstrated.[13] Light is probably the most exploited energy input in this context. This is not surprising, because photochemical reactions intrinsically violate the principle of microscopic reversibility, that needs to be not respected in dissipative systems at the steady state.

11.3 Photochemically driven dissipative systems

In principle, a thermally unstable photoswitch can be considered a dissipative system when operated under continuous irradiation. Indeed, a constant energy supply is needed to regenerate the photogenerated and thermally unstable state. In this case the continuous consumption of energy is

necessary only because the chemist has not been capable of obtaining a thermally stable photogenerated species. If the photogenerated species is thermally stable the concentrations of A and B are dictated by the relative speed of the forward and backward photoreactions. Under irradiation with monochromatic light this corresponds to:

$$\frac{[B]}{[A]} = \frac{k_f}{k_b} = \frac{\epsilon_{A\lambda_{irr}}\Phi_{A\to B}}{\epsilon_{B\lambda_{irr}}\Phi_{B\to A}} = K_{\lambda_{irr}} \tag{11.2}$$

where $k_{f/b}$ are the bulk speed of the forward and backward photoreaction, $\epsilon_{A/B\lambda_{irr}}$ are the absorption coefficients of A and B at the irradiation wavelength and Φ are the photoreaction quantum yields. $K_{\lambda_{irr}}$ indicates that for a given irradiation condition the ratio [B]/[A] is fixed, i.e. light constraints the concentration of A and B to a fixed ratio. $K_{\lambda_{irr}}$ is not an equilibrium constant, but at the photostationary state (PSS) the relation must hold.

It will be clear from the following discussion that depending on the reaction network that describes the dissipative system, significant differences in the properties of the dissipative state arise. For this reason a distinction is made: photoswitches are described as a type (I) dissipative system; linear network of reactions that include a photoreaction are described as type (II) dissipative systems, and cyclic network of reactions that include a photoreaction are described as type (III) dissipative systems. For the ease of discussion, an example for each of the three systems is represented in figure 11.2 and the discussion will refer to such examples.

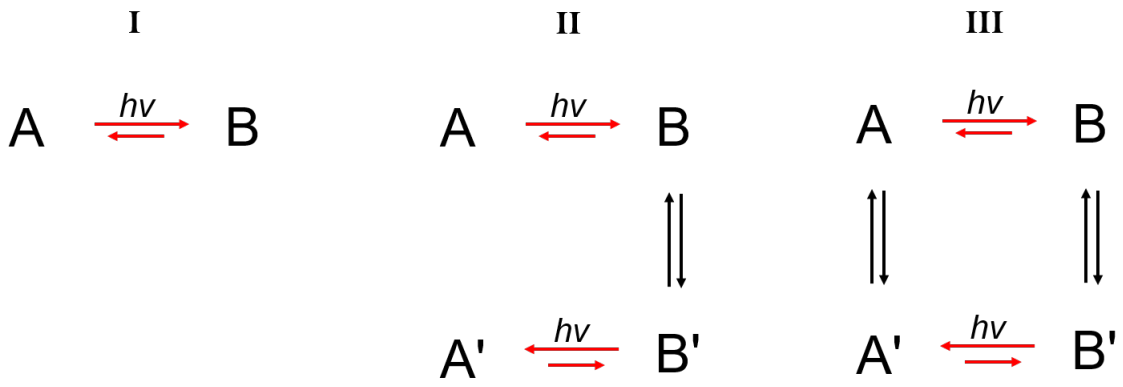

Figure 11.2: *Different types of photochemically dissipative systems described in the text: type (I), type (II) and type (III), differing in the sort of network in which photoreactions are included. Red arrows highlight the photochemical steps.*

Type (I) dissipative systems are a well known class of molecules and their properties will not be further discussed. A final premise is useful before moving to the description of type (II) and type (III) dissipative systems: the PSS of the photoreaction, at which $K_{\lambda_{irr}}$ is respected, is different from the PSS of the system, where both chemical and photochemical reactions are at the steady state. For type (I) dissipative systems the two PSS coincide, as no chemical reaction is present. In the case of type (II) and type (III) dissipative systems this is not always the case. The condition that allows to clearly distinguish between the two is that the kinetic of the photoreaction (i.e. the rate of the bulk photoreaction, that is determined by the rate of absorption, weighted for the quantum yield of the desired reaction) has to be fast in comparison with the rate of the thermal steps.[1] The following discussion is based on this condition, together with the constraint that photoproducts are thermally stable, but the conclusions are general: these conditions are used only to simplify the discussion and possibly make the concepts more clear.

In starting the discussion of the properties of type (II) dissipative systems it is highlighted the difference between the PSS of the reaction and the PSS of the system as a whole. Considering the reaction scheme in figure 11.2-II, when starting from A, under continuous irradiation the photoreaction that interconverts A and B reaches its PSS. At this stage A' and B' have not been formed yet. Only upon continuous irradiation both A' and B' form. When the PSS of the system has been reached, every single reaction is at the stationary state, that for thermal reactions coincides with equilibrium[2]. This particular reaction network can be found for example in the work of Prof. Tamaoki,[14] where a pure enantiomer was isolated and its photoracemization was obtained according to the scheme reported in figure 11.2-II. The similar scheme in which the initial system is the thermally equilibrated B ⇌ B' reaction has also been exploited in real cases. Indeed when the two photoreactions have different PSSs under the same irradiation conditions, the thermal equilibrium is affected, i.e. [B']/[B] respects the related equilibrium constant, but ([A]+[B])/([B']+[A']) does not.[3] Indeed an information ratchet effect is in place. Examples are the seminal paper of Prof. Leigh describing an information ratchet[15] and the work of Prof. Hecht demonstrating how light can affect a dynamic covalent reaction.[16] To aid the reader in the understanding of the properties of this particular reaction network, a numerical example of a hypothetical system analogue to the molecular information ratchet from Leigh [15] is provided in figure 11.3.

[1] It is worth highlighting that very often this does not correspond to reality, as chemical reactions can be very fast, whereas the bulk speed of a photoreaction is often in the range of several minutes.

[2] This is true even if the photochemical steps have different PSSs.

[3] It should be noted that there is no equilibrium constant associated to this ratio, however it is a choice that provides an informative description of systems of this type: see the following examples.

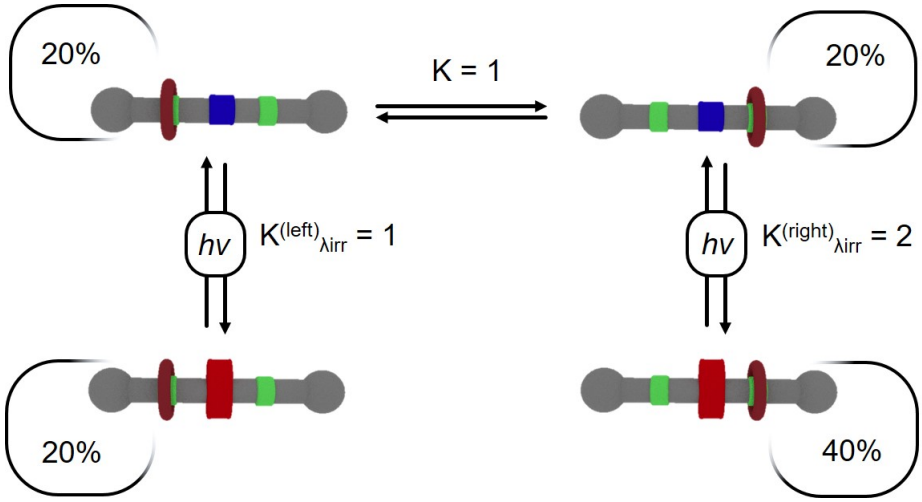

Figure 11.3: *Numerical example of a linear network of reactions in which an information ratchet mechanism is active (based on reference [15]). The thermal reaction is the shuttling reaction in a bistable rotaxane. Photochemical reactions convert the rotaxane to a conformation in which shuttling is prevented; the photoreaction has a photostationary state with a higher content of "blocked" conformation when the ring is on the right side (the information ratchet - light distinguishes the left and right co-conformations). The % reported in the corners represent the concentration of each species at the PSS of the system. Each K value is respected, however the population of rings on the right side is higher than that on the left side (60% vs 40% respectively).*

Also in these cases, to reach the PSS of the photoreactions is not enough to affect the thermal reaction, therefore continuous irradiation is needed. However, as the PSS of the system is reached, the energy source is not needed any more and can — in principle — be removed. In other words the dissipative operation of the system occurs only until as the PSS of the system is reached. This follows from the fact that at the PSS of the system each thermal step is at equilibrium.

This is not the case for type (III) dissipative systems. In this case continuous irradiation is necessary, because when the photoreaction is part of a cycle and the symmetry of the system is broken, i.e. an effective ratcheting mechanism is active, at the PSS of the whole system each reaction is not at equilibrium, instead the steady state is characterized by net fluxes. For example, the net speed of conversion of A into B will be equal to the net speed of conversion of B into B'. Ratcheting mechanisms can be engineered at the molecular level[see for example 4, 17–20] but also spatial differentiation at the macroscopic level can provide the ratcheting requirement in a simple setup[see for example 21, 22]. In the presence of a ratcheting mechanism included in a cyclic reaction network, it is also possible to calculate the ΔQ associated to a directional cycle, that will

be different from zero. This means that when such cycle is travelled in its preferential direction, the amount of energy ΔQ is available to perform work on the environment. Therefore the three types of dissipative systems are very different, in particular in the amount of energy that can be stored. In type (I) systems the stored energy is the energy that can be obtained upon conversion of the photogenerated B into A. In type (II) systems a second contribution is added: the energy that is stored in terms of shift of concentrations from their equilibrium value.[see 15, 16] Finally in type (III) systems a third possibility arise: some energy can be stored at each cycle by performing work on the environment.

The field of molecular devices and machines has obtained a very important recognition in 2016, with the Nobel prize in chemistry to Sauvage, Stoddart and Feringa; however, a clear definition of molecular motor in terms of the utilization of the energy source is still missing. From the above discussion it seems reasonable to consider any cyclic network of reactions that include a photoreaction, where symmetry-breaking ratcheting mechanisms are active, as a light-driven chemical motor. Often in defining a chemical motor the mechanical movement occurring at the molecular level is discussed,[23] however it is opinion of the author that this point (intrinsically related to molecular conformations) should not be a discriminant parameter in the definition of motor, as it is extremely difficult to make distinctions on the basis of this parameter.

In the next chapter a type (III) dissipative system will be illustrated. In particular the system acts as a molecular pump module, since in a cycle an asymmetric molecular axle goes through a macrocycle in a preferential direction.

11.4 References

[1] M. Baroncini, S. Silvi, M. Venturi, and A. Credi. *Angew. Chem. Int.Ed.*, 51:4223–4226, 2012. 111

[2] H. Li, C. Cheng, P. R. McGonigal, A. C. Fahrenbach, M. Frasconi, W. Liu, Z. Zhu, Y. Zhao, C. Ke, J. Lei, R. M. Young, S. M. Dyar, D. T. Co, Y. Yang, Y. Y. Botros, W. A. GoddardIII, M. R. Wasielewski, R. D. Astumian, and J. F. Stoddart. *J. Am. Chem. Soc.*, 135:18609–18620, 2013. 111

[3] C. Cheng, P. R. McGonigal, S. T. Schneebeli, H. Li, N. A. Vermeulen, C. Ke, and J. F. Stoddart. *Nat. Nanotechnol.*, 10:547–553, 2015. 111

[4] G. Ragazzon, M. Baroncini, S. Silvi, M. Venturi, and A. Credi. *Nat. Nanotechnol.*, 10:70–75, 2015. 111, 116

[5] G. Ragazzon, M. Baroncini, S. Silvi, M. Venturi, and A. Credi. *Beilstein J. Nanotechnol.*, 6:2096–2104, 2015.

[6] M. Baroncini, G. Ragazzon, M. Venturi S. Silvi, and A. Credi. *Pure Appl. Chem.*, 87:537–545, 2015. 111

[7] P. W. Anderson and D. L. Stein. *Self-Organizing Systems: The Emergence of Order, E. E. Yate (Ed.).* Plenum Press, New York, 1987. 112

[8] J. England. *Nat. Nanotechnol.*, 10:919–923, 2015. 112

[9] J. Boekhoven, W. E. Hendriksen, G. J. M. Koper, R. Eelkema, and J.H. van Esch. *Science*, 349:1075–1079, 2015. 113

[10] J. Boekhoven, A. M. Brizard, K. N. K. Kowlgi, G. J. M. Koper, R. Eelkema, and J. H. van Esch. *Angew. Chem. Int. Ed.*, 49:4825–4828, 2010. 113

[11] S. Maiti, I. Fortunatiand C. Ferrante, P. Scrimin, and L. J. Prins. *Nat. Chem.*, 8:725–731, 2016. 113

[12] M. R. Wilson, J. Solá, A. Carlone, S. M. Goldup, N. Lebrasseur, and D. A. Leigh. *Science*, 534:235–240, 2016. 113

[13] S. O. Krabbenborg, J. Veerbeek, and J. Huskens. *Chem. Eur. J.*, 21:9638–9644, 2015. 113

[14] N. Tamaoki and M. Wada. *J. Am. Chem. Soc.*, 128:6284–6285, 2006. 115

[15] V. Serreli, C. Lee, E. R. Kay, and D. A. Leigh. *Nature*, 445:523–527, 2007. 115, 116, 117

[16] R. Göstl and S. Hecht. *Angew. Chemie Int. Ed. Engl.*, 53:8784–8787, 2014. 115, 117

[17] N. Koumura, R. W. J. Zijlstra, R. A. van Delden, N. Harada, and B. L. Feringa. *Nature*, 401:152–155, 1999. 116

[18] Q. Li, G. Fuks, E. Moulin, M. Maaloum, M. Rawiso, I. Kulic, J. T. Foy, and N. Giuseppone. *Nat. Nanotechnol.*, 10:161–165, 2015.

[19] L. Greb and J.-M. Lehn. *J. Am. Chem. Soc.*, 136:13114–13117, 2014.

[20] V. Balzani, M. Clemente-León, A. Credi, B. Ferrer, M. Venturi, A. H. Flood, , and J. F. Stoddart. *Proc. Nat. Acad. Sci. USA*, 103:1178–1183, 2006. 116

[21] E. Chevallier, A. Mamane, H. A. Stone, C. Tribet, F. Lequeux, and C. Monteux. *Soft Matter*, 7:7866–7874, 2011. 116

[22] A. Diguet, R. Guillermic, N. Magome, A. Saint-Jalmes, Y. Chen, K. Yoshikawa, and D. Baigl. *Angew. Chem. Int. Ed.*, 48:9281–9284, 2009. 116

[23] E. Kay and D. A. Leigh. *Nature*, 440:286–287, 2006. 117

12

An autonomous artificial molecular pump

12.1 Introduction

Molecular machines and motors are extensively used by living organisms to perform crucial functions such as transport of substrates and mechanical actuation.[1, 2] The realization of artificial molecular machines, based on either fully synthetic components or biomolecular constructs, that couple directionless Brownian motion with an external energy source to generate directional movements is a fascinating goal in nanoscience.[3–5] Molecular machines capable of performing tasks as motor proteins do, must exhibit directionally controlled motion by dissipating energy from an external source in an autonomous fashion (that is, under constant environmental conditions). As illustrated in the previous chapter, both aspects are strictly related to the ability of the device to operate away from chemical equilibrium — a condition which is inherent to biochemical systems[6] but represents a formidable challenge for artificial ones.[5, 7, 8] Despite laboratory demonstration of the potential utility of molecular machines for application in catalysis,[9, 10] materials science,[11, 12] information and communications technologies,[13] and nanomedicine,[14], the realization of directional and autonomous molecular movements remains a very difficult endeavor, usually tackled with sophisticated chemical structures and/or operation procedures.[3–5] It was previously described in

This chapter is partially derived — with permission — from G.Ragazzon, M. Baroncini, S. Silvi, M. Venturi, A. Credi, "Light-powered autonomous and directional molecular motion of a dissipative self-assembling system" *Nature Nanotech.*, **2015**, 10, 70 - 75.

our laboratory[15] the directionally controlled transit of a non-symmetric molecular axle through a macrocycle, obtained by ratcheting the self-assembly potential energy profile by means of sequential photochemical and chemical stimulation.[16] Building upon these results, the autonomous relative unidirectional transit of an oriented axle through a macrocyclic ring, using light as the sole stimulus has been obtained. This molecular machine exhibits autonomous behaviour as it can repeat its operation cycle indefinitely under photostationary conditions. The experimental investigation demonstrated that the device takes advantage of light energy to operate away from equilibrium, thus representing a significant example of dissipative self-assembling system.[8] The results also suggest that both energy and information ratchet mechanisms can account for the rectification of thermal fluctuations brought about by photons.[17] A further element of interest is that the system consists of wholly synthetic unsophisticated compounds and its operation is based on one of the most efficient, reversible and clean photoreactions, namely, azobenzene $E \rightleftharpoons Z$ photoisomerization.[18]

12.2 System characterization

The employed molecular components are (figure 12.1a) the macrocyclic ring 2,3-dinaphtho[24]crown-8 ether **12.1**[19] and the molecular axle *E*-**12.2**H^+, comprising a photoswitchable *E*-azobenzene unit at one end, a central ammonium recognition site for the macrocycle, and a passive methylcyclopentyl pseudo-stopper at the other end.[15]

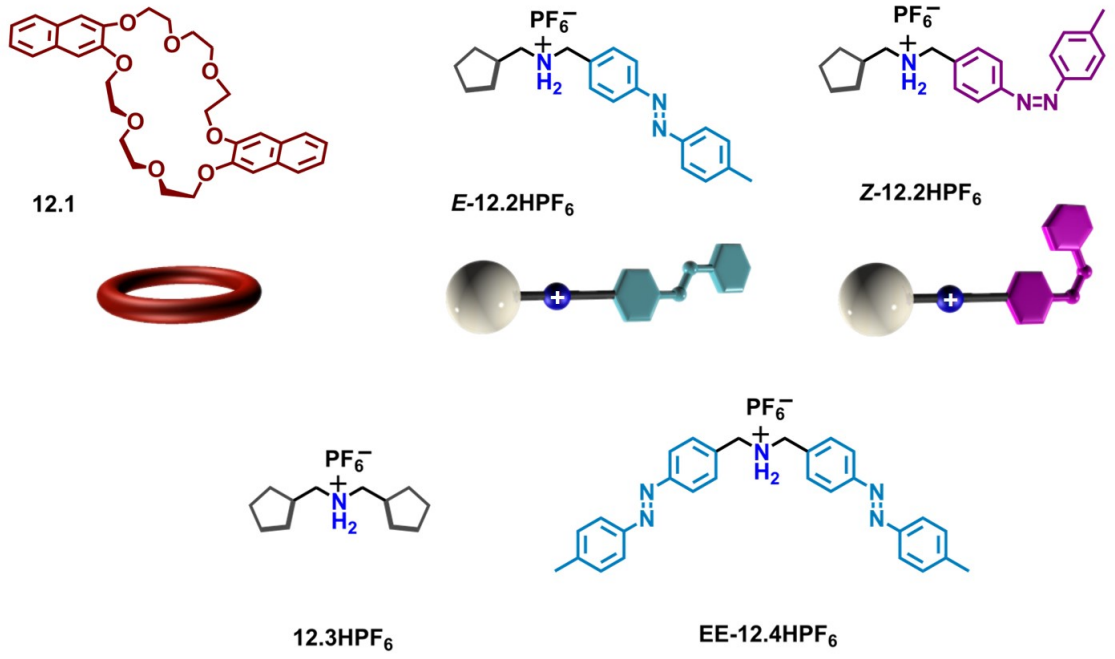

Figure 12.1: *Structure formulas and cartoon representation of macrocycle* **12.1**, *non-symmetric axles* E- *and* Z-**12.2**H^+ *and symmetric model axles* **12.3**H^+ *and* EE-**12.4**H^+.

As shown schematically in figure 12.2, the ring should enter exclusively from the *E*-azobenzene side of the axle for kinetic reasons, affording a pseudorotaxane in which the macrocycle encircles the recognition site on account of hydrogen bonding interactions between the oxygen atoms and the ammonium centre and, possibly, π-stacking forces involving the naphthalene and azobenzene units.[20] Subsequently, light irradiation converts the *E*-azobenzene unit into the bulkier *Z* form, a process which should also cause a destabilization of the supramolecular complex and dethreading of the components. If the extrusion from the ring is faster for the pseudo-stopper of the axle than for its *Z*-azobenzene unit, dethreading occurs preferentially along the same direction originally followed for threading. Reset is obtained by photochemical or thermal conversion of the azobenzene gate back to the *E*-isomer, thereby regenerating the starting form of the axle and causing directionally controlled threading once again (figure 12.2).

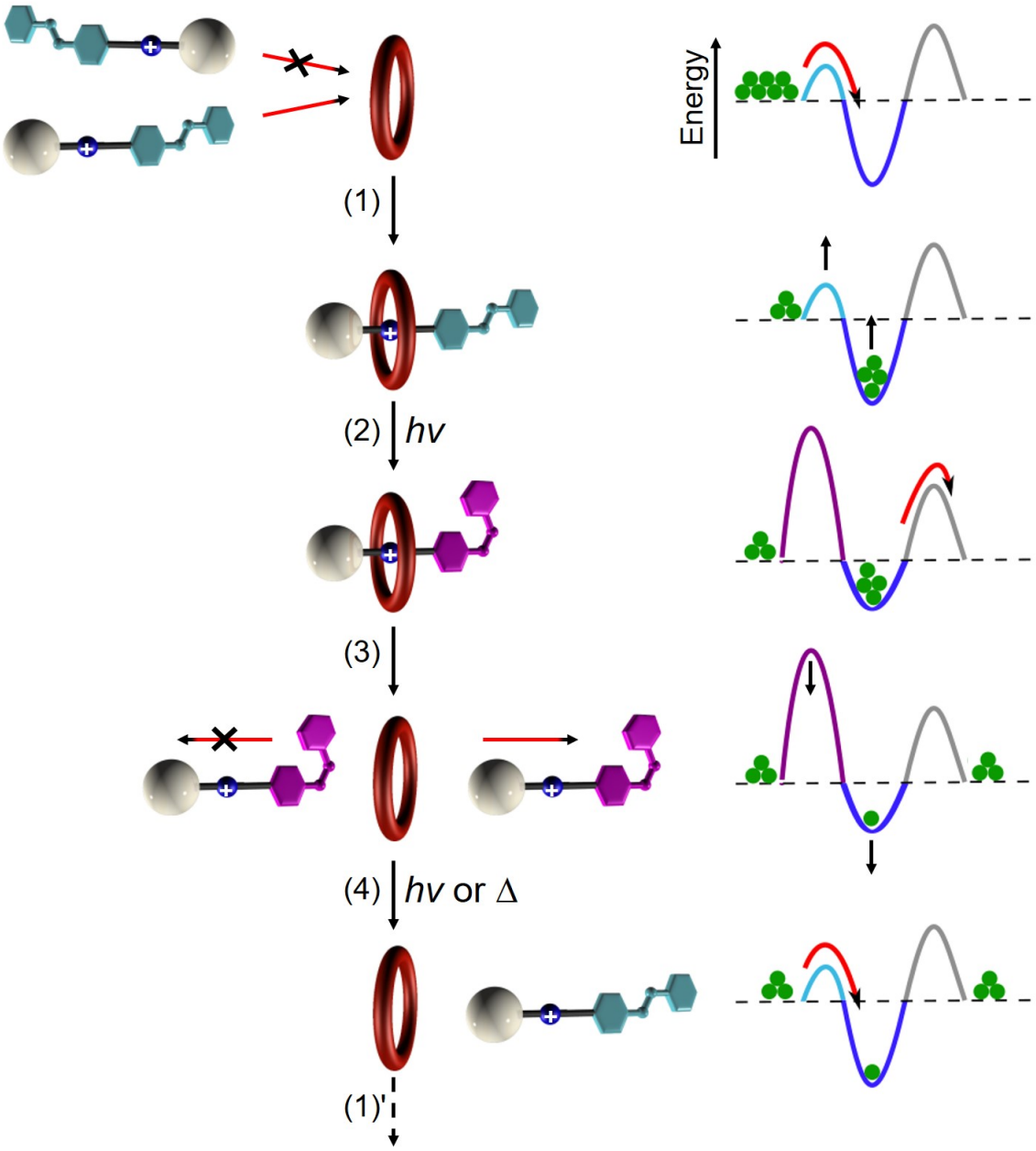

Figure 12.2: *Schematic representation of the relative unidirectional translations of the ring and axle components triggered by light (left) and simplified potential energy curves (free energy versus ring-axle distance) for the states shown on the left side (right). (1) directional threading; (2) photochemical gate locking; (3) directional dethreading; (4) gate unlocking (reset). This reaction sequence is induced by the periodic modulation of the energy barriers and wells induced by light, thus producing directional and repetitive threading-dethreading movements.*

Notice that, because of the overlapping absorption spectra and photoreactivity of *E*- and *Z*-azobenzene, the same photons can trigger both *E*→*Z* and *Z*→*E* photoisomerizations, thus enabling autonomous light-powered repetition of the sequence shown in figure 12.2 under steady irradiation (i.e. autonomous cycling in the cyclic reaction scheme shown in figure 12.5 - *vide infra*).[21–23] Overall, the photoinduced relative unidirectional transit of the axle through the macrocycle would be obtained according to a flashing energy ratchet mechanism (figure 12.2), in which a single photonic stimulus controls both the relative stabilities of the assembled and disassembled states (i.e. switching) and the relative heights of the kinetic barriers for threading/dethreading over either extremities (i.e. gating).[17] ^{1}H NMR spectra show that both *E*- and *Z*-**12.2**H$^+$ form 1:1 pseudorotaxane-type complexes with macrocycle **12.1**. The association of **12.1** and **12.2**H$^+$ causes also changes in the UV-visible absorption and luminescence spectra; in particular, the intense fluorescence of **12.1** (λ_{max} = 345 nm) is completely quenched when the ring is complexed by either isomer of axle **12.2**H$^+$. The thermodynamic and kinetic data for self-assembly of these complexes, together with those of the complexes formed by the symmetric model axles **12.3**H$^+$, *EE*-**12.4**H$^+$ and *ZZ*-**12.4**H$^+$ with macrocycle **12.1**, are reported in table 12.1 and 12.2. Axles *Z*-**12.2**H$^+$ and *ZZ*-**12.4**H$^+$, as well as their complexes with **12.1**, can be obtained by exhaustive irradiation of the corresponding *E*-isomers at 365 nm; in all cases the *E* → *Z* conversion yield at the photostationary state is >95%.

Table 12.1: *Thermodynamic data for the self-assembly of the investigated complexes (dichloromethane, 20° C).*

Complex	K[a] (M^{-1})	$-\Delta G^{\circ}$[b] (kcal mol^{-1})
[**12.1**⊃*E*-**12.2**]H$^+$	6.3×10^5	7.8
[**12.1**⊃*Z*-**12.2**]H$^+$[c]	1.7×10^5	7.0
[**12.1**⊃**12.3**]H$^+$	3.2×10^4	6.0
[**12.1**⊃*EE*-**12.4**]H$^+$	$>10^7$	>9.4
[**12.1**⊃*ZZ*-**12.4**]H$^+$[c]	[d]	[d]

[a] Determined by luminescence titration experiments. [b] Free energies of association (ΔG°), calculated from the K values by using the expression $\Delta G^{\circ} = -RT \ln K$. [c] Obtained upon exhaustive irradiation of the corresponding *E*-isomer at 365 nm; the *E*→*Z* conversion yield at the photostationary state was >95%. [d] Not measured because equilibrium cannot be reached before substantial thermal *Z*→*E* back isomerization occurs.

Table 12.2: *Kinetic data for the self-assembly of the investigated complexes (dichloromethane, 20° C).*

Complex	k_{in}[a] (M^{-1} s^{-1})	$\Delta G^{\ddagger}_{in}$[b] (kcal mol^{-1})	k_{out} (s^{-1})	$\Delta G^{\ddagger}_{out}$[b] (kcal mol^{-1})
[**12.1**⊃*E*-**12.2**]H^+	54	15	2.2×10^{-5}[a]	23
			8.6×10^{-5}[c]	
[**12.1**⊃*Z*-**12.2**]H^+[d]	0.81	17	4.7×10^{-6}[c]	24
[**12.1**⊃**12.3**]H^+	2.2	17	3.8×10^{-5}[a]	23
			6.9×10^{-5} [c]	
[**12.1**⊃*EE*-**12.4**]H^+	55	15	$<5.5\times10^{-6}$[c]	>24
[**12.1**⊃*ZZ*-**12.4**]H^+[d]	3.9×10^{-2}[e]	19	[f]	[f]

[a] Determined by UV-vis absorption or luminescence spectroscopy; see the text for details. [b] Free energies of activation for the threading ($\Delta G^{\ddagger}$in) and dethreading ($\Delta G^{\ddagger}$out) processes, calculated by using the relationships $\Delta G^{\ddagger}_{in} = -RT \ln(k_{in}h/kT)$ and $\Delta G^{\ddagger}_{out} = -RT \ln(k_{out}h/kT)$. [c] Calculated from the k_{in} and K values by using the expression $k_{out} = k_{in}/K$. [d] Obtained upon exhaustive irradiation of the corresponding *E*-isomer at 365 nm; the *E*→*Z* conversion yield at the photostationary state was >95%. [e] Estimated from the initial part of the time-dependent luminescence changes upon mixing **12.1** and *ZZ*-**12.4**H^+, after deconvolution of the contribution of *Z*→*E* isomerization and threading from the *E*-azobenzene terminus. [f] Not determined.

Photochemical experiments performed on the [**12.1**⊃*E*-**12.2**]H^+ complex show that the *E*→*Z* isomerization of the azobenzene unit of **12.2**H^+ is sensitized upon irradiation in the absorption bands of **12.1**, indicating that excitation energy is transferred from the naphthalene units of the ring to the *E*-azobenzene moiety of the axle. Such an energy-transfer process is also responsible for the emission quenching, as confirmed by the fact that the luminescence is quenched when **12.1** is complexed by *EE*-**12.4**H^+, while it is unaffected in the [**12.1**⊃11.3]$^+$ complex. Conversely, the photosensitization of the Z → E transformation in the [**12.1**⊃*Z*-**12.2**]H^+ complex is not efficient. A much faster photoinduced ring-to-axle energy transfer for *E*-**12.2**H^+ than for *Z*-**12.2**H^+ can be anticipated because of the different overlap of the emission spectrum of **12.1** with the absorption spectrum of either isomer of the axle. The significant quenching of the emission of **12.1** in the [**12.1**⊃*Z*-**12.2**]H^+ complex can be ascribed to electron transfer from the photoexcited naphthalene moiety of the ring to the LUMO orbital of the azobenzene axle. The fact that the threading rate constant for *E*-**12.2**H^+ is close to that of *EE*-**12.4**H^+ and 25 times faster than that of **12.3**H^+ (table 12.2, figure 12.3) indicates that axle *E*-**12.2**H^+ enters ring **12.1** almost exclusively (>95%)

with its *E*-azobenzene terminus. On the other hand, the rate constant for self-assembly of **12.1** and *Z*-**12.2**H$^+$ compares with that for threading of **12.3**H$^+$ which, in its turn, is 50 times faster than that for threading of *ZZ*-**12.4**H$^+$. All these observations clearly indicate that *Z*-**12.2**H$^+$ threads the ring with its methylcyclopentyl terminus, and confirm that the $E \rightleftharpoons Z$ photoisomerization can effectively be used to control the self-assembly kinetics.[24]

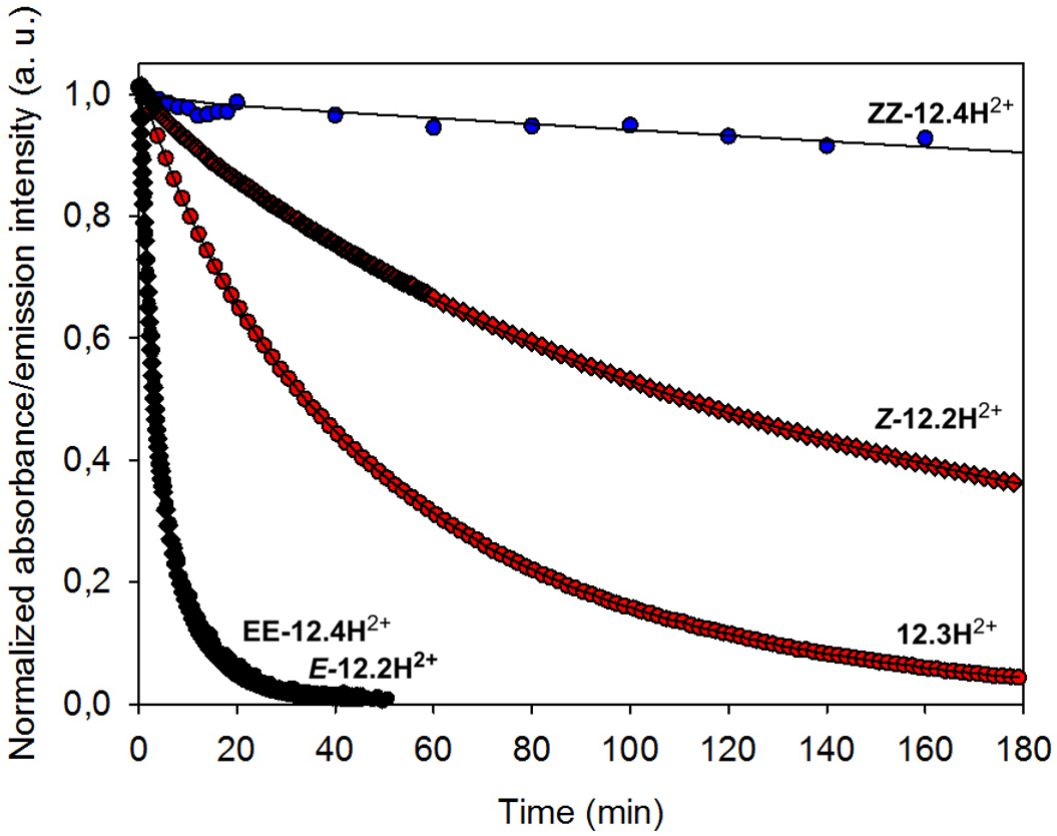

Figure 12.3: *Time-dependent luminescence changes associated with the self-assembly of the studied axles with* **12.1**. *Conditions:* CH_2Cl_2, *20 °C, 100 μM in both components,* λ_{exc} *= 272 nm. Black and red symbols are associated to axles that thread preferentially through the* E*-azobenzene and cyclopentyl units, respectively. Blue dots are indicate threading throug* Z*-azobenzene. Black lines represent numeric fitting of the experimental data, see experimental part for details. Data points and fitting curves for* E-**12.2***H*$^{2+}$ *and* E*E*-**12.2***H*$^{2+}$ *are largely superimposed in this representation.*

In contrast with the behaviour of an earlier system,[15] the $E \rightleftharpoons Z$ photoisomerization of **12.2**H$^+$ affects the stability of the resulting pseudorotaxane, as shown by luminescence titration curves

(figure 12.4). The association constant with **12.1** drops from 6.3×10^5 M^{-1} for *E*-**12.2**H^+ to 1.7×10^5 M^{-1} for *Z*-**12.2**H^+, most likely as a consequence of a diminished π-stacking of the naphthalene units of **12.1** with the non-planar Z-azobenzene moiety. Under typical experimental conditions (1:1 mixture of 50 μM **12.1** and **12.2**H^+), exhaustive irradiation at 365 nm affords the dethreading of about 15% of the pseudorotaxanes species. Hence, the reversible photoisomerization of the axle can be exploited also for switching the system, i.e., change the relative stabilities of the self-assembled and disassembled states (figure 12.2).

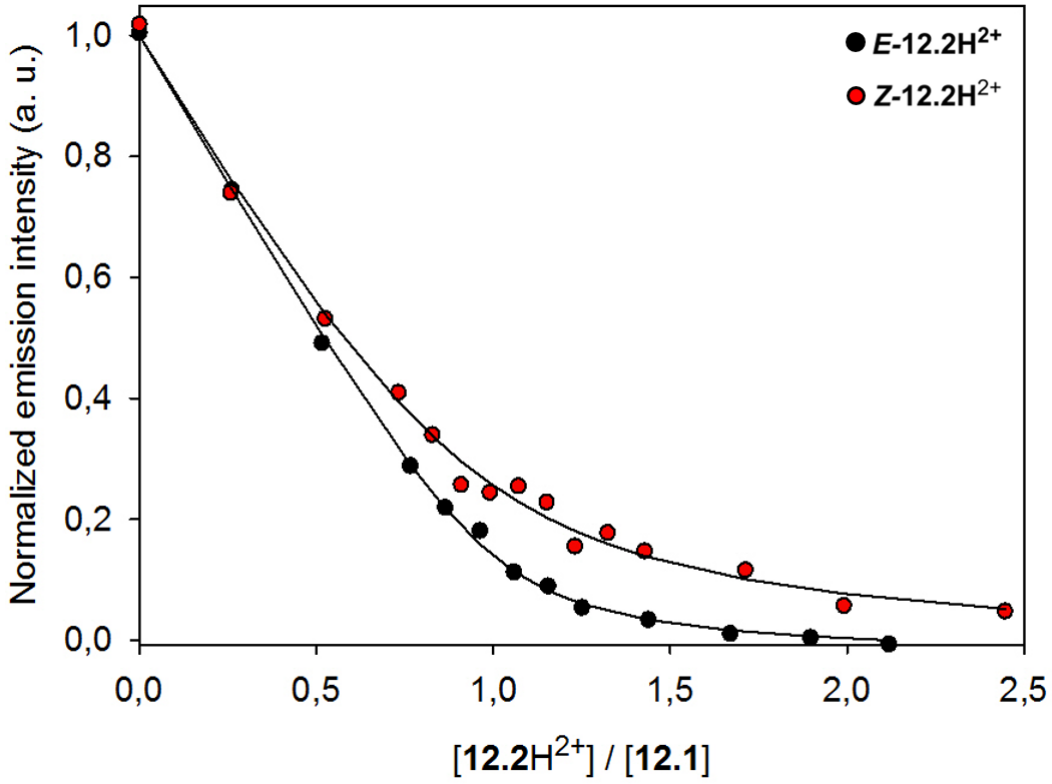

Figure 12.4: *Titration curves, obtained from luminescence data, observed upon addition of either* E-**12.2***H*$^+$ *(back dots) or* Z-**12.2***H*$^+$ *(red dots) to a 54 μM solution of* **12.1** *in* CH_2Cl_2 *at 20 °C (λ_{exc} = 272 nm). Black lines are numeric fitting of the experimental data, see experimental part for details.*

The direction of photoinduced dethreading can be determined considering that barriers (or rate constants) for threading with the different termini of a non-symmetric axle give information about the relative height of the corresponding dethreading barriers. On the basis of the threading rate

constants for **12.3**H$^+$ and *ZZ*-**12.4**H$^+$ with **12.1** it can be calculated that more than 98% of *Z*-**12.2**H$^+$ axles will enter the macrocycle with the methylcyclopentyl stopper. Therefore it can be concluded that extrusion of the methylcyclopentyl unit is kinetically preferred over *Z*-azobenzene in the dethreading of [**12.1**⊃*Z*-**12.2**]H$^+$. It should also be noted that the latter process (k = 4.7×10^{-6} s^{-1}) is faster than the thermal *Z*→*E* isomerization (k = 1.6×10^{-6} s^{-1}); these numbers indicate that, on average, the complex should have approximately three dethreading chances before its azobenzene gate is thermally converted back to the *E* configuration. The full reset of the system is determined solely by the *Z*→*E* isomerization, which restores the original potential energy landscape (figure 12.2) and promotes the re-threading of *E*-**12.2**H$^+$ into **12.1** preferentially with the azobenzene terminus (figure 12.2), thus completing the operation cycle.

12.3 Autonomous operation

To understand how our system can continue to operate once a steady state is reached under light irradiation, thereby establishing a net flux around the cycle in one way even if the concentration of each species remains static, it is useful to consider first a square scheme composed only of chemical reactions (figure 12.5).

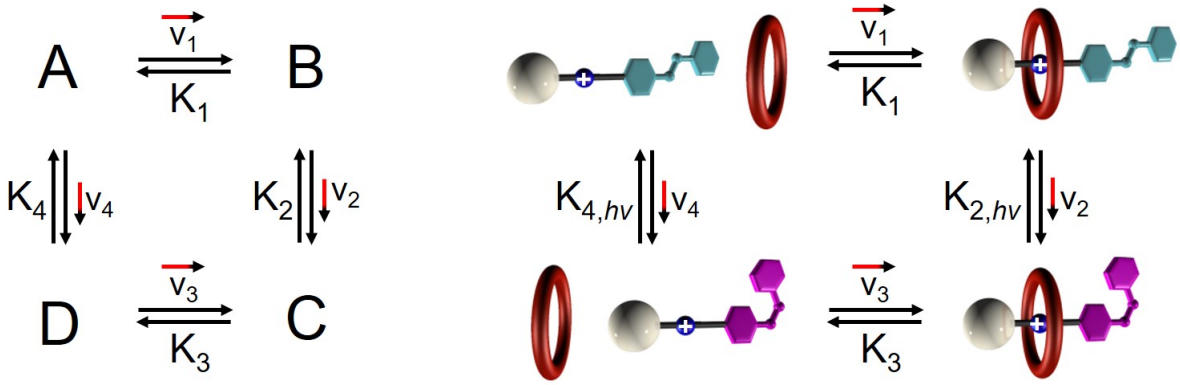

Figure 12.5: *Square cycle consisting of four chemical equilibria (left). Detailed balance states that, at equilibrium, all rates are zero. Square cycle representing the operation of the present system (right). Horizontal and vertical arrows denote the self-assembly equilibria and photochemical isomerization reactions, respectively. The indicated parameters refer to the reactions read from left to right and from top to bottom.*

For such a cycle at thermal equilibrium, detailed balance — a consequence of microscopic re-

versibility — states that each individual process has to be at equilibrium, that is, its net rate must be zero ($v_1 = v_2 = v_3 = v_4 = 0$)[17, 25] Such a condition implies the following relationship between the equilibrium constants (equation 12.1)

$$K_1/K_3 = K_4/K_2 \tag{12.1}$$

In the present case, however, two of the four processes — namely, isomerization of the free and complexed axle (figure 12.5, right, processes 2 and 4) — are photochemically driven and hence are not subjected to microscopic reversibility.[25, 26] In fact, once the steady state under light irradiation is reached, one can define $K_{2,h\nu}$ and $K_{4,h\nu}$ as the ratio of the photostationary concentrations of the products and reactants for the respective reactions. Our results show that the photostationary states reached upon irradiation of the free and complexed axle at λ >400 nm have the same E/Z composition. This means that $K_{2,h\nu} = K_{4,h\nu}$ but, since $K_1 > K_3$ (the ring associates more strongly with *E*-**12.2**H$^+$ than with *Z*-**12.2**H$^+$, table 12.1), eq. 12.1 does not hold and detailed balance is not fulfilled. In other words, at the steady state the net rates of the individual processes in the closed cycle must be equal but are not zero, and the system travels through the cycle one way; in the present case the cycling path (clockwise in figure 12.5; $v_1 = v_2 = -v_3 = -v_4 > 0$) is dictated by the fact that $K_1 > K_3$. It is worthwhile to remember that, for the reasons described above, the threading-dethreading processes represented in figure 12.5 are directionally controlled, i.e., *E*- and *Z*-**12.2**H$^+$ thread/dethread the ring with their *E*-azobenzene and methylcyclopentyl termini, respectively. Gaining direct experimental evidence of photostationary cycling, however, is not straightforward because the collective chemical and physical properties of the ensemble exhibit no change at the steady state. On the basis of the above discussion the supply of light energy is expected to cause cycling, thus bringing the system out of equilibrium. Therefore, a proof for autonomous light driven cycling would be the observation that the static concentration reached at the photostationary state for any species involved is not consistent with its expected equilibrium value. As the fluorescence of **12.1** is completely quenched when the ring is complexed by either *E*- or *Z*-**12.2**H$^+$, the fluorescence signal measured under appropriate spectral conditions[27] can be correlated to the amount of uncomplexed macrocycle present in the solution. We therefore monitored the concentration of the free ring in a solution containing **12.1** and **12.2**H$^+$ kept under steady irradiation at 365 nm.

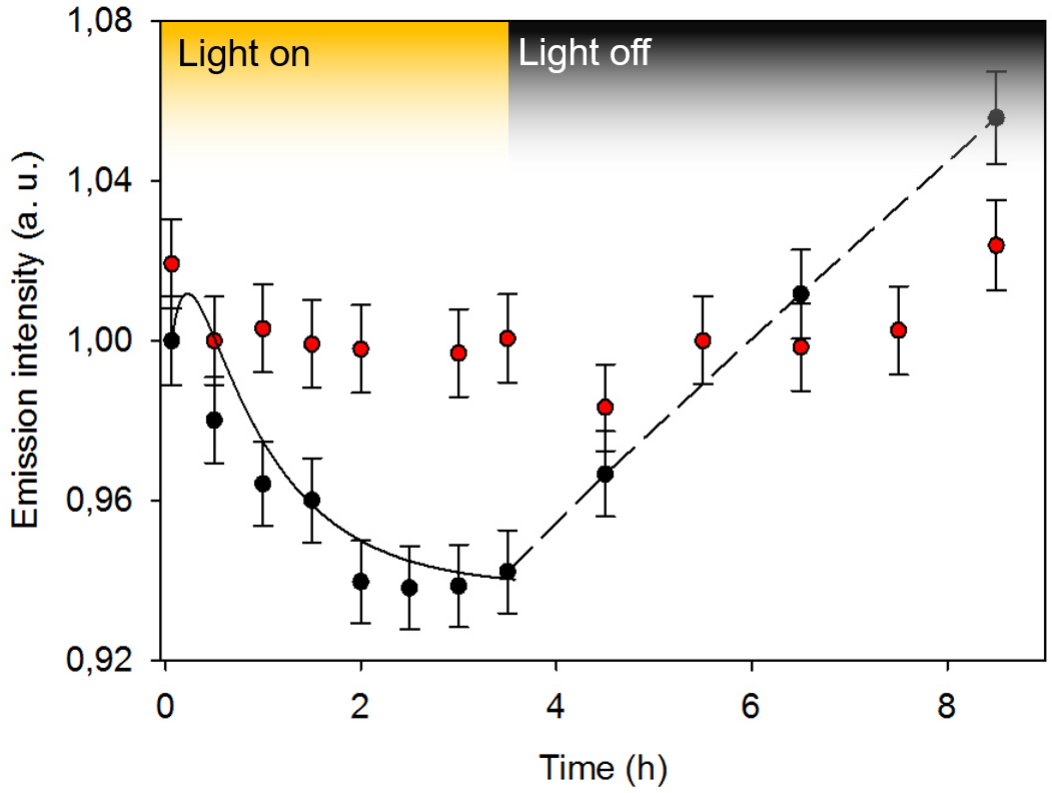

Figure 12.6: *Observation of photostationary cycling of the system away from equilibrium. Fluorescence intensity values of uncomplexed macrocycle* **12.1** *(λ_{exc} = 272 nm) upon prolonged low-intensity 365-nm irradiation of a mixture of ring and axle at the* E⇌Z *photostationary state in CH_2Cl_2 at 20°C (black dots, up to 3.5 h). After 3.5 h the irradiation at 365 nm had been switched off, and the luminescence was observed (black dots, after 3.5 h). Significant absorption changes, due to* Z→E *thermal isomerization, are observed, therefore strong inner filter effects prevent the analysis of data points after 8 h. The solution was argon-purged to minimize photodecomposition effects and was prepared by mixing 50 μM* **12.1** *and 150 μM* E-**12.2**H^+ *(98% complexation of* **12.1***) followed by quick exhaustive irradiation at 365 nm (5 min). The red dots show the fluorescence intensity values in an identical experiment in which the deprotonated axle* **12.2**, *lacking the ammonium center and thus unable to associate with* **12.1**, *is used in place of* **12.2**H^+. *In both cases no absorption changes are detected throughout the irradiation. The full line is a numeric simulation of the process, based on the scheme shown in figure 12.5 and performed by using the experimentally determined values for threading, dethreading, photoisomerization and thermal isomerization rates. The dashed black line serves as guide for the eye. Error bars correspond to the standard deviation for the luminescence intensity of* **12.1** *alone during the same experiment. See the text and ref. [28] for more details.*

In an optimized experiment, a solution containing 50 μM **12.1** and 150 μM *E*-**12.2**H^+ was

let to equilibrate in the dark at 20 °C; the self-assembly of [**12.1**⊃*E*-**12.2**]H^+ was revealed by a strong decrease of the emission intensity. Irradiation of the solution with relatively high intensity (2.8×10^{-8} Einstein min^{-1}) 365-nm light afforded nearly complete $E\rightarrow Z$ conversion, in such a short time (5 min) that the self-assembly equilibria cannot keep up with the photoisomerization changes. As a result, both the free and complexed axles are photoisomerized while maintaining the initial concentrations of the respective *E*-forms. In fact, the concentration of the free ring was unchanged within errors after the irradiation, confirming that the dethreading of a fraction of the [**12.1**⊃*Z*-**12.2**]H^+ species, expected because its stability constant is lower than that of [**12.1**⊃*E*-**12.2**]H^+, does not take place on this time scale. Once the system had been completely photoisomerized (that is, when the absorption spectrum became invariant), the irradiation was resumed with a lower light intensity (1.7×10^{-9} Einstein min^{-1}) to prevent any photodecomposition effect. A further decrease of the concentration of the free macrocycle was indeed observed, which reached a plateau at −6% after ca. 2 h of continuous irradiation (figure 12.6a). It should be noted that these emission measurements are very accurate as they do not suffer from inner filter effects since, as noted above, the absorption spectrum of the solution is constant throughout the irradiation. Such a lower concentration of free **12.1** indicates a degree of complexation even larger than that expected for *E*-**12.2**H^+ — that is, the guest form exhibiting the highest affinity for the ring — and it is clearly incompatible with any equilibrium mixture of **12.1** and *E*- or *Z*-**12.2**H^+. A control experiment performed on a solution containing the macrocycle and the deprotonated guest *E*-**12.2** (lacking the ammonium recognition site and thus unable to associate with **12.1**) under otherwise identical conditions showed no change in the emission intensity upon prolonged irradiation (figure 12.6), confirming that the observed effect arises from the interplay of photoisomerization and self-assembly processes (figure 12.5). The lower concentration of the free ring under photostationary operation can be understood considering that, in a sequence of reactions in which a perturbation determines non-equilibrium conditions, the slowest reaction is the farthest away from equilibrium.[29] In other words to have equal speeds in all the steps of the cycle, the concentration of the species that interconvert with processes characterized by the smaller kinetic constants need to adapt their concentration to values that are further away from their equilibrium ones. In the present case, dethreading of [**12.1**⊃*Z*-**12.2**]H^+ through the methylcyclopentyl group is the slowest of all processes of the cycle (figure 12.5); hence, a larger concentration of this species at the photostationary state with respect to dark equilibrium conditions is expected. In practice, while the cycle operates, reaction 2 (figure 12.5, right) populates the [**12.1**⊃*Z*-**12.2**]H^+ state, characterized by very slow dissociation kinetics, scavenging [**12.1**⊃*E*-**12.2**]H^+ and thus fostering the complexation of *E*-**12.2**H^+ generated in reaction

4 (figure 12.5). When the light is switched off, [**12.1**⊃*Z*-**12.2**]H^+ begins to dethread because its concentration is higher than the equilibrium value, and the amount of the free ring increases (figure 12.6). In particular, since the axle is almost completely present as *Z*-isomer, the system evolves toward a kinetically trapped state, for which the concentration of free ring is close to the equilibrium value for the **12.1** + *Z*-**12.2**H^+ ⇆ [**12.1**⊃*Z*-**12.2**]H^+ reaction. Since the association constant for the *Z*-complex is lower than that of the *E*- isomer, the emission intensity (the amount of free ring) associated to such kinetically trapped state is higher than the initial one, that was related to a fully *E*-isomer equilibrium state. The absorption changes associated with the concomitant *Z*→*E* thermal isomerization prevent again an accurate determination of the fluorescence intensity because of the strong reabsorption of the emitted light, for times longer than 8 h.[27] Nevertheless, after 20 days in the dark at room temperature — that is, when all the isomerization and self-assembly processes have reached equilibrium — the observed emission intensity is identical to that measured for the equilibrated solution of **12.1** and *E*-**12.2**H^+ before irradiation. This result highlights the full reversibility and a remarkable fatigue resistance of this ensemble.

To verify our interpretation of the observed results, numeric simulations of the cycle shown in figure 12.5 were performed (see [28] for details). The excellent match between the simulation and the measured data points (figure 12.6) confirms the validity of the mechanistic hypotheses. A few interesting facts can be extracted from the simulation to assess the performance of the cycle. The cycling rate, which is also the net rate of each reaction, is 1.7×10^{-10} M s^{-1}, and the efficiency is 2.3×10^{-3} cycles per photon; that is, about 430 photons need to be absorbed on average to complete a cycle. The product of the rate constants of the clockwise processes divided by the product of the rate constants of the counterclockwise ones (figure 12.5) indicates that, on average, the system loops in the "wrong" way (i.e., counterclockwise) once every 160 cycles. The net energy change of the system,[17, 30] which corresponds to the maximum amount of work that can be performed in a cycle, is 5.1 k_BT or 3.0 kcal mol^{-1} at 20°C. i.e., about one fourth of the energy provided by ATP hydrolysis. Considering that, under the conditions employed, one cycle uses ca. 430 photons of 365 nm light (78 kcal mol^{-1}), the upper limit for the energy conversion efficiency is 8×10^{-5}. A closer look at the photochemical data enables a discussion about the mechanism used by the system to rectify Brownian fluctuations. It was found that the *E*→*Z* conversion at the photostationary state upon irradiation at 365 nm is slightly larger for the complex than for the free axle. As the photoisomerization quantum yields are not affected by the presence of the macrocycle, the more efficient *E*→*Z* transformation in the complex must arise from its slightly higher molar absorption coefficient at 365 nm in comparison with the free axle. Under these conditions $K_{2,h\nu} > K_{4,h\nu}$ and

with equation 12.1 cannot be valid for an additional reason. The situation is even more interesting when the system is irradiated with light absorbed also by the ring component (e.g., 287 nm). Because excitation energy is efficiently transferred from **12.1** to *E*-**12.2**H$^+$ but not to *Z*-**12.2**H$^+$ in their respective complexes (and, as noted above, the inherent photoisomerization efficiency of the axle does not change when it is surrounded by the ring), irradiation of the ring-axle mixture at this wavelength generates a photostationary state with a larger E/Z composition than for the axle alone and, again, $K_{2,h\nu} > K_{4,h\nu}$. For what has been discussed, the device operation is described as based on pure energy ratcheting[17, 31] if irradiation is performed with λ >400 nm, whereas a contribution from information ratcheting [17, 32, 33] takes place upon irradiation at 287 or 365 nm. Different physical phenomena enable information ratcheting at either wavelength. The light absorbed by the ring at 287 nm causes the transfer of excitation energy to the *E*-axle — a process that can only occur when the components are bound — and triggers the $E \rightarrow Z$ isomerization of the latter.[32] Conversely, the ring does not absorb light at 365 nm but its presence enhances the absorption of the *E*-axle, leading to the preferential light-triggered closure of the azobenzene gate in the pseudorotaxane compared to the free axle. In both cases, the information about the location of the ring with respect to the axle can control the gating.[25]

12.4 Conclusions

Although the system as such cannot be used to perform work in a bulk solution,[30] it provides a viable route for the construction of rotary motors based on catenanes[34] or linear motors[35] based on polymeric motifs,[36] capable of moving — and possibly transporting — cargos over long distances. It can also be regarded as a precursor of artificial molecular pumps[31] capable of generating concentration gradients across membranes.[37–40] Besides practical applications, this system epitomizes the conceptual and practical elements at the basis of repetitive directionally controlled molecular motion powered by light.[17, 25, 30] In conclusion, in this chapter a dissipative self-assembling ensemble that uses light energy to perform directed molecular movements in a repetitive fashion out of equilibrium has been described.[8]

12.5 References

[1] R. A. L. Jones. *Soft machines: Nanotechnology and Life.* Oxford University Press, Oxford, 2008. 121

[2] *Molecular Motors, Ed.: M. Schliwa.* Wiley-VCH, Weinheim, 2003. 121

[3] V. Balzani, A. Credi, and M. Venturi. *Molecular Devices and Machines, 2nd Ed.* Wiley-VCH, Weinheim, 2008. 121

[4] W. Browne and B. Feringa. *Nat. Nanotechnol.*, 1:25–35, 2006.

[5] E. R. Kay, D. A. Leigh, and F. Zerbetto. *Angew. Chem. Int.Ed.*, 46:72–191, 2007. 121

[6] S. Mann. *Angew. Chem. Int. Ed. Engl.*, 47:5306–5320, 2008. 121

[7] J.-M. Lehn. Toward complex matter: supramolecular chemistry and self-organization. *Proc. Nat. Acad. Sci. U. S. A.*, 99(8):4763–4768, 2002. 121

[8] B. A. Grzybowski, C. E. Wilmer, J. Kim, K. P. Browne, and K. J. M. Bishop. *Soft Matter*, 5:1110–1128, 2009. 121, 122, 134

[9] R. Eelkema, M. M. Pollard, J. Vicario, N. Katsonis, B. S. Ramon, C. W. M Bastiaansen, D. J. Broer, and B. L. Feringa. *Nature*, 440:163, 2006. 121

[10] V. Blanco, D. A. Leigh, V. Marcos, J. A. Morales-Serna, and A. L. Nussbaumer. *J. Am. Chem. Soc.*, 136:4905–4908, 2014. 121

[11] K.-Y. Chen, O. Ivashenko, G. T. Carroll, J. Robertus, J. C. M. Kistemaker, G. London, W. R. Browne, P. Rudolf, and B. L. Feringa. *J. Am. Chem. Soc.*, 136:3219–3324, 2014. 121

[12] V. N. Vukotic, K. J. Harris, K. Zhu, R. W. Schurko, and S. J. Loeb. *Nat. Chem.*, 4:456–460, 2012. 121

[13] A. Coskun, J. M. Spruell, G. Barin, W. R. Dichtel, A. H. Flood, Y. Y. Botros, and J. F. Stoddart. *Chem. Soc. Rev.*, 41:4827–4859, 2012. 121

[14] Z. Li, J. C. Barnes, A. Bosoy, J. F. Stoddart, and J. I. Zink. *Chem. Soc. Rev.*, 41:2590–2605, 2012. 121

[15] M. Baroncini, S. Silvi, M. Venturi, and A. Credi. *Angew. Chem. Int.Ed.*, 51:4223–4226, 2012. 122, 127

[16] G. Haberhauer. *Angew. Chem. Int. Ed. Engl.*, 50:6415–6418, 2011. 122

[17] R. D. Astumian. *Phys. Chem. Chem. Phys.*, 9:5067–5083, 2007. 122, 125, 130, 133, 134

[18] H. M. D. Bandara and S. C. Burdette. *Chem. Soc. Rev.*, 41:1809–1825, 2012. 122

[19] G. J. E. Davidson, S. J. Loeb, P. Passaniti, S. Silvi, and A. Credi. *Chem. Eur. J.*, 12:3233–3242, 2006. 122

[20] P. R. Ashton, P. J. Campbell, P. T. Glink, D. Philp, N. Spencer, J. F. Stoddart, E. J. T. Chrystal, S. Menzer, D. J. Williams, and P. A. Tasker. *Angew. Chem. Int. Ed. Engl.*, 34:1865–1869, 1995. 123

[21] N. Koumura, R. W. J. Zijlstra, R. A. van Delden, N. Harada, and B. L. Feringa. *Nature*, 401:152–155, 1999. 125

[22] M. Klok, N. Boyle, M. T. Pryce, A. Meetsma, W. R. Browne, and B. L. Feringa. *J. Am. Chem. Soc.*, 130:10484–10485, 2008.

[23] V. Balzani, M. Clemente-León, A. Credi, B. Ferrer, M. Venturi, A. H. Flood, , and J. F. Stoddart. *Proc. Nat. Acad. Sci. USA*, 103:1178–1183, 2006. 125

[24] M. Baroncini, S. Silvi, M. Venturi, and A. Credi. *Chem. Eur. J.*, 16:11580–11587, 2010. 127

[25] R. D. Astumian. *Nat. Nanotechnol.*, 7:684–688, 2012. 130, 134

[26] J.-M. Lehn. *Chem. Eur. J.*, 12:5910–5915, 2006. 130

[27] A. Credi and L. Prodi. *J. Mol. Struct.*, 1077:30–39, 2014. 130, 133

[28] G. Ragazzon, M. Baroncini, S. Silvi, M. Venturi, and A. Credi. *Nat. Nanotechnol.*, 10:70–75, 2015. 131, 133

[29] F. G. Helfferich. *Kinetics of Multistep Reactions, 2nd Ed.* Elsevier, Amsterdam, 2004. 132

[30] A. Coskun, M. Banaszak, R. D. Astumian, J. F. Stoddart, and B. A. Grzybowski. *Chem. Soc. Rev.*, 41:19–30, 2012. 133, 134

[31] M. N. Chatterjee, E. R. Kay, and D. A. Leigh. *J. Am. Chem. Soc.*, 128:4058–4073, 2006. 134

[32] V. Serreli, C.-F. Lee, E. R. Kay, and D. A. Leigh. *Nature*, 445:523–527, 2007. 134

[33] M. Alvarez-Pérez, S. M. Goldup, D. A. Leigh, and A. M. Z. Slawin. *J. Am. Chem. Soc.*, 130:1836–1838, 2008. 134

[34] J. V. Hernandez, E. R. Kay, and D. A. Leigh. *Science*, 306:1532–1537, 2004. 134

[35] M. von Delius, E. M. Geertsema, and D. A. Leigh. *Nat. Chem.*, 2:96–101, 2010. 134

[36] P. Thordarson, E. J. A. Bijsterveld, A. E. Rowan, and R. J. M. Nolte. *Nature*, 424:915–918, 2003. 134

[37] G. Steinberg-Yfrach, P. A. Liddell, S. Hung, A. L. Moore, D. Gust, and T. A. Moore. *Nature*, 385:239–241, 1997. 134

[38] I. M. Bennett, H. M. V. Farfano, F. Bogani, A. Primak, P. A. Liddell, L. Otero, L. Sereno, J. J. Silber, A. L. Moore, T. A. Moore, and D. Gust. *Nature*, 420:398–401, 2002.

[39] H. Zhang, X. Hou, L. Zeng, F. Yang, L. Li, D. Yan, Y. Tian, and L. Jiang. *J. Am. Chem. Soc.*, 135:16102–16110, 2013.

[40] X. Xie, G. A. Crespo, G. Mistlberger, and E. Bakker. *Nat. Chem.*, 6:202–207, 2014. 134

13

Insights in the operation of a dissipative pump

13.1 Lessons from other fields

In the previous chapter a light-driven molecular pump has been described. In particular a fluorescence signal was shown to be correlated with the concentration of the free ring and allowed the experimental observation of the system while operating autonomously in a dissipative fashion. A kinetic simulation was also associated to the experiment. When arbitrarily changing some of the kinetic constants used in the simulation it is not straightforward to predict how the system adapts, in particular it is not straightforward to predict how the cycling speed will be affected. From considerations like this an attempt has been done to rationalize the operation of the pump module. To this aim lessons from other fields have been very important.

When discussing the properties of thermally evolving systems the potential energy surface (PES) is probably the most used tool by chemists. Even when very simplified it can provide useful indications about the behaviour of the system. The PES of the studied pump module is reported in figure 13.1.

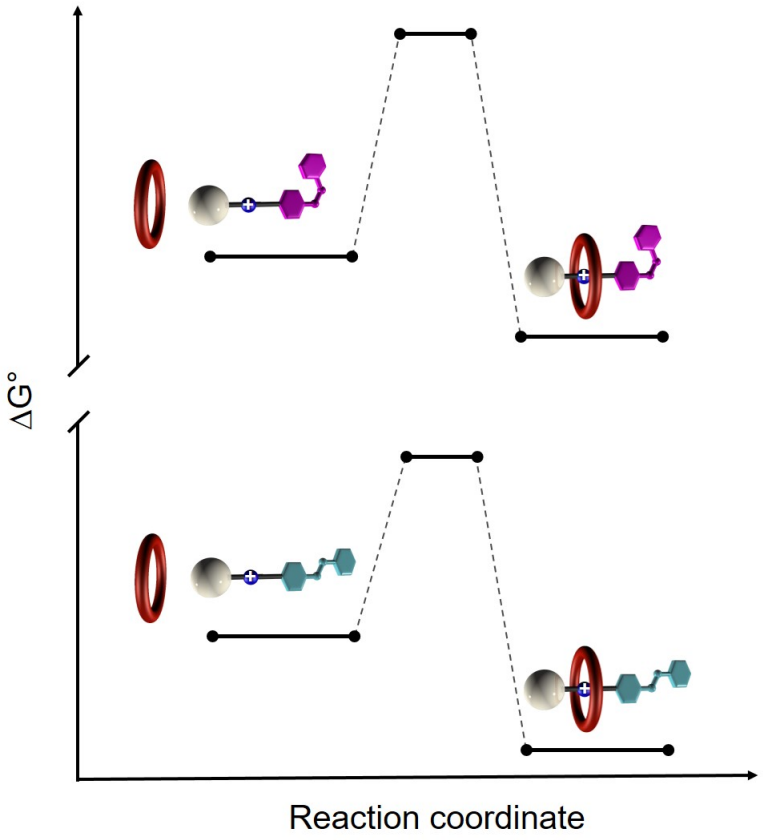

Figure 13.1: *Potential energy surface describing the studied molecular pump, obtained using the experimental data reported in table 12.1 and 12.2. The energy of difference between the* E- *and* Z- *surfaces is not determined.*

This representation is not very informative, indeed as an example, an increase in the incident photon flux does not affect the PES, whereas it has an effect on the operation of the pump — therefore this representation does not seem very informative. To try to deepen the understanding on such system it was natural to look at the rationalization of naturally occurring chemically driven molecular machines. In particular from the work of Bustamante[1] it appears very clearly that natural autonomous molecular machines operate on a periodically descending PES. The fact that the PES is periodic and descending is intrinsically related with the fact that the motor operates in an autonomous fashion. Indeed the fact that something keeps happening is possible only in the presence of a downhill PES, moreover the fact that the same processes are repeated several times indicates that the PES is periodic. Also the studied pump is autonomous and the same reaction

sequence takes place several times in an autonomous fashion, therefore it behaves as if it was on a periodic and downhill PES. Naturally occurring molecular machines are not the only case of chemical system described by a periodic and downhill PES. Catalytic cycles are also described by PES with the same characteristics. Indeed at each cycle the catalyst produces a certain amount of product of an exergonic reaction that would be otherwise slower. Indeed it is known that chemically driven molecular motors can be viewed as catalysts (of an exoergonic reaction involving a fuel) that during their catalytic cycle perform some kind of directional motion, that would not occur when the catalysis is not taking place.[2] To this regard the work of Prof. Kozuch and Prof. Shaik has been particularly important.[3–6] They showed that what determines the speed of a catalytic cycle is not the rate determining step, rather, it is the overall energy span that is experienced in the cycle. In other words even if there are several steps that are going uphill in energy, what matters for the overall rate is the energy difference between the most stable intermediate and the highest energy transition state.

13.2 Building an apparent potential energy surface

Because of the occurrence of photochemical steps it is not possible to directly apply the energy span theory to our molecular machine. To this aim a new energy profile was obtained. This energy profile is obtained from kinetic constants applying the Eyring equation:

$$\Delta G^{\ddagger} = -RTln\frac{kh}{k_B T} \tag{13.1}$$

When equation 13.1 is applied to thermal reactions a $\Delta G^{\ddagger}$ is obtained. Instead when the kinetic constants of bulk photoreactions (see chapters 11 and 12) are used, a value unrelated to the reaction profile is obtained. Indeed photokinetic constants only reflect the frequency of a photochemical event and are not correlated with the energy of the transition state. However, calculating an energy value from the frequency gives the opportunity to effectively compare visually the speed and the influence of the photochemical reactions in the cycle. For what has been just discussed the obtained energy values will be denoted as apparent $\Delta G^{\ddagger}$'s: $\Delta G^{\ddagger}_{app}$. This precedure has been applied to the studied molecular pump: its operation scheme is reported in figure 13.2 and the obtained $\Delta G^{\ddagger}$ and $\Delta G^{\ddagger}_{app}$ values are reported in table 13.1.

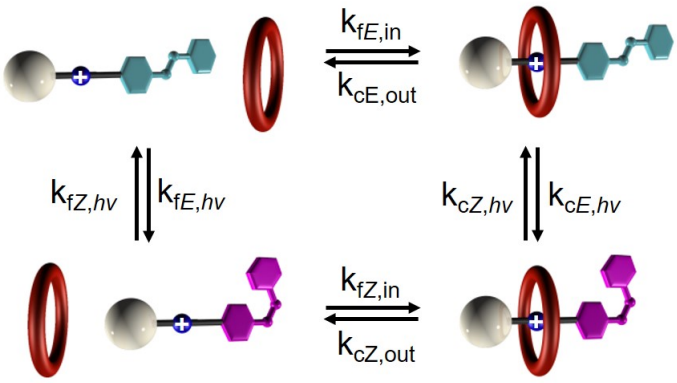

Figure 13.2: *Square cycle representing the operation of the present system. Horizontal and vertical arrows denote the self-assembly equilibria and photochemical isomerization reactions, respectively.*

Table 13.1: *Kinetic constants associated to the dissipative operation of the studied molecular pump (see chapter 12 for details) and the corresponding* $\Delta G^{\ddagger}$ *and* $\Delta G^{\ddagger}_{app}$*. Notation follows the one used in figure13.2:* f = *free axle*, c = *complex*, in = *threading process*, hν = *photochemical step*, Δ = *thermal step.*

Constant	k (s^{-1} or s^{-1} M^{-1})	$\Delta G^{\ddagger}_{app}$ (kcal mol^{-1})
$k_{fE,in}$	54	14.8
$k_{cE,out}$	8.6×10^{-5}	22.6
$k_{cE,h\nu}$	1.8×10^{-3}	20.8
$k_{cZ,h\nu} + k_{cZ,\Delta}$	1.8×10^{-6}	24.8
$k_{cZ,out}$	4.7×10^{-6}	24.3
$k_{fZ,in}$	0.81	17.3
$k_{fZ,h\nu} + k_{fZ,\Delta}$	8.0×10^{-5}	22.6
$k_{fE,h\nu}$	1.6×10^{-3}	20.9

Using the obtained values, it is possible to build the apparent potential energy surface reported in figure 13.3. State I is the starting point and its energy is arbitrarily set to zero. Transition state II is placed at 14.8 kcal mol^{-1} accorging to the $\Delta G^{\ddagger}$ reported in table 13.1 for $k_{fE,in}$. Then intermediate state III is placed at -7.8 kcal mol^{-1} from the following energy difference: 14.8 kcal mol^{-1} (state II) -22.6 kcal mol^{-1} (associated to $k_{cE,out}$) $= -7.8$ kcal mol^{-1}. The same procedure is used for all the following states.

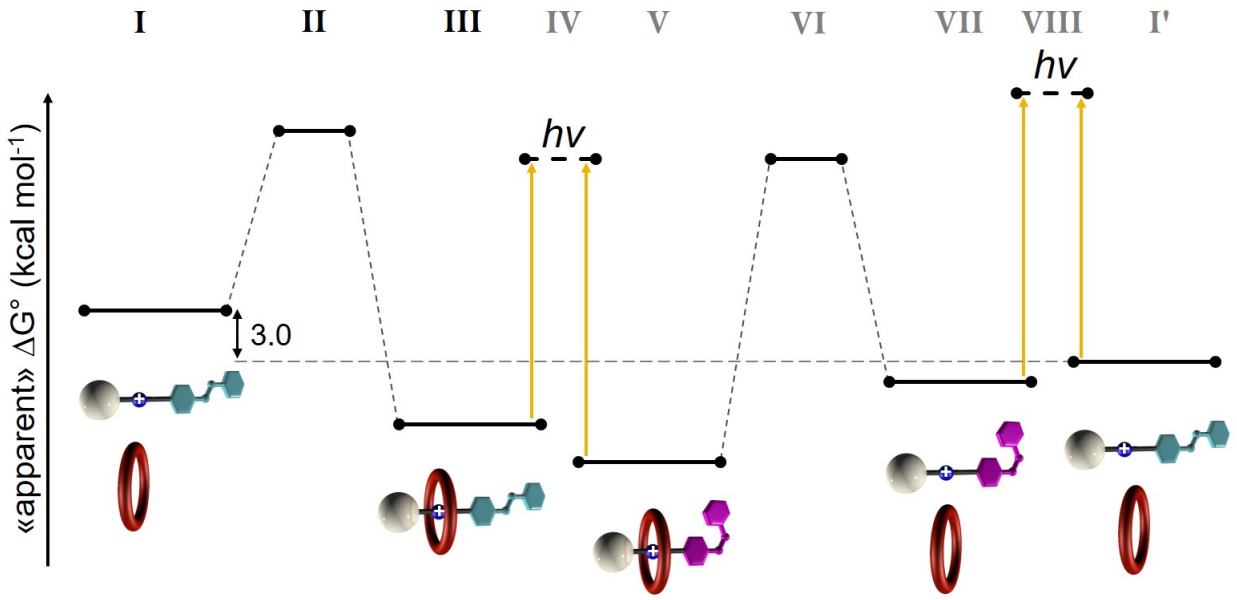

Figure 13.3: *Apparent potential energy surface, built from the* $\Delta G^{\ddagger}_{app}$ *values reported in table 13.1. The apparent* ΔG *of the starting state* **12.1** + E-**12.2**H^+ *has been arbitrarily set to zero. Photochemical transitions are indicated by yellow arrows, and are associated to virtual photochemical transition states, denoted by dashed levels. The apparent energy difference after one clockwise cycle is reported in kcal* mol^{-1}.

The obtained apparent PES has some interesting features that are worth of discussion. This PES is not the traditional PES (reported in figure 13.1), however the system evolves "as if" it was on a PES with this shape. Therefore it can be considered as the PES that is experienced by the system. It can be observed that the apparent energy of the final state (i.e. of the initial state after one clockwise cycle) is not at the same apparent energy as the initial state, meaning that the apparent PES is going downhill in energy along with the occurrence of a cycle, and is periodic, as in the case of chemically driven molecular machines and catalytic cycles. This counterintuitive result implies that the system can distinguish between clockwise and anticlockwise cycling. This happens for two reasons, that both originate in the photochemical steps, and are related to the energy and information ratchet effects that allow the pump operation. The energy ratchet effect comes from the different stabilities of the *E*- and *Z*- complexes. In an hypothetical thermally driven cycle this difference is cancelled in the isomerization steps, indeed the thermal transition (never experimentally observed in this system) from *E*-**12.2**H^+ to *Z*-**12.2**H^+ is easier that that from [**12.1**⊃*E*-**12.2**H]$^+$ to [**12.1**⊃*Z*-**12.2**H]$^+$, because in the latter case, also the destabilization energy of the complex

has to be included (i.e. the transition converts *E*-azobenzene complex in its *Z*-isomer, and also destabilizes the adduct). When the isomerization is driven by light, if the isomerization is equally probable in the free or complexed axle, than the energy difference between *E*- and *Z*- complexes is not counterbalanced any more, and it is therefore apparently preferred to cycle clockwise, in order to associate the *E*-isomer and dissociate the *Z*-isomer. The difference in the stability constants is associated to a $\Delta\Delta G^\circ$ of 0.8 kcal mol^{-1}, that contributes partially to the energy difference observed in figure 13.3 between the initial and final state. Along with this effect comes the energy ratchet effect. Indeed the photoreaction has different efficiency (i.e. different photostationary states) in the free or complexed species. In particular in the current system the isomerization of [**12.1**⊃*E*-**12.2**H]$^+$ to [**12.1**⊃*Z*-**12.2**H]$^+$ under 365 nm light irradiation is even more favoured than the isomerization of the free axle. This effect contibutes for the remaining energy that originates the apparent energy difference of 3.0 kcal mol^{-1} for a clockwise cycle. This energy difference is not generated "for free", indeed two photons of 365 nm have been used in a net clockwise cycle. For the discussion of the energetic efficiency of the pump please refer to chapter 12.

A second interesting fact is noted, in relation to the energy span explored by the system: the lowest-lying intermediate is the *Z*-complex, however the highest apparent transition state is the photochemical conversion of *Z*-**12.2**H$^+$ to *E*-**12.2**H$^+$. This means that the photochemical reaction is crucial in determining the overall speed of the reaction. By using this representation it is very easy to recognize the importance of this photochemical step in determining the reaction speed, instead it would have been more difficult to understand it just from the kinetic constants, because the smallest kinetic constant is the one associated with the dethreading of the axle from [**12.1**⊃*Z*-**12.2**]$^+$.

13.3 Conclusions

In this chapter the operation of the molecular pump introduced in chapter 12 has been rationalized in terms of a newly-built apparent potential energy surface. The surface is built using the experimentally determined values for the chemical equilibria and the bulk rates of photoreactions, and allowed to rapidly grasp the elements that influence the pump operation. In particular the role of photoreactions — that would have been otherwise hidden — is highlighted in this representation. The main features of the obtained apparent PES resemble those of natural molecular motors and catalytic cycles.

13.4 References

[1] C. Bustamante, D. Keller, and G. Oster. *Acc. Chem. Res.*, 34:412–420, 2001. 140

[2] M. R. Wilson, J. Solá, A. Carlone, S. M. Goldup, N. Lebrasseur, and D. A. Leigh. *Science*, 534:235–240, 2016. 141

[3] S. Kozuch and S. Shaik. *J. Am. Chem. Soc.*, 128:3355–3365, 2006. 141

[4] S. Kozuch and S. Shaik. *Acc. Chem. Res.*, 44:101–110, 2011.

[5] S. Kozuch. *WIREs Comput. Mol. Sci.*, 2:795–815, 2012.

[6] S. Kozuch and J. M. L. Martin. *ChemPhysChem*, 12:1413–1418, 2011. 141

Part V

Radicals in supramolecular polymers

14

A radical-cation based supramolecular polymer

14.1 Aim & introduction

The main body of this thesis is dedicated to the study and characterization of molecular devices and machines. Six months of the PhD were spent in the laboratories of Prof. Aida at The University of Tokyo: considering my background experience with supramolecular interactions and spectroscopic techniques, including some experience with radicals, the work at The University of Tokyo has been mostly dedicated to the supramolecular polymerization of triamide triphenylamine (TPA) radical cations. The project initially developed from some preliminary attempts to extend the concept of chain-growth supramolecular polymerization[1] to triamide triphenylamine radical cations. Indeed preliminary results indicated that the radical cation of TPA monomers does not spontaneously polymerize, even in conditions where analogue neutral TPA form linear supramolecular polymers. However, polymerization of the radical cation was observed in selected cases, although it was not possible to clearly establish the reason for the occurrence of polymerization. For this reason I synthesized the radical cation of several TPA derivatives and investigated its behaviour, to possibly disclose the mechanism of polymerization.

14.2 Synthesis and stability of triphenylamine radical cations

The investigated triamide derivatives were synthesized in the group respectively by Kim (**14.1** and **14.3**) Nihonyanaghi (**14.2**) and Dr. Rao (**14.4**) and are reported in figure 14.1.

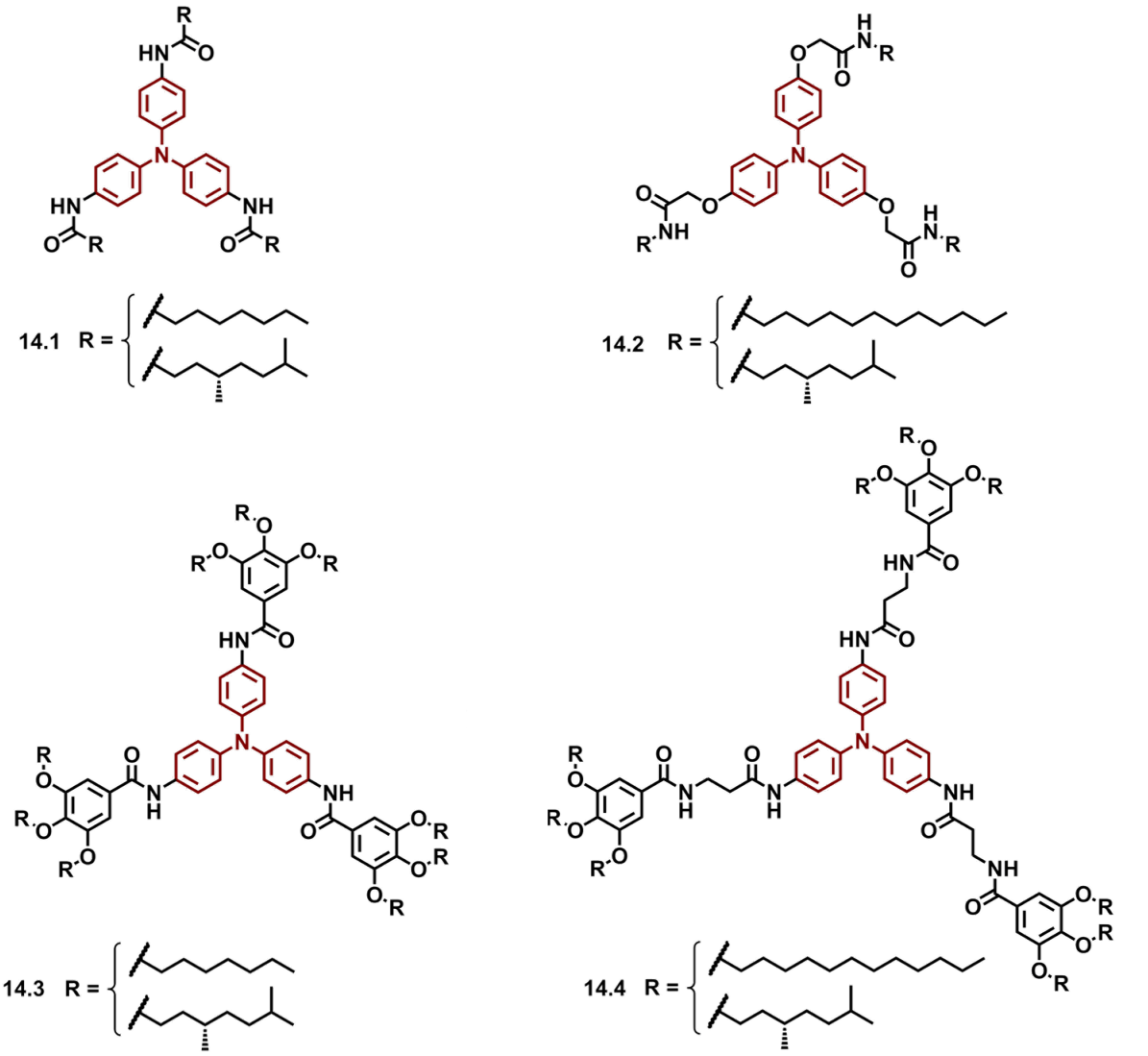

Figure 14.1: *Molecular structure of the investigated triaarylamine derivatives. Use of derivatives with chiral side chains will be specified throughout the text.*

14.2.1 Oxidation of 14.1 with triethyloxonium hexachloroantimonate

The first TPA to be examined has been derivative **14.1**, as it had been the subject of preliminary investigations. In a typical synthesis a solution of the neutral triamide **14.1** in DCM (1 mg in ca. 10 mL, concentration ca. 150 μM) was prepared. $SbCl_6Et_6O$ (stoichiometric amount, that as

a consequence of the particular oxidation mechanism of this chemical oxidant corresponds to 1.5 equivalents, ca. 1 mg) was dissolved separately in 3 mL of DCM. The oxidant solution was then added at −78 °C to the triamide solution, using a CO_2/acetone bath to control the temperature. After 5 minutes the solution was transferred to a water-ice bath and vigorously stirred for 1 h. Finally, the solution was brought to room temperature while under vortex-stirring. The solution was then dried and the solid was washed with hexane to remove the excess neutral monomer. The oxidation reaction proved to be rather slow; indeed, avoiding the first step at −78 °C did not change the outcome of the reaction. On the contrary, heating to 40 °C, stirring overnight at room temperature, or concentrating the solution sped the reaction up significantly. Even with these modifications the reaction was not complete when a stoichiometric amount of oxidant was used, as evidenced by the presence of the neutral monomer band at 325 nm in the absorption spectrum of the crude. Performing the synthesis under an inert atmosphere did not improve the radical stability or the required amount of oxidant. At least two equivalents were necessary to fully convert the neutral TPA in its radical cation. While optimizing the synthesis it was observed that an excess of chemical oxidant could induce spectral changes overnight at room temperature, compatible with the supramolecular polymer formation (i.e. consistent with preliminary results, see figure 14.2). This suggests that chemical oxidant itself is able to promote the aggregation. In particular the degradation of Et_3OSbCl_6 is a well known process in solution and constitutes the initial step of a series of reactions leading to the formation of the active one-electron oxidant species, however, when the one-electron oxidant is not consumed in a redox reaction, such reaction generates other non-innocent species,[2] that are likely playing an important role in the observed aggregation process. Unfortunately the aggregation was concomitant with a partial disappearance of the lowest energy band of the radical cation, evidencing its degradation.

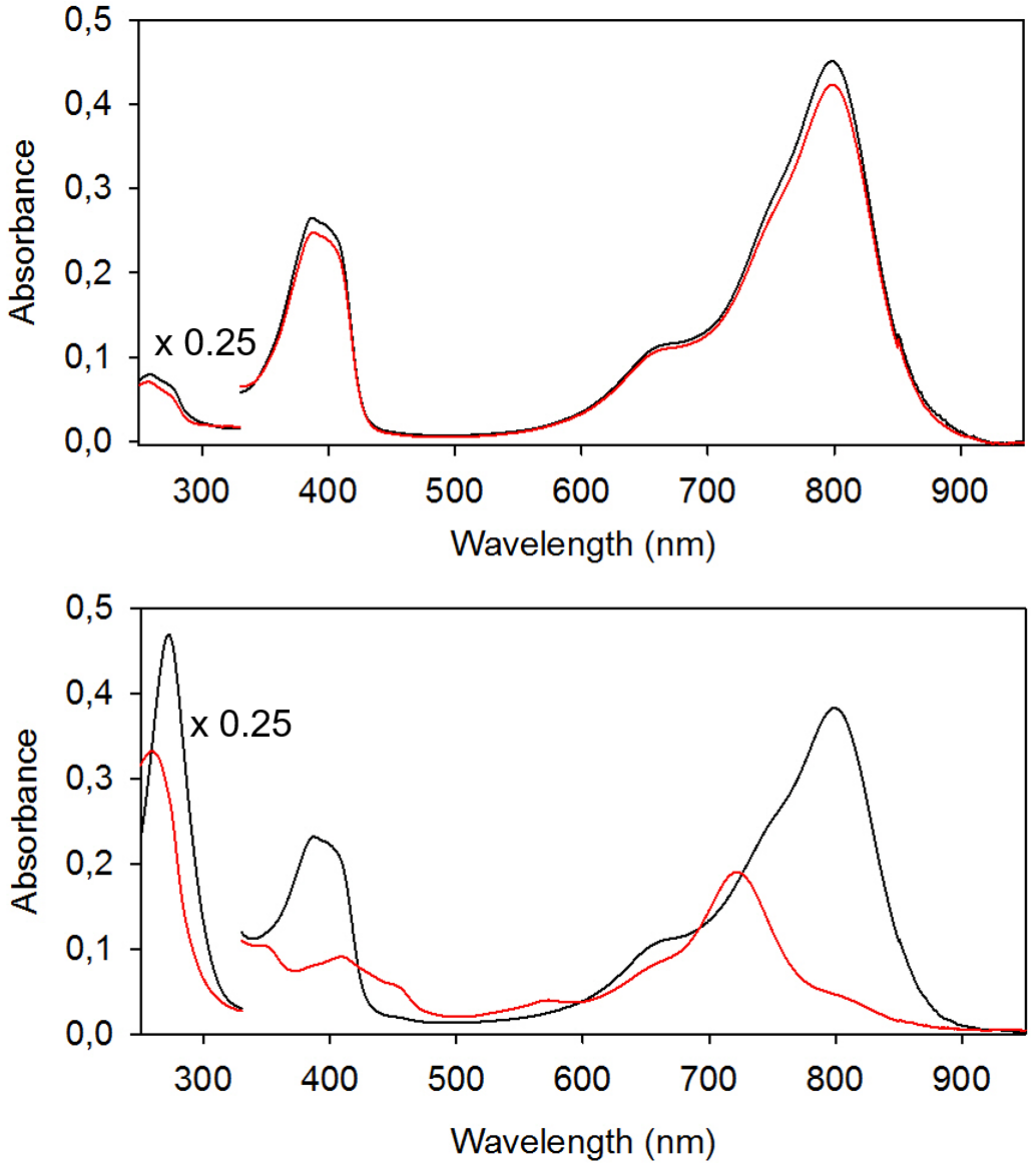

Figure 14.2: *Absorption spectra of radical cation* **14.1**$^{+\bullet}$ *in DCM as synthesized (black spectra) and after standing overnight at 20 °C (red spectra). The two graph differ in the amount of chemical oxidant used: 2 eq. (top) and 15 eq. (bottom).*

Efforts to optimize the amount of added chemical oxidant to avoid degradation and obtain the supramolecular polymer proved to be unsuccessful. Moreover, the complicate behavior of the chemical oxidant, related to its degradation, refrained us from a detailed investigation of the chemical

oxidant role. For these reasons it was decided to abandon the use of this chemical oxidant and to investigate others, that could possibly afford a pure and stable radical cation.

14.2.2 Oxidation of 14.1 with different chemical oxidants

On the basis of literature reports, it was decided to use tris(4-bromophenyl)ammoniumyl hexachloroantimonate (**TBPA**$SbCl_6$), nitrosonium hexafluoroantimonate ($NOSbF_6$) and nitrosonium tetrafluoroborate ($NOBF_4$) as oxidizing agents. Here it is discussed the procedure used with **TBPA**$^{+\bullet}$, since it proved to be the better oxidant and will be later applied also to other derivatives. To isolate the radical cation upon oxidation with **TBPA**$^{+\bullet}$, the neutral triamide was mixed with the oxidant in DCM, in which both compounds are soluble, with the former in slight excess. Evaporation of the resultant solution to dryness, redissolution of the obtained solid in cold ACN and filtration of the obtained mixture was functional to the removal of the excess neutral triamide, that is not soluble in cold ACN. Next, the solution was dried and the solid was washed with methylcyclohexane (MCH), that washes away the neutral **TBPA**, but is not able to dissolve the radical cation. Using this procedure, it was possible to obtain a radical cation that was almost completely pure, even if two remaining absorption peaks of little intensity around 270 nm were still noticeable. These two impurities could not be removed by a second dissolution in ACN or washing with hexane. The synthesis using $NOSbF_6$ was performed successfully, but in this case the impurity peaks around 270 nm were more pronounced in comparison with those remaining in the radical cation obtained with **TBPA**$SbCl_6$. The synthesis performed using $NOBF_4$ was unsuccessful, in line with the fact that smaller counterions are associated with a lower stability. The stability of the resulting radical cations was evaluated by monitoring the decrease in absorbance of the lowest energy band after keeping the samples in the dark overnight at r.t.. This was based on the assumption that the degradation product did not absorb light in that region: this is partially supported by the fact that even after substantial degradation, the shape of the absorption band did not change appreciably.

Table 14.1: *Degradation (%) of a 40 μM DCM solution of* **14.1**$^{+\bullet}$ *after 11 h at r.t.; the reported value is based on the decrease in the absorbance at the maximum of the lowest energy band of the radical cation.*

	Et_3OSbCl_6	**TBPA**$SbCl_6$	$NOSbF_6$	$NOBF_4$
Degradation (%)	7[a]	6 (3[a])	19	*high*

[a] the synthesis was performed under aerated conditions.

In the case of **TBPA**$SbCl_6$, performing the synthesis under ambient conditions gave even better results in terms of stability, possibly because quick operation avoided the formation of unwanted byproducts while the samples were in unstable conditions, e.g. in ACN or in contact with hexane. Using special precautions to avoid ambient light did not lead to any improvement of the stability. In light of these results, **TBPA**$SbCl_6$ was chosen as chemical oxidant.

14.2.3 Stability of 14.1, 14.2 and 14.3 hexachloroantimonate radical cation

In order to further improve the stability of the radical cation, different molecular structures of the triphenylamine were tested (derivatives **14.2** and **14.3** in figure 14.1). At this stage of the investigation, derivatives bearing linear (thus achiral) side chains were used.

With respect to **14.1**, **14.2** was chosen because the presence of oxygen atoms at *para*-positions was shown to greatly stabilize a structurally analogue radical cation.[3] At the same time **14.3** was also investigated, to assess the effect of an extended conjugation on the radical stability. Since **14.3** is soluble also in MCH, a minor amount of neutral monomer could not be removed from the reaction mixture using the same procedure previously adopted. Degradation percentages after 10 h at room temperature are reported in table 14.2.

Table 14.2: *Degradation (%) of a 40 μM DCM solution of* $\mathbf{14.1}^{+\bullet}$, $\mathbf{14.2}^{+\bullet}$ *and* $\mathbf{14.3}^{+\bullet}$ *in MCH after 10 h at r.t.; the reported value is based on the decrease in the absorbance at the maximum of the lowest energy band of the radical cation.*

	$\mathbf{14.1}^{+\bullet}$	$\mathbf{14.2}^{+\bullet}$	$\mathbf{14.3}^{+\bullet}$
Degradation (%)	3	2	6

Since $\mathbf{14.2}^{+\bullet}$ showed the lowest degradation, the study continued focusing on this type of monomer. Although in DCM at 20 °C the radical cation can be considered stable for 10 h, the solvent is not appropriate to induce the formation of a supramolecular polymer. For this reason, the stability of the radical cation had to be investigated in different solvents. MCH is known to be a good solvent for the polymerization of the neutral counterpart of this radical cation, however the radical cation itself is insoluble in this solvent. Therefore a 1:1 mixture DCM:MCH was used as solvent, along with toluene, that has a polarity intermediate between DCM and MCH. Unfortunately, in both these conditions a significant degradation was observed. After 10 h the decrease in the lowest energy absorption band amounted to 36% and 37% respectively (figure 14.3). A

DCM:CH (cyclohexane) 1:1 mixture was also investigated: the rational for this choice has been that in CH there are no tertiary carbons, that could possibly be oxidized by the radical cation. Indeed a moderate decrease in the degradation was observed. However, since the improvement was minor, and the use of CH (m.p. = 6 °C) limits the range of temperature that can be used to induce the polymerization, (compare with MCH, m.p. = −126 °C), it was chosen to avoid the use of CH. Considering the possibility that degradation involves adventitious species present in solution, the dependence of the stability from the sample concentration was also investigated. As expected, the more concentrated sample showed less degradation, although still substantial. The kinetic profile of the degradation reactions suggests that the degradation occurs through two different pathways. In particular, after 4 h the degradation speed is very similar between the two samples, suggesting an intramolecular degradation reaction, or a reaction with the solvent (figure 14.3).

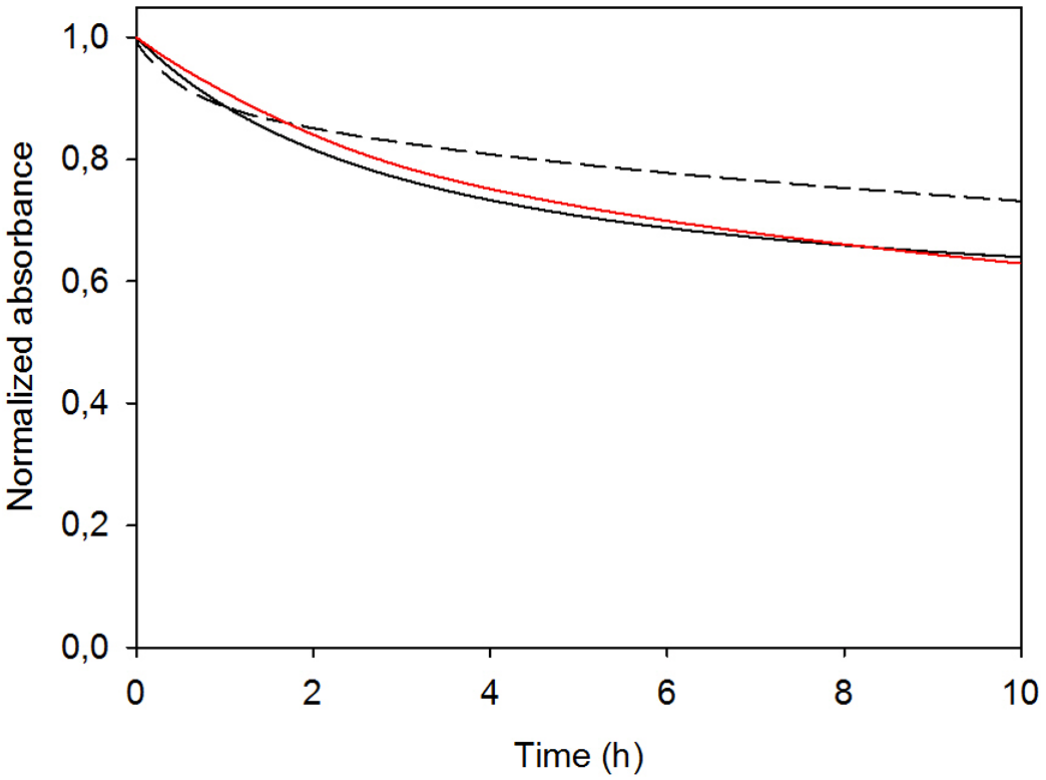

Figure 14.3: *Time-dependent degradation profile of* **14.2**$^{+\bullet}$ *in toluene at 40 and 400 μM concentration (black, solid and dashed line, respectively) or in DCM:MCH 1:1 mixture (40 μM, red line). Profiles are obtained monitoring the decrease in absorbance of the lower-energy band (ca. 800 nm) at r.t..*

Finally, the effect of temperature on the degradation was also investigated. Keeping the sample at 2 °C avoided almost completely the degradation. Therefore, DCM:MCH mixture kept at 2 °C was chosen as the working condition for further studies.

14.3 Polymerization attempts

To investigate the formation of the supramolecular polymer, circular dichroism (CD) was chosen as the preferred technique to screen the polymerization conditions. Indeed, when neutral triamide triphenylamine molecules assemble, the polymer adopts a preferential chirality, if the side chain carries a chiral center.[4] The assumption that this process would be effective also in the case of the monomer radical cation (as suggested by preliminary results) prompted us to use CD as a convenient and clear screening technique. To this regard, derivatives bearing a chiral side chain were investigated (see figure 14.1 for structures). Since it was shown that increasing the temperature promptly lead to radical cation degradation, different methods to induce nucleation – thus polymerization – had to be investigated, other than increasing the temperature.

Three different possibilities were investigated:

(1) addition of chloride ions in the form of tetrabuthylammonium salt. This strategy was chosen because Giuseppone and coworkers showed that the polymerization of metastable triamide triphenylamine was induced upon light-induced generation of radical cations, with chloride counterion[5]. In light of these results we hypothesized that if partial counterion exchange could take place, this would favor the nucleation process;

(2) addition of seeds of the neutral polymer. In this case the neutral polymer should act as a nucleus for the growth of the radical cation polymer. The seeds were obtained by dissolving the neutral monomer in MCH and subsequently an aliquot of the polymer solution was added to the radical cation solution. Since in DCM:MCH 1:1 solution the polymer seeds are thermodynamically unstable, this strategy relies on the fact that the elongation kinetic should be faster than depolymerization;

(3) cooling the solution. In this case the aim was to increase the thermodynamic stability of the polymer, thus inducing its formation at low temperature. In this case samples were kept at −30 °C overnight.

In order to find the optimal conditions for polymerization, solvent composition and radical cation monomer concentration were also changed. Concentration was increased as much as possible under every solvent condition, whereas several DCM:MCH 1:X mixtures, where X is the relative amount

of MCH, were tested. Figure 14.4 graphically represents the investigated conditions. Unfortunately all attempts to polymerize were not successful.

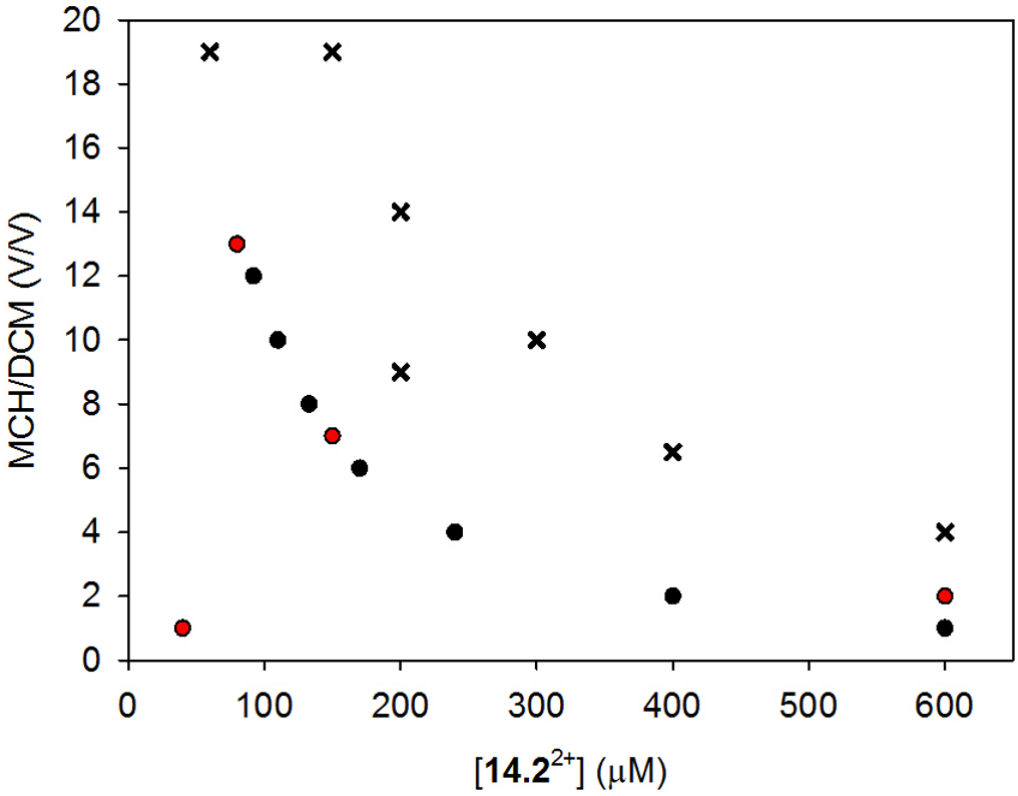

Figure 14.4: *Conditions investigated to attempt the supramolecular polymerization. Dots are referred to conditions in which the monomer was stable in solution at least overnight; in particular, polymerization was attempted with the three outlined methods in correspondence to the red dots. Black crosses indicate conditions where the monomer was not stable and precipitated.*

14.3.1 Investigation of the double amide derivative 14.4

Examining these results, it was reasoned that polymerization was possibly not taking place because of an insufficient thermodynamic driving force. Therefore it was decided to investigate an hexaamide derivative bearing two amides for each arm (**14.4**, figure 14.1). In the case of its analogue neutral polymer, it is known that increasing the number of amide units leads to a much greater stability of the resulting polymer, that remained stable even in the presence of little amounts of DCM (e.g. 5%

v/v)[1]. Moreover, the presence of the phenolic part imparted solubility to the radical cation also in pure MCH, as in the case of the single-amide analogue previously discussed. Analogously to what previously discussed, some residual neutral **TBPA** was also present in the studied solution.

Our previous investigation showed that going from the neutral monomer to its radical cation decreased the compound solubility in MCH, indeed radical cations were not soluble in MCH (with the exception of those bearing a phenolic part), whereas neutral monomers were soluble in MCH. Moreover, decreasing the polarity of the solvent, from DCM to toluene or DCM:MCH mixtures decreased the stability of the monomers. Based on these results, with regards to the double amide derivative, it was expected a lower solubility, compared to its neutral counterpart. Morover, a lower stability in MCH with respect to DCM was also expected. Contrary to our expectations, both these predictions were not verified. Indeed the radical cation was soluble at least up to 80 μM (solubility of the neutral monomer in MCH ca. 10 μM), and only a minimum degradation was observed overnight (2% after 10 h at 2 °C). Unfortunately, no CD signal was observed, excluding the formation of a chiral supramolecular polymer. The same behavior (good solubility and high stability on MCH) was also observed in the case of the analogue single amide derivative **14.3** (figure 14.1), implying that this behavior is not a consequence of the presence of the double amide, instead it is related to the presence of the phenolic part, that imparts solubility in MCH. To further investigate this behavior, EPR was performed. Both for the single and double amide derivatives the EPR signal in DCM was significantly different from that observed in MCH (figure 14.5).

[1]Dr. V. R. Kotagiri, unpublished work

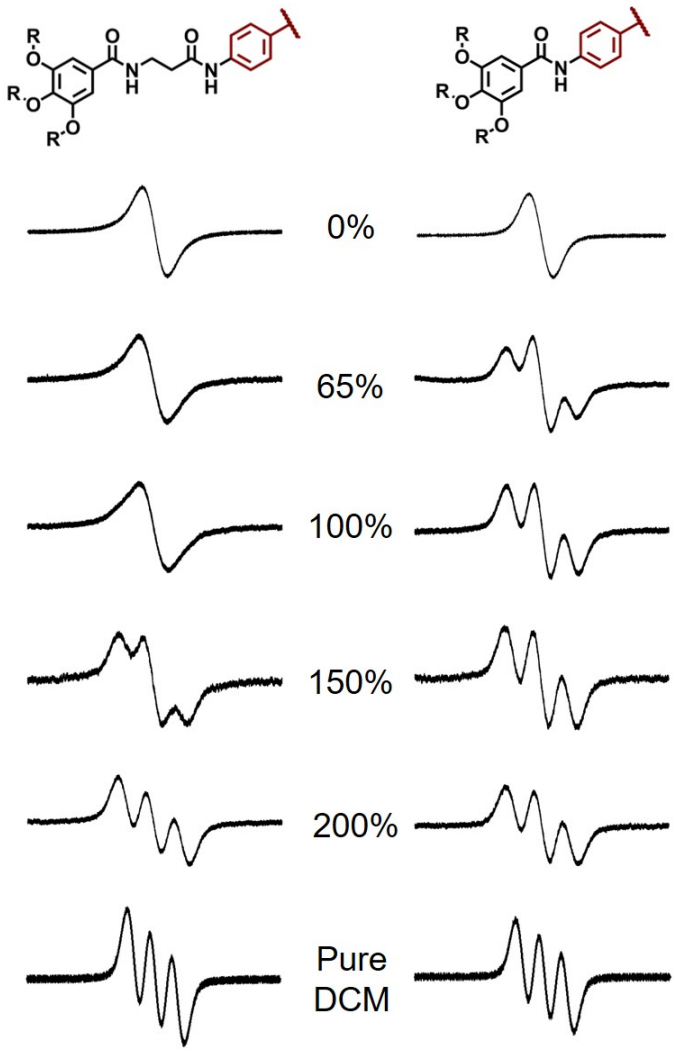

Figure 14.5: *EPR signal obtain for derivatives* **14.3**$^{+\bullet}$ *(right) and* **14.4**$^{+\bullet}$ *(left) in MCH (top), DCM (bottom), and upon addition of DCM (volume %) to the initial MCH solutions (top to bottom). Oxygen was not removed from the samples.*

The EPR signal observed in DCM is consistent with a radical centered on the nitrogen atom and coupled with the aromatic protons, thus originating the broad signal observed. On the contrary, the MCH signal could be originated from an aggregate of radicals. To further support the fact that a hydrogen bonded aggregate formed in MCH, the following experiment was performed: DCM was gradually added to MCH solutions of the mono or double amide derivative, and the transition between the two spectral shapes was observed. As expected the transition occurred first for the single

amide and a larger amount of DCM had to be added to induce the transition in the double amide sample (figure 14.5). Further evidence of the formation of aggregates was obtained from AFM of a dip-coated MCH sample of the double amide cation radical (figure 14.6). Round-shaped objects with height ranging from 15 to 20 nm were observed; however, control-images of the neutral monomer and the radical cation of the mono-amide derivative were not collected due to time limitation.

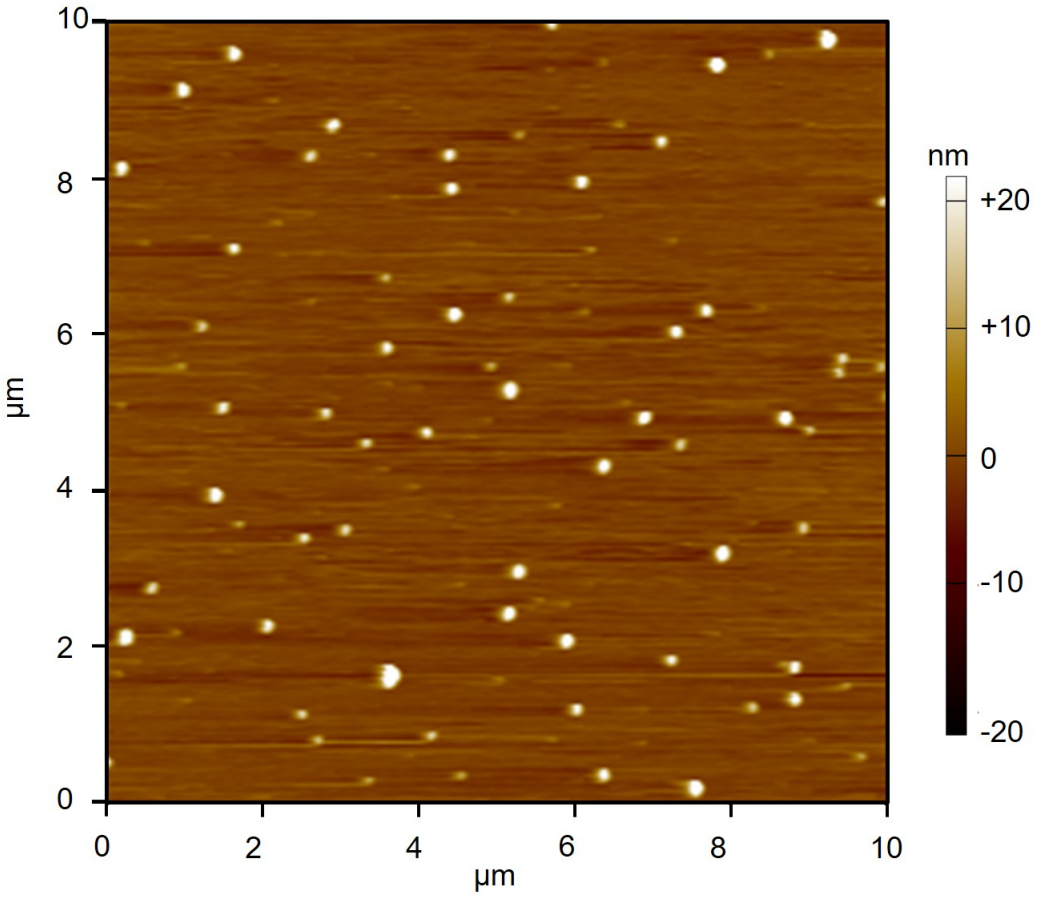

Figure 14.6: *Tapping-mode AFM image of a dip-coated sample of* $\mathbf{14.4}^{+\bullet}$ *dissolved in MCH.*

14.4 Conclusions

With respect to the initial aim of the project, it was concluded that degradation of $SbCl_6Et_6O$ may be responsible for the polymerization of TPA radical cations. Besides this, an adapted procedure to obtain a pure radical cation monomer of amide-bearing triphenylamine derivatives was developed,

and the effect of various parameters on the stability of this class of monomers was investigated (counterion, substituents, solvent, temperature, concentration). In particular, it was found that lowering the temperature greatly improved the radical stability, even in an apolar solvent mixture as DCM:MCH 1:1, where the radical cation is intrinsically less stable with respect to more polar solvents like pure DCM. Judging from circular dichroism spectra, all attempts to obtain linear polymers of these radical cation monomers proved to be unsuccessful, even in very favorable conditions (e.g., six amide present in the molecular structure of the monomer and using MCH as a solvent). Instead, the radical cation monomers that were soluble in MCH likely formed irregular aggregates, as evidenced by EPR spectroscopy and AFM. The observed behaviour is tentatively rationalized in terms of the preferential position of the $SbCl_6^-$ counterion, that according to computational simulations[6] is located on top of the nitrogen atom, thus hampering supramolecular polymerization. Possibly, the $SbCl_6Et_6O$ degradation process lead to the formation of different counterions, that might have been more easily moved to the side of the radical monomer (a higher valency of the counterion might favour this) thus inducing supramolecular polymerization.

14.5 References

[1] J. Kang, D. Miyajima, T. Mori, Y. Inoue, Y. Itoh, and T. Aida. *Science*, 347:646–651, 2015. 149

[2] Z. V. Todres. *Organic ion radicals: chemistry and applications.* Marcel Dekker Inc., New York and Basel, 2003. 151

[3] L. Ebersonn and B. Larsonn. *Acta Chem. Scand., Ser. B*, 41:367–378, 1987. 154

[4] T. Kim, T. Mori, T. Aida, and D. Miyajima. *Chem. Sci.*, 16:6689–6694, 2016. 156

[5] E. Moulin, F. Niess, M. Maaloum, E. Buhler, I. Nyrkova, and N. Giuseppone. *Angew. Chem. Int. Ed.*, 49:6974—6978, 2010. 156

[6] I. Nyrkova, E. Moulin, J. J. Armao, M. Maaloum, B. Heinrich, M. Rawiso, F. Niess, J. Cid, N. Jouault, E. Buhler, A. N. Semenov, and N. Giuseppone. *ACS Nano*, 8:10111–10124, 2014. 161

Conclusions

The key advancement presented in this thesis has been the experimental demonstration that a functional supramolecular system can operate autonomously away from thermodynamic equilibrum, exploiting light energy in a repetitive fashion. To achieve this goal, an innovative way of rationalizing photodriven dissipative systems has also been devised and employed. These results have been described in **Part IV** of the manuscript. One message that emerges very clearly from this part is the crucial importance of ratcheting mechanisms for the development of active nonequilibrium matter. Hopefully this work will contribute to foster research in this domain.

The key finding of **Part III** of this manuscript is that allosteric behaviours within an interlocked structure can be engineered by means of "frustrated" noncovalent interactions. Further studies on this topic may contribute to disclose some aspects of allostery in biologically relevant molecules. Moreover, using the very same rotaxane architechture it was demonstrated the sequential pick-up, transport and release of a molecular cargo – a metal complex. To the best of my knowledge, the illustrated system is the sole able to pick-up a substrate from solution, while binding it with a stable covalent bond: this is a key experimmental requirement to ensure that the cargo does not detach while being transported.

Parts II and **V** collect results at a more basic level, still, this part of the manuscript provides solid bases for future developments. In particular in **Part II** it was shown that in isomeric rotaxanes bearing a cali[6]arene as wheel component, the orientation of the wheel with respect to the axle imparts a clear thermodynamic preference for shuttling in one of the two isomers. Building on this result it may be possible to obtain rotaxanes in which the direction of motion is dictated solely by the orientation of the wheel component, and not by the symmetry of the axle. In **Part V** the investigation of triarylamine radical cations suggested that it is not possible to obtain linear supramolecular polymers of such species, when the radical counterion is monovalent. The obtained results suggest that the use of counterions with a higher valency may induce the formation of linear supramolecular polymers composed of radical cations.

List of publications

originated from this thesis

Original research articles

listed as discussed in the manuscript

I "Plugging a bipyridinium axle into multichromophoric calix[6]arene wheels bearing naphthyl units at different rims"
G. Orlandini, G. Ragazzon, V. Zanichelli, L. Degli Esposti, M. Baroncini, S.Silvi, M. Venturi, A. Credi, A. Secchi, A. Arduini, *ChemistryOpen*, **2017**, 6, 64 - 72.

II "Covalent capture of oriented calix[6]arene rotaxanes by a metal-free active template approach"
G. Orlandini, G. Ragazzon, V. Zanichelli, A. Secchi, S.Silvi, M. Venturi, A. Arduini, A. Credi, *ready for submission.*

III "Synthesis and characterization of constitutionally isomeric oriented calix[6]arene-based rotaxanes"
V. Zanichelli, G. Ragazzon, A. Arduini, A. Credi, P. Franchi, G. Orlandini, M. Venturi, M. Lucarini, A. Secchi, S. Silvi, *European Journal of Organic Chemistry*, **2016**, 1033 - 1042.

IV "Synthesis by ring closing metathesis and properties of an electroactive calix[6]arene [2]catenane"
G. Orlandini, V. Zanichelli, A. Secchi, A. Arduini, G. Ragazzon, A. Credi, M. Venturi, S. Silvi, *Supramolecular Chemistry*, **2016**, 28, 427 - 435.

V "Thermodynamic insights on a bistable acid-base switchable molecular shuttle with strongly shifted co-conformational equilibria"
G. Ragazzon, A. Credi, B. Colasson, *Chemistry - a European Journal*, **2017**, 23, 2149 - 2156.

VI "Structural Changes of a Doubly Spin-Labeled Chemically Driven Molecular Shuttle Probed by PELDOR Spectroscopy"

P. Franchi, V. Bleve, E. Mezzina, C Schäfer, G. Ragazzon, M. Albertini, D. Carbonera, A. Credi, M. Di Valentin, M. Lucarini, *Chemistry - a European Journal*, **2016**, 22, 8745 - 8750. Journal inside back cover.

VII "An artificial molecular transporter"
C. Schäefer, G. Ragazzon, B. Colasson, M. La Rosa, S. Silvi, A. Credi, *ChemistryOpen*, **2016**, 5, 120 - 124.

VIII "Light-powered autonomous and directional molecular motion of a dissipative self-assembling system"
G.Ragazzon, M. Baroncini, S. Silvi, M. Venturi, A. Credi, *Nature Nanotechnology*, **2015**, 10, 70 - 75. Journal cover. Highlights: "Nanomachines: a light-driven molecular pump" E. Sevick, *Nature Nanotechnology*, **2015**, 10, 18 - 19; "Photoisomerization: molecular motors driven by light" O. Graydon, *Nature Photonics*, **2015**, 9, 13.

Review and conference papers

IX "Light-driven molecular machines based on Ruthenium polypyridine complexes: strategies and recent advances"
B. Colasson, A. Credi, G. Ragazzon, *Coordination Chemistry Review*, **2016**, 325, 125 - 134.

X "Light powered artificial molecular pumps: a minimal approach"
G. Ragazzon, M. Baroncini, S. Silvi, M. Venturi, A. Credi, *Beilstein Journal of Nanotechnology*, **2015**, 6, 2096 - 2104.

XI "The ethernal youth of azobenzene: new photoactive molecular and supramolecular devices"
M. Baroncini, G. Ragazzon, S. Silvi, M. Venturi, A. Credi, *Pure and Applied Chemistry*, **2015**, 87, 6, 537 - 545.

XII "Photochemically controlled molecular machines with sequential logic operation"
T. Avellini, M. Baroncini, G. Ragazzon, S. Silvi, M. Venturi, A. Credi, *Israer Journal of Chemistry*, **2014**, 54, 553 - 567.

Book chapters

XIII "Electrochemically Controlled Supramolecular Switches and Machines"
G. Ragazzon, M. Baroncini, P. Ceroni, A. Credi, M. Venturi in "Comprehensive Supramolecular Chemistry II", J. Atwood, G. Gokel (Eds.), Elsevier, Amsterdam, *in press*.

XIV "Azobenzene photoisomerization: an old reaction for activating new molecular devices and materials"

M. Baroncini, G. Ragazzon, S. Silvi, M. Venturi, A. Credi in "Photochemistry", **2017**, 44, 296 - 323, A. Albini, E. Fasani (Eds.), RSC Press, Cambridge.

Divulgative articles

XV "Molecole a senso unico", (One way molecules - in italian)
G. Ragazzon. Independent contribution to "European Young Chemist Award: premiata la Chimica Italiana"
M. Pavone, G. Ragazzon, D. Leonori, F. Monti, F. Bella *La Chimica e l'Industria WEB*, **2016**, 3, 8 - 13.

XVI "Pompe molecolari azionate dalla luce" (Light-driven molecular pumps - in italian)
G. Ragazzon, M. Baroncini, S. Silvi, M. Venturi, A. Credi, *La Chimica e l'Industria*, **2015**, 97, 35 - 39.

XVII "Molecole in azione" (Molecules in action - in italian)
G. Ragazzon, *Sapere*, **2015**, 2, 45.

Grazie!

Questa tesi è il frutto anche del lavoro e dell'aiuto di molte persone. Mi fa piacere ringraziarle.

Le più importanti sono state Alberto e Serena. In questi anni ho pensato più volte che un ottimo punto di partenza per fare un buon dottorato è lavorare con persone che hanno un approccio al mondo simile al proprio, almeno in una parte considerevole: non è solo questione di avere gli stessi interessi scientifici. Quantomeno questa è stata la mia percezione. Grazie per avermi ascoltato sempre ed avermi lasciato la libertà di provare e sbagliare.

Alberto, sono fortunato per la fiducia che mi hai dato e mi dai. Vorrei avere sempre l'entusiasmo che trasmetti per la ricerca e spero che continuerò ad apprezzare ogni aspetto del lavoro in Università: la ricerca, l'insegnamento, la divulgazione.
Serena, sei una sicurezza. Sempre presente, molto lineare, ben organizzata: è facile lavorare con te. A entrambi dico che spero di avere molte altre occasioni di lavorare assieme.

Per me è stato molto importante Benoit. Dove lo si trova un Prof. così? Un approccio alla scienza veramente molto diverso da Serena, ma dalla mia prospettiva perfettamente complementare. Se penso che ha lavorato molto "per me" una persona che ha imparato il mestiere da due Premi Nobel mi metto a ridere. Ci vediamo presto di fronte a un birrino.

Spending half a year in the word-class laboratory of Prof. Takuzo Aida has been a very unique opportunity that turned into an absolutely special experience. I was not expecting to develop a personal relation with Aida Sensei and to breath such a scientific broadness; neither to be followed so closely by Miyajima san and to meet a group of exceptionally talented students: I still am very impressed. Rao san, you have been a great colleague and helped me a lot to adapt to the new lab; I hope that one day you'll be able to enjoy Eejanaika at Fuji-Q like me, Miyajima san and Kang san did.
In my laptop I have a file entitled "Things that surprised me": I wrote it while in Japan and it's always nice to go back to it from time to time and have a look. Some pieces of that half a year will

last forever.

In questi anni ho lavorato su molecole sintetizzate da altre persone, che ringrazio. In particolare Massimo, Christian e Benoit all'interno del nostro gruppo, Kim san, Rao san and Nihonyanaghi san nel gruppo del Prof. Aida all'Università di Tokyo, i Prof. Arduini e Secchi assieme ai loro collaboratori all'Università di Parma e il Prof. Lucarini coi suoi collaboratori, presso il nostro Dipartmento. Il gruppo Lucarini va doppiamente ringraziato, per le misure EPR (fatte sempre a tempo di record!). Guardando oltre i composti sintetizzati e le misure fatte, vi ringrazio per tutta la scienza discussa assieme e la condivisione delle vostre conoscenze con me.

Un grazie anche ai collaboratori il cui lavoro non è incluso in questa tesi — citati nel summary, perchè hanno contribuito alla mia maturazione scientifica. In particolare ad Armaroli, che in più occasioni ha avuto modo di dimostrarmi la sua fiducia.

Alle persone del laboratorio devo molto, in particolare ai più vecchi per avermi insegnato con pazienza e ai più giovani per le piccole cose di ogni giorno.
Poi per me il trucco è stato farsi una o due pause caffè al giorno e una colazione al bar ogni tanto assieme a Marianna: spacchi, e forse avrei dovuto iniziare i ringraziamenti da te.

L'inizio del dottorato, alcuni momenti in Giappone e il periodo della scrittura sono stati mentalmente molto impegnativi. Senza dei buoni amici chissà...
Se una cosa è davvero nuova non viene al primo colpo. Non è facile fare scienza, anche se dall'esterno magari a qualcuno sembra che io abbia avuto sempre fortuna o sia riuscito a far funzionare le cose. Comunque mi è molto chiaro che per riuscire in questo ambiente non è questione di chi ha più intelligenza logica e stop. Anzi, superata una certa soglia quasi non fa differenza. Penso che mi abbia aiutato molto leggere "A PhD in not enough! — A guide to survival in Science" ben prima di iniziare il dottorato. Suggerito.

Alla fine se ho fatto un dottorato penso sia merito della mia famiglia. Con l'implicita spinta allo studio ricevuta non avrebbe potuto andare diversamente; e con Davide a fare l'apripista (oltre che il primo e più tosto reviewer) è tutto più semplice.